



Université Paris 7 - Denis Diderot
Unité de Formation et de Recherche de Physique
Ecole Doctorale de Matière Condensée et Interfaces

Modélisation du bruit acoustique d'ébullition du sodium lors des bouchages d'assemblage

Modeling of the acoustic boiling noise of sodium during an assembly blockage

Matthias Vanderhaegen

Commission d'Examen :

Prof. Dr. Ir. Arnaud Tourin	Directeur de thèse
Prof. em. Michel Giot	Examineur
Prof. Dr. Valentin Leroy	Examineur
Dr. Ir. K. Paumel	Invité
Prof. Dr. Ir. Arnaud Tourin	Directeur de thèse
Prof. Dr. Ir. Greet Maenhout	Examineur
Prof. Dr. Ir. G. Gavriluk	Examineur
Dr. Ir. K. Paumel	Invité – Tuteur CEA

Thèse de doctorat soutenue le 1 octobre 2013
devant la Commission d'Examen
pour obtenir le titre de docteur ingénieur



Modélisation du bruit acoustique d'ébullition du sodium lors des bouchages d'assemblage

RÉSUMÉ

Thèse de doctorat préparée au sein du CEA Cadarache avec une bourse CFR
Laboratoire d'Instrumentation et des Essais Technologiques
Département de Technologie Nucléaire, Direction de l'Energie Nucléaire
F-13108 Saint-Paul-lès-Durance, France



Thèse de doctorat soutenue le 1 octobre 2013
devant la Commission d'Examen
pour obtenir le titre de docteur ingénieur



University Paris 7 - Denis Diderot
Faculty of Physics
School of Condensed Matter and Interfaces



Institut Langevin
ONDES ET IMAGES

Modeling of the acoustic boiling noise of sodium during an assembly blockage

ABSTRACT

PhD thesis prepared at CEA Cadarache with a research scholarship
Laboratory of Instrumentation and Technological Tests
Department of Nuclear Technologie, Nuclear Energy Division
F-13108 Saint-Paul-lès-Durance, France



PhD thesis defended on October 1, 2013
before the PhD Commission in fulfillment of the
requirements for the degree of Doctor of Philosophy

Foreword

During my PhD many things happened in the world.

Aix-En-Provence, 2013
Matthias Vanderhaegen

Table of Contents

Foreword	i
Table of Contents	iii
List of Figures	vii
List of Tables	xi
List of Acronyms	xiii
List of Symbols	xvii
Résumé Français	xxv
1 Introduction	1-1
1.1 Introduction	1-1
1.2 Sodium-cooled Fast Reactor Accidents	1-2
1.3 A Boiling Detection System	1-3
1.4 This Study	1-4
References	1-4
2 Nuclear Energy	2-1
2.1 Introduction	2-1
2.2 Nuclear Energy	2-2
2.2.1 Nuclear Energy Worldwide	2-4
2.2.2 Nuclear Energy in France	2-5
2.2.3 Nuclear Energy in Belgium	2-8
2.2.4 Sustainable Nuclear Energy?	2-11
2.2.4.1 Nuclear Fuel and Waste	2-11
2.2.4.2 Environmental Impact	2-13
2.2.4.3 Final Remarks	2-15
2.3 The Future of Nuclear Energy	2-16
2.3.1 Generation IV	2-16
2.3.2 The future	2-20
References	2-21

3	Sodium Fast Reactors	3-1
3.1	Introduction	3-1
3.2	Fast Reactor Physics	3-2
3.2.1	Elastic Collisions and Energy Loss	3-2
3.2.2	Inelastic Collisions and Energy Loss	3-5
3.2.3	Fuel Design	3-5
3.2.4	Neutron Production	3-6
3.2.5	Transmutation and Breeding	3-9
3.2.6	Core Neutron Leakage and Reactor Dynamics	3-10
3.3	Historical Development and Operating Experience	3-11
3.3.1	Clementine	3-11
3.3.2	The Experimental Breeder Reactor	3-12
3.3.3	Fermi	3-13
3.3.4	SuperPhenix Blockage Incident	3-16
3.3.5	The Prototype Fast Reactor Oil Spill	3-16
3.4	The Reactor System	3-17
3.4.1	The Sodium Coolant	3-17
3.4.2	Structures, Systems and Components	3-19
3.4.2.1	The Primary Loop	3-20
3.4.2.2	The Reactor Core	3-24
3.4.2.3	The Fuel Assembly	3-25
3.4.2.4	The Fuel Pin	3-27
3.4.2.5	Defense-In-Depth	3-29
3.4.2.6	Examples	3-29
3.5	SFR and GEN-IV	3-29
3.6	Accident Analysis	3-30
3.6.1	Introduction	3-30
3.6.2	Core Disruptive Accidents	3-32
3.6.3	Design Basis Accidents	3-33
3.6.4	The Total Instantaneous Blockage Accident	3-35
3.7	Conclusion	3-37
	References	3-38
4	Liquid Metal Boiling	4-1
4.1	Introduction	4-1
4.2	Boiling Fundamentals	4-2
4.2.1	Nucleation	4-2
4.2.1.1	The Origin of Superheat	4-2
4.2.1.2	Homogeneous vs. Heterogeneous Nucleation	4-7
4.2.1.3	Nucleation of Liquid Sodium	4-9
4.2.2	Condensation-Evaporation Heat Transfer	4-17
4.3	Subassembly Boiling	4-21
4.3.1	Introduction	4-21
4.3.1.1	Departure of Nucleate Boiling Heat Flux	4-23
4.3.1.2	Minimum Film Boiling Temperature	4-23

4.3.1.3	Hydraulic Diameter	4-24
4.3.2	Wall Superheat	4-27
4.3.3	Subchannel Temperature Profile	4-30
4.3.3.1	Reduced Flow	4-37
4.3.3.2	Local Blockages	4-38
4.3.4	Boiling Regimes	4-40
4.3.4.1	Water boiling regimes	4-40
4.3.4.2	Sodium boiling regimes	4-41
4.3.5	Two-Phase Flow Patterns	4-43
4.3.5.1	Flow Pattern Classification in a Vertical Tube	4-43
4.3.5.2	Flow Pattern Classification in a Pin Bundle	4-45
4.3.5.3	Flow Patterns in a Small Vertical Tube	4-46
4.3.5.4	Identified Flow Patterns for Sodium Boiling	4-47
4.3.6	Boiling Zone	4-49
4.4	Boiling Crisis	4-50
4.5	Conclusion	4-51
	References	4-51
5	Acoustic Boiling Noise Analysis	5-1
5.1	Introduction	5-1
5.2	Hydrodynamic Noise	5-2
5.2.1	Introduction	5-2
5.2.2	Two-Phase flow equations	5-2
5.2.2.1	Vapor phase equation	5-2
5.2.2.2	Liquid phase equation	5-3
5.2.2.3	Liquid-Vapor interface	5-4
5.2.2.4	Solution	5-6
5.2.3	Simplified form	5-7
5.3	Bubble Dynamics	5-7
5.3.1	Analytical Development	5-7
5.3.1.1	Bubble Growth	5-7
5.3.1.2	Bubble Oscillation	5-7
5.3.1.3	Bubble Condensation	5-7
5.3.2	Condensation Dynamics	5-7
5.3.3	Condensation Models	5-7
5.4	Acoustic Development	5-7
5.5	Theory vs. Documented Experimental Data	5-7
5.6	Conclusion	5-7
	References	5-7
6	Acoustic Boiling Noise Experiments	6-1
6.1	Introduction	6-1
7	Acoustic Boiling Noise Detection	7-1
7.1	Introduction	7-1

8 Conclusion	8-1
A Conversion and Breeding: from fertile to fissile isotopes	A-1
A.1 Introduction	A-1
B Sodium Properties	B-1
B.1 Introduction	B-1
B.2 Thermodynamic Properties	B-2
B.2.1 Vapor Pressure	B-2
B.2.2 Heat Of Vaporization	B-3
B.2.3 Density	B-4
B.2.4 Heat Capacity	B-4
B.2.5 Surface Tension	B-6
B.2.6 Sensitivity	B-6
B.3 Transport Properties	B-7
B.3.1 Viscosity	B-7
B.3.2 Thermal Conductivity	B-8
B.3.3 Prandtl number	B-10
B.4 Non-Condensables	B-10
References	B-12

List of Figures

2.1	A photograph of the historical electricity production with EBR-I. . .	2-2
2.2	A futuristic 1960s newspaper advertisement, suggesting futuristic nuclear powered trains	2-3
2.3	The fractional contribution of different fuel sources to the total total worldwide primary energy supply in 2010.	2-5
2.4	The evolution of nuclear power reactors.	2-17
2.5	The six Generation-IV nuclear reactor systems.	2-20
3.1	Comparison between a thermal and a fast neutron spectrum. . . .	3-2
3.2	The Slowing down density.	3-3
3.3	The neutron absorption cross-section for several reactor materials. . . .	3-7
3.4	The coolant-to-fuel ratio for a triangular and rectangular lattice. . . .	3-8
3.5	The neutron production per absorption.	3-8
3.6	The fission-to-absorption ratio for several minor actinides.	3-9
3.7	The EBR-I Mark II core.	3-12
3.8	The EBR-I Mark III core.	3-13
3.9	The BR-5, Fermi and EBR-II fuel assembly design.	3-14
3.10	Comparison between an SFR and PWR containment building. . . .	3-20
3.11	Comparison between pool and loop type design.	3-21
3.12	A representation of the reactor vessel of Superphenix.	3-22
3.13	The Low void core concept of CEA	3-25
3.14	The typical fuel assembly structure.	3-26
3.15	The typical fuel pin structure.	3-28
3.16	A schematic representation of the Bethe-Tait accident.	3-33
3.17	A schematic evolution of the Total Instantaneous Blockage accidental scenario.	3-35
4.1	A Representation of the surface conditions for a plane and a spherical interface.	4-4
4.2	A comparison between the model and realistic situation at a boundary.	4-4
4.3	Typical conditions at a flat solid interface with an attached bubble. . . .	4-8
4.4	Typical wetting angle on a stainless steel surface for liquid sodium. . . .	4-10
4.5	The typical expulsion behavior in a superheated channel.	4-12

4.6	A conceptual visualization of the non-condensable behavior in a thermal hydraulic sodium loop.	4-14
4.7	The non-condensable bubble behavior in liquid sodium.	4-16
4.8	The non-condensable bubble behavior in liquid sodium.	4-17
4.9	The thermal diffusivity ratio of the vapor and liquid of saturated water and sodium	4-18
4.10	The experimental data of Misra and Bonilla for condensing sodium compared to the original Nusselt theory and the low Prandtl number corrections	4-20
4.11	The variation of the condensation coefficient.	4-21
4.12	The typical boiling heat transfer curve.	4-22
4.13	Representation of bubble nucleation at a surface.	4-27
4.14	The bubble's reference frame close to a wall boundary.	4-29
4.15	The temperature profile inside a subassembly during normal operating conditions.	4-31
4.16	The temperature profile at boiling inception for water and sodium.	4-38
4.17	Influences on the temperature profile at boiling inception for water and sodium.	4-39
4.18	The qualitative temperature and flow profile inside an SFR subassembly with an 21% corner blockage.	4-39
4.19	The typical convective water boiling pattern inside a uniformly heated tube.	4-40
4.20	The typical boiling zones in a 19-pin bundle with wire spacer.	4-42
4.21	The velocity profile.	4-42
4.22	Typical liquid/gas two-phase flow patterns in a vertical tube.	4-44
4.23	Typical liquid/gas two-phase flow map for a vertical tube.	4-45
4.24	Slug flow patterns in a vertical pin bundle.	4-46
4.25	Typical liquid/gas two-phase flow patterns in a small vertical tube.	4-47
4.26	A graphical representation of the flow patterns in a typical boiling SFR subchannel.	4-50
4.27	A graphical representation of dryout and Departure from Nucleate Boiling.	4-51
5.1	Graphical representation of the flow properties at a liquid/vapor interface.	5-5
B.1	The relative molar dimer Na_2 content in sodium vapor.	B-2
B.2	The vapor pressure at saturation for sodium and water, as a function of the absolute temperature.	B-3
B.3	The heat of vaporization of sodium and water	B-4
B.4	The density of saturated liquid sodium and water.	B-5
B.5	The density of saturated sodium vapor and steam.	B-5
B.6	The saturated heat capacity at constant pressure of water, liquid sodium and their vapor.	B-6

B.7	The surface tension between the saturated liquid and the saturated vapor of sodium and water.	B-7
B.8	The surface tension variation for an alcohol-water system and a cesium-sodium system.	B-8
B.9	The kinematic viscosity of saturated water and liquid sodium . . .	B-9
B.10	The kinematic viscosity of saturated steam and sodium vapor . . .	B-9
B.11	The saturated thermal conductivity of water, liquid sodium and their vapors	B-10
B.12	The saturated thermal diffusivity of water, liquid sodium and their vapors.	B-11
B.13	The Prandtl number at saturation conditions for liquid sodium and water.	B-11

List of Tables

3.1	The slowing down power for several materials	3-4
3.2	Typical impurity content of nuclear grade sodium	3-18
3.3	Sodium Properties at 450°C	3-19
3.4	Fast Reactor Data: Rapsodie, Phenix and SuperPhenix	3-30
3.5	Simplified thermal time constant analysis for a BWR and an SFR	3-32
4.1	The Superheat properties for liquid metals compared to water	4-7
4.2	Typical SFR subchannel data.	4-25
4.3	Typical SFR boiling inception wall superheat data.	4-29
B.1	Solubility of typical non-condensables in sodium and water.	B-12

List of Acronyms

A

ADS	Accelerator Driven System
ANL	Argonne National Laboratory
ANS	American Nuclear Society
ASTRID	Advanced Sodium Technological Reactor for Industrial Demonstration

B

BR	Belgian Reactor
BWR	Boiling Water Reactor

C

CEA	Commissariat à l'énergie atomique et aux énergies alternatives (before 2010: Commissariat à l'énergie atomique – The Atomic Energy Commission)
CHF	Critical Heat Flux

E

EBR-I	Experimental Breeder Reactor – I
EdF	Électricité de France – France's electrical utility
ENDFB	United States Evaluated Nuclear Data File

G

GEN	Generation
GFR	Gas-cooled Fast Reactor
GIF	The Generation-IV International Forum

I

IAEA	International Atomic Energy Agency
ICRP	International Commission on Radiological Protection
IEA	International Energy Agency
IHX	Intermediate Heat Exchanger

L

LFR	Lead-cooled Fast Reactor
LMFBR	Liquid Metal Fast Breeder Reactor
LWR	Light Water Reactor

M

MFBT	Minimum Film Boiling Temperature
MOX	Mixed Plutonium-Uranium Oxides
MSR	Molten Salt Reactor
MYRRHA	Multi-purpose hYbrid Research Reactor for High-tech Applications

P

PWR	Pressurized Water Reactor
-----	---------------------------

S

SCK-CEN	Studiecentrum Kernenergie - Centre d'Etude de l'énergie Nucléaire (Belgian Nuclear Research Centre)
SCWR	Supercritical-Water-Cooled Reactor
SFR	Sodium-cooled Fast Reactor

T

TIB	Total Instantaneous Blockage
TOP	Transient OverPower
TUC	Transient UnderCooling

U

UNGG	Réacteur à Uranium Naturel-Graphite-Gaz (Natural Uranium-Graphite-Gaz reactor)
UNSCAER	United Nations Scientific Committee on the Effects of Atomic Radiation
USNRC	United States Nuclear Regulatory Commission

V

VHTR	Very-High-Temperature Reactor
------	-------------------------------

List of Symbols

A - α

α	Scattering energy loss fraction
α_l	The liquid thermal diffusivity
α_v	The vapor thermal diffusivity
A	Atomic mass number
A	Surface Area
A_C	Coolant Flow Area
A_F	Fuel Surface Area
Ag	Silver
Al	Aluminum

B - β

β	Evaporation / Accommodation / Condensation constant
Ba	Barium
Be	Beryllium
Bi	Bismuth

C

c_g	Dissolved gas concentration
c_p	Heat capacity
C	Carbon
Ca	Calcium
Cd	Cadmium
Co	Cobalt
C_o	The confinement number

Cr	Chromium
Cs	Cesium
Cu	Copper

D - δ

Δp	Pressure losses
$\Delta p_{buoyancy}$	Buoyancy driving pressure
ΔL	Height difference
$\Delta \rho$	Density difference
$\Delta \rho_{lv}$	Liquid-vapor density difference
ΔT	Temperature difference
D	Diameter
D_h	Hydraulic diameter
D_p	Pin outer diameter
D_v	Vapor bubble diameter
D	Diffusion coefficient

E - η

η	Neutron production factor
E	Energy

F

f	Utilization factor
Fe	Iron

G

g	Acceleration due to gravity: 9.81 m/s^2
g_l	Liquid specific Gibbs free energy
g_v	Vapor specific Gibbs free energy
G	Gibbs free energy
\dot{G}	Mass flux

H

h_{lv}	Latent heat of vaporization
$H_2O_{(g)}$	Steam
$H_2O_{(l)}$	Water
H	Hydrogen
H	Enthalpy
H	Height
He	Helium
Hg	Mercury

K

k_{∞}	Infinite multiplication factor
k_H	Henry constant]
K	Potassium

L

log	Natural logarithm
-----	-------------------

M - μ

μ	Dynamic viscosity
m	Mass
m_l	Liquid mass
m_v	Vapor mass
M_i	Molar mass of substance i
Mg	Magnesium
Mn	Manganese
Mo	Molybdenum

N - ν

ν	Kinematic Viscosity
n	Neutron density
N	Atomic, molecular or particle density
N	Nitrogen
Na	Sodium
Ni	Nickel
NaK	Sodium-Potassium Eutectic Alloy

P - ϕ

ϕ	Neutron flux
p	Pressure
p_l	Liquid pressure
p_g	Gas pressure
p_{sat}	Saturation pressure
p_v	Vapor pressure
P	Pitch
P	Perimeter
P_w	Wetted perimeter
Pr	Prandtl number
Pb	Lead
Pu	Plutonium

Q

q''_{av}	The average pin heat flux
q''_{max}	The maximal pin heat flux
q''_w	Wall heat flux

R - ρ

ρ	Reactivity
ρ_l	Liquid density
ρ_v	Vapor density
r	radial distance in a cylindrical or spherical coordinate system
R	Radius
\mathcal{R}	Specific gas constant

S - σ

σ	Surface tension
σ_i	Microscopic cross-section for the nuclear reaction of type i
Σ_i	Macroscopic cross-section for the nuclear reaction of type i
s_i	Specific entropy
S	Entropy
Sn	Tin
Sr	Strontium

T - τ - θ

t	Time
τ_w	Wall shear stress
T	Temperature
T_l	Liquid temperature
T_{sat}	Saturation temperature
T_v	Vapor temperature
T_w	Wall temperature
Th	Thorium
Ti	Titanium
θ	Wetting angle

U

U	Uranium
---	---------

V

v	Specific volume
v_l	Liquid specific volume
v_g	Vapor specific volume
V	Vanadium

X - ξ

ξ Average lethargy gain
 x_g Dissolved gas mole fraction

Z

Zn Zinc
Zr Zirconium

Résumé Français –French Summary–

nederlandse samenvatting

1

Introduction

*“Je fais toujours bien le premier vers, mais j’ai peine à faire les autres” –
Marquis de Mascarille, **Les Précieuses ridicules***

*Molière
1659*

1.1 Introduction

In France, the research on the disposal and management of nuclear waste is regulated by a law of 1991, the Law of Bataille. In 2006, before the 15 year revision period was over, this law was extended to include the study of a reactor from a new generation that could be used to control and destroy some of the radioactive waste. Following this law, the French research agency CEA (French Atomic Energy Commission) studied fast reactor systems that are particularly efficient for the incineration of nuclear waste. After 4 years of research, it was decided to continue with the sodium-cooled fast reactor (SFR) systems and to construct such a reactor on the horizon of 2020 according to the law of 2006. This is the ASTRID – Advanced Sodium Technological Reactor for Industrial Demonstration – project.

In the framework of this renewed interest in SFRs, the ASTRID reactor project, emphasis is put on the Generation - 4 (GEN-IV) objectives because the new prototype should come from a new reactor generation. Among the objectives for this new generation of reactors we can find some notes on risk and safety [3]:

- The GEN-IV reactors will have to excel in safety and reliability.
- The likelihood and the extent of possible core damage will have to be very low.

Although SFRs have a good safety record, the GEN-IV recommendations on SFRs state that additional research is necessary. This research needs to ensure that the events considered for the licensing approach can be handled without external consequences. The latter becomes even more important, taking into account the recent Fukushima accident.

1.2 Sodium-cooled Fast Reactor Accidents

These recommendations are not that surprising because SFRs can be considered to be neutronically and thermodynamically unstable¹ (i.e. the reactor isn't in its optimal, most reactive, configuration from neutronic point of view). The liquid sodium coolant is highly reactive; the reactor core lacks many of the inherent forgiving feedback mechanisms of a typical Light Water Reactor. This latter explains the consideration of so-called core disruptive accidents, even in the early stages of fast reactor development (the 1950s). Waltar and Reynolds [4] classify two types of events that are related to a cooling-heating imbalance: the Transient Over Power (TOP) and Transient UnderCooling (TUC) events.

Whereas TOP events are more or less related to sudden changes in power or the level of the neutron density in the core that may lead to core damage e.g. the extraction of a control rod, core compaction. . . TUC events are more or less related to any event that reduces the cooling of the nuclear fuel e.g. loss of pumping power, subassembly blockages. . . These events can result in a temperature increase and even sodium boiling. Coolant boiling in an SFR can increase the reactivity of the core and rapidly cause fuel damage. Once fuel damage occurs, dispersion of the nuclear fuel and a propagation of the accident are possible. In the best case this leads to a severe contamination of the coolant, or in the worst case this leads to a core disruptive accident that endangers the integrity of the containment system.

These are of course very pessimistic considerations and there is sufficient margin in place to prevent such events. Additionally, technical solutions have been conceived to further reduce the probability and consequences of such events. Therefore the previous accident paths are very unlikely. Nonetheless, in view of the GEN-IV requirements and the recent Fukushima accident, it would be helpful if sodium boiling could be detected and the reactor could be scrammed before any

¹This is a famous expression used by Prof. F. Vanmassenhove – a former highly respected nuclear engineering professor at the University of Ghent, Belgium.

significant damage occurs. If not, a sodium boiling detection system could also be helpful to follow the core's state during accidents. Especially in France, a boiling detection system could be useful to strengthen the safety approach for the hypothetical total instantaneous blockage incident of a subassembly (i.e. a total and sudden stop of coolant flow). At the moment this incident is very difficult to detect with the current reactor surveillance instrumentation. As boiling occurs during this hypothetical incident, accident detection could be facilitated.

1.3 A Boiling Detection System

The idea of a boiling detection system for sodium fast reactors, far from new, has been reconsidered after the successes in the development of a boiling deterioration detection system by Courtois et al. [6, 7]. Such a detection is important for the cooling system of a fusion reactor's plasma facing components that have to withstand very high heat fluxes. To evacuate the heat load of these components, the latent heat and turbulence of a high pressure water flow is used. And although this turbulent subcooled boiling flow is an excellent coolant, a sudden rise in the heat flux may lead to a boiling regime with degraded heat transfer and a degradation of the component. This is known as burn-out caused by passing the maximal heat flux, the critical heat flux (CHF), for subcooled boiling. Courtois et al. refer to a publication of Celata et al. [8] who propose an acoustic method to detect this change in the subcooled boiling regime. Celata et al. explain that the principle is based on the process of nucleation, growth and collapse of vapor bubbles. They all generate acoustic signals, hence a change in the acoustic noise might form a precursor of a degradation of the heat removal as this degradation is a cause of change in the processes that create the acoustic signals.

Courtois et al. conducted several tests with different designs of the cooling circuit of the plasma facing components under extreme heat loads delivered by an electron beam. Among these designs were a hypervapotron (a cooling element with very small cavities machined on a surface to enhance the boiling heat exchange rate) and a cooling tube with a swirl tape to increase turbulent mixing. From these tests, it was possible to deduce acoustic precursors that indicate an approach or passage of the CHF threshold heat flux. These acoustic precursors could also be related to possible sources such as bubble implosion leading to shock waves, bubble detachment disturbances, turbulent flow noise, acoustic resonance phenomena. . .

1.4 This Study

Unlike Courtois et al. we do not have the resources to boil sodium in a geometry that is representable for a reactor and its subassembly. We do have publication and some old technical notes at our disposal but our information ends there. All the registered boiling noise measurement in reactors and sodium boiling loops haven't been preserved and most of the former experts have long been inactive in the field. Hence we commit ourself to study the inverse problem as that posed to Courtois and his team: the boiling phenomena of sodium in a reactor environment are studied and the possible acoustic signals in the reactor are deduced.

This is a very complicated study that covers boiling thermal hydraulics, bubble dynamics and fundamental acoustics. These fields are used to create an idea of the boiling noise spectra and amplitude. The following chapters will deal with the state of nuclear energy in the world that will clearly explain how we came to this situation. Afterwards the sodium-cooled nuclear reactors are described to have an idea of the geometry and the conditions for which the liquid metal boiling will be studied in a following chapter. With this information a theoretical study is undertaken to identify the main contributors to the boiling noise. From these theoretical results some experimental possibilities are explored. Then some additional information and conclusions about a boiling detection system are formulated.

References

- [1] *Loi 91-1381 du 30 décembre 1991 relative aux recherches sur la gestion des déchets radioactifs*. <http://www.Legifrance.gouv.fr>.
- [2] *Loi 2006-739 du 28 juin 2006 de programme relative à la gestion durable des matières et déchets radioactifs*. <http://www.Legifrance.gouv.fr>.
- [3] U.S. DOE Nuclear Energy Research Advisory Committee and the Generation IV International Forum. *A Technology Roadmap for Generation IV Nuclear Energy Systems*, December 2002.
- [4] Alan Edward Waltar and Albert Barnett Reynolds. *Fast Breeder Reactors*. Pergamon Press, 1981.
- [5] A.M. Tenter. *Severe Accident Approach – Final Report: Evolution of Design Measures for Severe Accident Prevention and Consequence Mitigation*. Technical Report ANL-GENIV-128, Nuclear Engineering Division, Argonne National Laboratory, March 2010.
- [6] X. Courtois, A. Durocher, F. Escourbiac, J. Schlosser, R. Mitteau, M. Merola, and R. Tivey. *In-situ monitoring of actively cooled plasma facing components*

-
- using acoustic and thermal methods*. Physica Scripta, 2007(T128):189–194, 2007.
- [7] X. Courtois, A. Durocher, B. Riccardi, M. Boinet, and M. Merola. *Acoustic Precursors of critical heat flux on actively cooled fusion reactor components*. In The 12th International Topical Meeting on Nuclear Reactor Thermal Hydraulics (NURETH-12), Pittsburgh, Pennsylvania, USA, September 30 - October 4 2007.
- [8] G.P. Celata, G. Dell’Orco, and G.P. Gaspari. *Detection of subcooled boiling heat transfer regimes up to critical heat flux by accelerometric equipment*. Fusion Engineering and Design, 28:44–52, 1995.

2

Nuclear Energy

“Too cheap to meter”

1954

Lewis L. Strauss

Chairman of the US Atomic Energy Commission

2.1 Introduction

Ever since the discovery of nuclear fission by Lise Meitner, Otto Hahn and Fritz Strassmann in 1939, together with the associated energy release predicted by the mass defect, interest in its applications flourished due to the foreseeable potential. Taking the historical background of these events, efforts were mainly focussed to weapon applications. Nonetheless, it still had to be proven that a chain reaction could be sustained. The 2nd of december 1942, in Chicago and during World War II, the first man-made¹ critical mock-up was assembled by Enrico Fermi and his team. Since that point, nuclear technology evolved incredibly with the development of numerous applications: nuclear weapons, nuclear energy, radiation treatments, ...

¹It would be wrong to state that it was the first critical mock-up on earth, because the ore from the Oklo-mine shows clear signs of a sustained fission reaction. For information, this was a French discovery



Figure 2.1: A photograph of the historical electricity production with EBR-I.

2.2 Nuclear Energy

Although all of the previous mentioned applications are scientifically interesting, only some of them are so from an ethical point of view. Nuclear energy is certainly interesting in both the ethical and scientific aspect: It is an energy source that has low or nearly no carbon emissions, an important aspect considering that global warming is most likely accelerated by man-made carbon emissions. Although this latter argument is generally recognized, there are some sources that claim nuclear energy to be emitting an amount of carbon that is equal or higher than for a gas-fired plant of the same power rating [1]. However, there is quite some criticism on this study's methodology and results.

As for the scientific aspect of nuclear power, it is a challenging technology that requires a vast knowledge of different fields of physics and their interactions. It was even during World War II that physicists studied these interactions and they started thinking about unlocking the energy of the atom. But it was not before the Experimental Breeder Reactor (EBR-I), built in the United States of America, that the first nuclear generated electricity was produced. Although the electricity output merely made a few light bulbs glow (figure 2.1), it was a great achievement considering that it was only 1951. But more important, EBR-I was a reactor operating on a fast neutron spectrum. This is contrary to the current reactor fleet that operates on a thermal spectrum. That type of reactor was mainly developed from experience gained from nuclear submarines. Nevertheless, the future of nuclear power looked bright during those initial years. Nuclear power was welcomed by some euphoria that sometimes was associated with a science fiction type of view on the future, which was typical for that time. The latter is demonstrated by a 1960s newspaper advertisement given in figure 2.2. Other interesting examples

are the Disney movie “Our Friend the Atom”, Strauss’s quote “Too cheap to meter”. There were even plans for a nuclear powered aircraft (demonstrated by the Aircraft Reactor Experiment). However, it never came that far that nuclear energy was applied at the large scale that was initially foreseen. . .

July 20, 1960

THE SATURDAY EVENING POST

Will atomic energy power tomorrow's railroads?



Some day you may see a train like this—powered by the energy locked up in the atom.

Possibly the locomotive will have its own nuclear reactor. Or perhaps it will use electricity generated at atomic power stations. But this much is certain. Of all forms of land transportation, railroads offer the greatest opportunities for the efficient use of nuclear energy.

Railroads are constantly exploring exciting possibilities like this. Such progressive thinking is important to all of us—for we're going to need railroads more than ever in the boom years ahead.

Clearly, it's in the national interest to give railroads equal opportunity and treatment with other forms of transportation. America's railroads—the lifeline of the nation—are the main line to your future.

**ASSOCIATION OF
AMERICAN RAILROADS**
WASHINGTON 6, D. C.

Figure 2.2: A futuristic 1960s newspaper advertisement, suggesting nuclear powered trains

This is hardly the place to discuss in-depth the reason of the incomplete development of nuclear power's potential, there are just too many details involved that are far beyond the scope of this chapter. However a small historical summary is given on the basis of Bodansky's work [2]. It can't be denied that a large part of the current fleet of reactors evolved from the United States Navy research on nuclear propulsion. This is the Pressurized Water Reactor (PWR) design and the Shippingport reactor was the first to be adapted for civil electricity production. There is however another Light Water Reactor (LWR) design that is commonly operated, the Boiling Water Reactor (BWR) design. This latter design has been developed by General Electric from early research at Argonne National Laboratory (ANL). Most of these developments were done in the 1950s with only occasional reactor orders and new-builds. But after 1965 there was a significant increase in the number of reactor orders and those reactors were actually deployed. However, the increased construction costs and increased opposition led to a reduced deployment of nuclear power. The 1970s oil crisis resulted furthermore in a reduced energy – and thus electricity – demand on the American markets, resulting even in reactor cancellations during the construction phase. The Three Mile Island accident, better known as the TMI accident, resulted in a practical halt in reactor orders and dissuaded further investments in nuclear power.

It is interesting to note how the oil crisis halted reactor construction in the United States, whereas in certain European countries (e.g. Belgium and France) this stimulated the evolution to nuclear electricity generation. In what follows, a presentation of the world wide nuclear energy contribution will be given, after which a more detailed description on the French and Belgian situation is presented.

2.2.1 Nuclear Energy Worldwide

At the time of writing, there are 666 known operational reactors of which 437 power reactors that have an installed capacity of 371 762 MWe [3, 4]. The total nuclear production of these reactors equals about 13% of the worldwide electrical energy production. Although this amount is far from negligible, a total of 2 756 TWh , electrical energy (and thus also nuclear power) contributes only for a small fraction to the total worldwide primary energy supply as can be seen in figure 2.3 that represents the figures of 2010 [5]. Nonetheless it would be wrong to conclude from this graph that nuclear energy is easily replaceable. In certain countries the nuclear contribution to energy generation is very high. The two countries that deduce most of their electricity from nuclear sources are Belgium and France, with a respective nuclear share of 54% and 77.7% in 2011. Another interesting figure is the number of power reactors that are currently under construction: a total of 64. Hence nuclear power is still developing. However, most of these construction

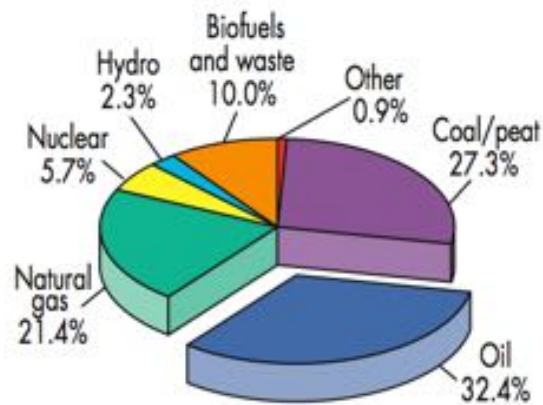


Figure 2.3: The fractional contribution of different fuel sources to the total total worldwide primary energy supply in 2010, according to the International Energy Agency (IEA) [5].

sites are located outside of Europe and the USA. In Europe and the USA, power upratings tend to increase the nuclear energy production.

Every country has a different history and it would be beyond the scope of this work to analyze every nuclear country in the world. However, it is interesting to look to Belgium and France: both have embarked on the nuclear route early after World War II but with a different strategy. Because the path to this thesis started in Belgium and ended in France, it is also appropriate to analyze these two countries with a special attention on fast reactors.

2.2.2 Nuclear Energy in France

It is indisputable that France has made an astonishing contribution to nuclear science and technology. At the end of the 19th century it were French scientist such as Becquerel, Pierre Curie and Marie Curie who made important contributions to the understanding of radioactivity; and indirectly they opened the pathway to nuclear energy generation. The new insights in radioactivity triggered research on the different types of radiation emitted and research on the nucleus of an atom. This research led to the hypothesis of a neutral particle in the nucleus of the atom, the neutron. A hypothesis later verified by Chadwick, just before the French scientists Frédéric and Irène Joliot-Curie were able to generate neutrons. However, they were able to induce artificial radioactivity in their experiments. This started a new wave of research on artificial radioactivity, especially with neutrons as they interact easily with matter. This led to the discovery of fission and the realization

that a huge amount of energy is released with the process. Frédéric Joliot repeated those experiments and found that neutrons are created during fission. Hence all elements were in place for the development of a chain reaction that releases of energy. Although French scientists, under whom Joliot, realised this; they were unable to act on it because of the war in Europe.

Joliot easily convinced De Gaulle² that nuclear development would help the post-war recovery and further industrialization of France. The CEA, The French Atomic Energy Commission, was thus created in 1945. Not much later, in 1948, French scientists attained criticality in the heavy water-moderated, natural uranium fueled, Zoë pile. The CEA continued with the fundamental research on the heavy water technology and constructed a prototype power plant later on. However, the first French nuclear electricity generation was done with a graphite moderated reactor.

Although it is undeniable that the heavy water technology has many drawbacks as Reuss mentions [6], Hecht [7] mentions that there might have been political and military grounds that inspired a shift to graphite technology. However, more officially, France chose the plutonium fuel cycle as it had an interest to go for fast reactor technology and it wanted to evade the difficult and expensive development of fuel enrichment. This led to the construction of the graphite-moderated, gas-cooled, natural uranium-fueled (UNGG) reactors at the Marcoule site. This type of reactor, especially with its design that allows short-term continuous irradiation and on-line refueling, is particularly suited for weapons grade Pu-production. It is at this point that the French electric utility, EdF, came into contact with nuclear power. Representatives of EdF suggested to equip these reactors with a turbine to generate electricity. As the Marcoule reactors (G1-G2-G3) main mission was the production of high quality Pu instead of electricity, EdF started the development of dedicated power reactors. Aided by the CEA, they developed a more efficient version of these reactors and constructed six of them.

In 1958 France decided to go ahead with a nuclear explosive development program. However by then everything was in place: theoretical studies on nuclear explosives, plutonium producing reactors at Marcoule, plutonium extraction, . . . EdF was even forced to put their UNGG reactors at disposition for the production of additional high quality Pu. It is thus not surprising that, a few years later in 1960, France was able to conduct explosive tests. Hence early military goals might have influenced the choice of a plutonium fuel cycle. However it would be wrong to condemn France of only having a military interest in a Pu-fuel cycle as the CEA started to study MOX – $(U, Pu)O_2$ – fueled sodium-cooled fast reactors (SFRs)

²General De Gaulle is a French wartime general that supervised the reinstallation of the French government after the French liberation. Later he entered into politics and became President of France

in the late 50s. This led to the construction of the Rapsodie reactor, with the aid of Euratom, at the Cadarache site. The success of the British and the American with this type of reactors in the mid-60s, encouraged the CEA to go ahead with the development of this reactor type. EdF also showed interest in the development of this reactor type and both collaborated on the Phenix project. Although EdF and CEA collaborated on the fast reactor project, the mid-60s is also known for the struggle between CEA and EdF on the thermal reactor future.

Whilst CEA continued to advocate the UNGG reactors, EdF started showing interest in the deployment of LWRs under a license of the American company Westinghouse. These reactors, according to the report of Horowitz³ and Cabanius⁴, had a much better production cost per *kWh*. Even though Horowitz argued that this result was obtained by assuming that sufficient fuel enrichment capacity was available in France, as otherwise France would become dependent on foreign nations⁵, this discussion was won in favor of the deployment of PWRs. To make matters worse, only days before the official decision to go ahead with PWR technology in late 1969, a loading error resulted in a cooling channel blockage that led to a core melt at the newest UNGG plant. The planned UNGG reactors at Fessenheim were thus replaced by the first large scale (900 *MWe*) PWRs in France, after earlier testing of a lower power design at Chooz (together with Belgium) and after its participation in a similar design in Tihange (Belgium). The 1970s oil crisis urged the French government to become more independent of foreign fuel sources and they ordered the construction of several more plants. Up to 58 Westinghouse PWRs were so constructed, with the aid of CEA, before 1982. Starting from 1981 Framatome, now AREVA NP, was able to renegotiate the Westinghouse license. This resulted in greater independence and led to the development of an entire French product: the N4 1450 *MWe* mastodons. Later on this product evolved, under European collaboration, to the well known EPR design which is now under construction in Finland, France and China.

However, before the first 900 *MWe* PWR was connected to the grid, a more evolutionary design started commercial operation in 1974: the Phenix reactor. This reactor's satisfactory operation led to the design and construction of a large scale prototype, SuperPhenix. Due to the general European interest in fast breeder technology, this project included German, Italian, Belgian and Dutch financing. And although the early years of operation, starting from 1986, can frankly be described as catastrophic, stable operation was attained afterwards. However, the world had changed importantly in 1997. Nuclear energy had, also in France, to cope with

³CEA

⁴EdF

⁵This was recognized and the military gaseous diffusion enrichment technology developed by CEA was used to develop the Eurodif enrichment complex at Tricastin

protests. The uranium scarcity, that threatened the PWRs and which hastened the development of breeder reactors and a Pu-fuel cycle, never became reality. Hence the political unacceptable, expensive (in comparison with PWRs) and unnecessary SuperPhenix reactor fell prey to an election promise and was abandoned. The end of the many successes of the French breeder project was in sight. And whilst the studies on SFRs continued until 1993 due to the European Fast Reactor project, the demise of the technology led to reduced needs and thus manpower.

With the law of 2006 [9] to develop a new generation reactor for the control and destruction of nuclear waste, interest in SFR technology flourished again and this led eventually to the ASTRID SFR reactor project. And although France has an enormous amount of information on SFR technology, it is obvious that important expertise has been lost. To make matters worse, crucial data has been destroyed. Luckily Phenix could operate until 2010 [3], delivering valuable information and expertise for the ASTRID project. And even in its current shutdown state, it remains a valuable tool. Nonetheless it is clear, even to the PhD student, that a lot of expertise has to be rebuilt.

2.2.3 Nuclear Energy in Belgium

Congo, a former colony of Belgium, contains rich uranium ores in the region of Katanga. And after the accidental discovery of these uranium-rich layers in 1913, a uranium/radium industry developed in the north of Belgium around 1921. This gave Belgium a monopoly position on the international radium market. Before the discovery of nuclear fission, uranium was mainly an ore for the extraction of radium. Afterwards, during World War II, uranium also became an important product. This led to the Belgian-Allied contract for the delivery of uranium. This uranium was used for the Manhattan project and for the construction of the first nuclear bombs. The contract also guaranteed the exclusive rights over the uranium stock for the USA and the United Kingdom over a period of 10 years, with “reasonable” uses for the Belgium industry and research. In return, Belgium was given access to nuclear expertise. Nonetheless, the USA’s nuclear knowledge exchange policy changed. The contract details were revised on demand of the Belgian government. As such, Belgium acquired a large budget that was to be used for nuclear research and the predecessor of the SCK-CEN was born in 1952. One of its main goals was the development of peaceful nuclear applications. But even with the knowledge exchange policy changed, Belgium still had a privileged position in obtaining nuclear knowledge and resources.

The money earned from the post-war compromise was first invested in the construction of a research reactor, proposed by researcher of the Oak Ridge National

Laboratories after lectures given there to Belgian scientific staff. This graphite moderated reactor “Belgian Reactor-1” resembles quite well the reactors G1-G2 and G3 reactors, although with a smaller thermal power output, no turbines and an obviously different goal. Nonetheless, Belgium was also interested in nuclear electricity generation. Already in 1954, plans were made to generate the electricity for the World Expo in 1958 by means of nuclear technology next to the royal palace. This plan was a little too ambitious⁶ and thus cancelled. But the minds were set, Belgium was going to become a nuclear-industrialized country. As such, a material testing reactor was planned and research on the use of Pu in civil reactors started. The new reactor, BR-2, was to be built in Mol, not so far from the BR-1 reactor. Again this reactor was developed with international, especially US, support. In the meantime, the plans for a nuclear power plant were preserved but only saw realization with a few years of delay and far away from the royal palace. It was thus as such that Mol housed in 1962 three reactors: BR-1, BR-2 and BR-3.

BR-3, the first Belgian nuclear power plant was a Westinghouse PWR design and the first of its kind in Europe. This reactor allowed the Belgian electricity utilities to get well acquainted with nuclear electricity production. But because pretty little Belgium was too little developed to install the bigger, newer and more economical PWR units; it collaborated with France to install a new PWR unit. This unit was installed at Chooz, under the international European Euratom treaty and started operating in 1967. Although the initial high cost of nuclear power and the uncertain cost improvement, the Belgian utilities were confident that it would contribute significantly on the long term. Therefore they ordered 2 medium sized reactors that were adapted to the Belgian grid: the Doel 1 & 2 units. However, in collaboration with the French utility a large 900 *MWe* unit was ordered that was more compatible with the French grid: Tihange 1. From this discussion it is clear that Belgium adopted directly the technology from Westinghouse. While it is true that these reactors need enriched fuel, the favorable American-Belgian relations made it initially easier to obtain such fuel. The 70s oil crisis, the foreseen growth in electricity demand and the fact that Belgium doesn't have energy resources and only a small potential for hydraulic power, all led to the decision to install 4 more large units of nuclear power: Doel 3 & 4 and Tihange 2 & 3. With the construction of internationally available enrichment capacity, Belgium gained further independence for its energy resources. The installation of a ninth unit at the Doel site was also foreseen and at the site preparatory works were undertaken in the end of 1985. However, with the Chernobyl accident in mind the Belgian government didn't find it suitable to continue with nuclear deployment. Afterwards, in 2003, it was decided to phase-out nuclear power as part of a political agreement to form a government.

⁶BR-1 only reached first criticality in 1956

But whilst Belgium utilities entered into the commercial exploitation of nuclear power, the accomplishments of the SCK-CEN shouldn't be forgotten nor minimized. It had at its disposal two very powerful research reactors to obtain these: a material testing reactor and a PWR prototype. And as such Belgium, also interested in the Pu-fuel cycle and fast breeders, participated with CEA under a joint USA - Euratom agreement to the development of MOX fuel for fast reactors. Satisfied with the results of the initial research, it was decided to load Pu-fuel in BR-3 for an irradiation cycle. The first PWR in Europe thus produced the first "Pu-containing" electricity, demonstrating the feasibility of Pu-fuels in thermal reactors and as thus contributing to the peaceful application of Pu. But Belgium, as a small country, had to look for partners to develop fast reactors. As such Belgium collaborated with Germany, France and the Netherlands. In this context the Belgian experience with Pu-fuel was important and this expertise was used to develop and fabricate the MOX fuel for the German breeder SNR-300. In the context of these programs the BR-2 reactor proved to be very useful. But with the general decline of interest for fast reactor programs and the declining market of the Belgian nuclear industry, the Belgian nuclear industry crumbled and over time the companies that were created around the Belgian expertise were closed or purchased. Hence also in Belgium a lot of knowledge and expertise has disappeared.

Starting from 1995, Ion Beam Applications and SCK-CEN studied a small accelerator driven system (ADS) for dedicated radioisotope production. The main interest was to create an efficient source for medical radioisotopes that are currently produced in the BR-2 reactor. In the period of 1997, when this project ended, an upgrade towards a multi-purpose irradiation facility was performed. This was the birth of the MYRRHA project, which is still continuing today. It is the aim that MYRRHA replaces the aging BR-2 reactor and contributes to the destruction of nuclear waste. As such Belgium research tries to contribute, as before, to a first of a kind as no ADS systems have been constructed yet. And again the main goal is to contribute to the peaceful application of nuclear technology. It must be noted that the MYRRHA-project isn't violating the phase-out agreement as the phase-out only applies to nuclear electricity generation [14]. As for the electricity generation, only seven reactors are operational at the moment. The BR-3, again taking the role as a first, is under decommissioning. The other reactors are scheduled for an operational lifetime of 40 years, in line with the phase-out law [14]. There are however governmental discussions to prolong the operation of some of the more modern units, again in line with the phase-out law, to guarantee the security of electricity supply. But the recent discovery of material defects in the Doel 3 and Tihange 2 reactor vessels makes these prolongations uncertain and at a moment their restart was even highly questioned.

2.2.4 Sustainable Nuclear Energy?

The French and Belgian projects for the future are only two examples, and each one claims to contribute to the sustainable development of nuclear power. Nonetheless, we should pose the question if nuclear power can be sustainable. But how can sustainability be defined? A very popular definition is proposed by the Brundtland report:

...Sustainable development is a development that meets the needs of the present generation without compromising the ability of future generations to meet their own needs...

However we can ask ourselves whether or not this definition is appropriate as we do not know the needs of the future generation for example. Erik Laes however gives, in his PhD thesis, a clear and well argued definition of sustainability that basically boils down to (for the purpose of simplicity):

Sustainable development should improve the quality of life and focus on the equality between, and in a generation on a global scale, whilst taking care of the environment. In the same time, sustainable development urges to be cautious about uncertainties that may result in greater harm.

It is clear that the two definitions given here are particularly useful to give a technical argumentation on the sustainability of nuclear power and we'll proceed as such without going into the details of economics etc.

The increased availability of more energy (and power)⁷ evidently results in a better quality of life. The increased availability, and thus reduced price, of low-carbon nuclear (electrical) power can also contribute to the preservation of the environment by facilitating more energy-intensive processes that are more environment-friendly. We can imagine e.g. electrical heating that reduces residential carbon emissions, hydrogen fueled (combustion) engines that also reduce the carbon emissions whilst eliminating the particulate matter emissions of typical diesel fuels, gaseous effluent scrubbing by an electrical plasma discharge (thus energy consuming), plasma sterilization of medical equipment, . . . and of course many more. Although questions might arise concerning the sustainability of abundantly available power, a more important question for our argumentation stems from the equality between generations and the possible harm caused by nuclear power.

2.2.4.1 Nuclear Fuel and Waste

At the moment a lot of countries operate on a once-through fuel cycle. That is to say: the uranium ore is mined, concentrated and converted to yellow-cake (U_3O_8).

⁷It is interesting to note that there is a scarcity of power, as energy is abundant on earth.

Afterwards this form of uranium is converted to uranium hexafluoride: UF_6 . This is a compound that is particularly useful for the enrichment process as it is gaseous above $56^\circ C$ whilst it is a solid below, facilitating its transport. The enrichment process, independent of the enrichment technology⁸, results in a product stream that has a ^{235}U -mass content that is higher than 0.711 wt% and a stream of material that has a ^{235}U content smaller than this natural fraction.

The enriched mixture is then converted to UO_2 for further fuel fabrication, whilst the “depleted” uranium is a waste stream that is stored for possible future use. Due to the fact that the current use of depleted uranium (for radiation shielding, depleted uranium ammunition, high density ballast, . . .) is rather limited compared to the production, a great amount of this depleted uranium “waste” tends to accumulate. As for the enriched UO_2 mixture, this is irradiated in a reactor and generates energy.

After irradiation, these elements are stored for a cool-down period before further treatment is possible. In a once-through fuel cycle, it can be decided to reprocess the waste and to dispose the vitrified high level waste mixture (containing both fission products and actinides) in geological layers. Another option in a once-through fuel cycle is the direct geological disposal of the cooled irradiated elements.

It is clear that mining of great quantities of uranium doesn't really leave much resources for the future generations. However we can argue that there are gigantic reserves of exploitable uranium. They simply differ in quality and it is thus more difficult to extract significant quantities of uranium from certain sources.

But even with sufficient resources, the enrichment process results in significant quantities of depleted uranium. And whilst gigantic amounts of energy can be extracted from the enriched uranium (exceeding 70 GWd/tU according to the AREVA EPR factsheet), the long-term storage of the fission products and the long-living actinides introduces uncertainties for the disposal of this waste. This becomes especially important if a once-through fuel cycle is maintained for several decades or centuries. Furthermore, it is a waste that the energy-rich plutonium generated during the fuel irradiation isn't used (for details on the Pu-generation, see appendix A). However there is an alternative: the closed fuel cycle.

In a closed fuel cycle, the plutonium present in the spent-fuel is recycled. Thus re-

⁸This is due to the conservation of mass, the enrichment technology will determine the energy requirements and the amount however.

ducing the needs for additional fissile uranium. Furthermore, in advanced fuel cycles with breeder reactors, more fissile material can be created than is consumed⁹. In such advanced fuel cycles, the need for new uranium is even further reduced and the stored depleted uranium can be used. It is this closed U-Pu fuel cycle that is often considered as being sustainable because there is conservation of the natural resources, leaving sufficient for the future generations. It is also this fuel cycle that France has been pursuing from the start of its nuclear program. However, even in this fuel cycle, fission products have to be extracted and stored. Furthermore the continued recycling of plutonium in thermal reactors has as a disadvantage that ^{241}Pu is created. This particular plutonium isotope decays to ^{241}Am . The presence of this isotope under irradiation can further lead to ^{242}Cm . These minor actinides have a relatively long decay chain, thus prolonging the storage considerations of the nuclear waste. On top of that they generate a lot of heat and are quite radiotoxic due to their α -decay, complicating storage. Hence it is foreseen to recycle these minor actinides, as these too contain valuable energy, in fast reactor systems. The latter is especially important due to the fact that fast reactor systems are particularly efficient in fissioning these minor actinides. Another option is to switch to the closed Th-U cycle, severely reducing the production of these minor actinides. Furthermore thorium is much more abundant than uranium and as such the Th-U fuel cycle is perceived as being even more sustainable.

Unfortunately, the fission of heavy isotopes leads inevitably to fission products. At the moment these, often radioactive and by some perceived as valuable, fission products do not have any economical value. Thus even in a closed fuel cycle, waste is generated. The treatment for this waste remains the same as in a once-through fuel cycle: immobilization by vitrification and disposal in geological layers. We must however add that this waste decays; after some time the fission products decay chain ends in a stable nuclide.

2.2.4.2 Environmental Impact

Due to the fact that fission products are created in any fuel cycle, there is always the need for disposal of these products. The option that has been retained is deep storage in stable geological layers. It is the aim that these layers retain the fission products long after the engineered barriers fail, because in the long term their integrity can not be guaranteed and these barriers will surely fail. The geological layers considered are at the moment not regarded as a possible resource for mining, nor is it likely that they will be in the future. The host layers do also not communicate with the aquifer, further isolating the highly radioactive fission products and preventing dispersal. We try thus to maintain the equality between

⁹This isn't a violation of the first law of thermodynamics. For more information see appendix A.

generations. The long term assessment of this geological containment show that the dose results at the surface due to the repository degradation are well within acceptable limits. And although the concentrated fission products are stored in geological layers, some fission products and minor actinides escape in the discharge waste streams of the extraction processes. These nuclides are thus dispersed and normally highly diluted. Thus, given the fact that radioactivity exists in nature, a highly diluted additional activity does normally not significantly increase the doses received.

For the waste, the environmental impact boils down to the impact of a dose that is higher than the dose because of natural exposure. Hence from a technical point of view, and in view of our definitions of sustainability, the harm done by small additional doses of radiation should be evaluated on a global scale and for several generations. This is a problem treated by the United Nations Scientific Committee on the Effects of Atomic Radiation (UNSCEAR) that evaluates and reports continuously on the effects of radiation. Other notable documents come from the International Commission on Radiological Protection (ICRP). They all adopt a no threshold model, that is to say, a model that predicts an excess health risk by an additional radiation dose received. There exists some arguments that this model might be too conservative. And despite using this conservative model, it is the author's personal belief that improvement of the quality of life outweighs the small health risks.

As for the impact of mining the ore that is necessary in all fuel cycles, it should be admitted that any mining process has a relatively important impact on the environment. This is even worsened by the fact that the uranium ore is more radioactive than the actual uranium. Hence fuel cycles that reduce the need of additional ore can only increase the sustainability of nuclear energy.

Last but not least, we have to add a few words about the potential of a nuclear accident. We can not deny that serious accidents happened in the past. Without going into detail here, Mosey [17] mentions a few: Some of these accidents resulted in valuable lessons and didn't have serious health consequences e.g. The Fermi-I accident¹⁰, but there are also some accidents that are plain inexcusable e.g. the Tokaimura accident¹¹ that resulted in the death of two people. However, the current regulations demand an increasing level of safety that should severely reduce the health risk, or in the words of the American USNRC regulation [18]:

The risk to an average individual in the vicinity of a nuclear power

¹⁰See chapter 3, section 3.3 for more

¹¹The processing of highly enriched uranium in an aqueous solution resulted in a foreseeable criticality accident

plant of prompt fatalities that might result from reactor accidents should not exceed one-tenth of one percent (0.1%) of the sum of prompt fatality risks resulting from other accident to which members of the population are generally exposed

and

The risk to the population in the area of nuclear power plant of cancer fatalities that might result from nuclear power plant operation should not exceed one-tenth of one percent (0.1%) of the sum of cancer fatality risks resulting from all other causes

Hence the probability of such an accident should, due to the industries current safety standards be approximately zero. Nonetheless, a real zero-risk doesn't exist¹² as the Fukushima accident demonstrated. But it might be too early to deduce any conclusion for the long term environmental effects of this accident. Thus we have to look at the impact of another accident with significant off-site consequences: the Chernobyl accident. The effects of that accident were of course far from negligible. In this case it is true that usable land is contaminated and it isn't possible to develop it before the dose rate has been sufficiently reduced. This possibly severe impact isn't compatible with the definitions of sustainability. It is therefore that most sustainable nuclear initiatives, notably "The Sustainable Nuclear Energy Technology Platform" and GEN-IV, insist on optimizing and maintaining the highest level of safety.

2.2.4.3 Final Remarks

It is true that the discussion here has been given in a qualitative and brief fashion, which was also the aim for the sake of simplicity. And it is true that some topics such as proliferation were not mentioned, again to limit this chapter to an introductory level. However, some of the claims given here can be found in the excellent works of Cohen [19], Bodansky [2] or Lamarsh [20], where they are put into context with a quantitative analysis. Some other remarks or claims are personal views and are the result of a critical analysis of several works and lectures. From all the previous, and from a personal perspective, it can be concluded that the nuclear industry isn't completely sustainable at the moment. Nonetheless, again from a personal interpretation, it is possible for the nuclear industry to evolve to a sustainable industry that supplies low-carbon power for a global well-being whilst seeking the best conservation of the environment over many generations.

¹²This is true for any technology!

2.3 The Future of Nuclear Energy

Having acknowledged that nuclear energy can be sustainable, we can look to the possible future of nuclear energy. And before the Fukushima accident, a hot topic during this study, this section would have been totally different. It would have contained many phrases relating to the so-called “Nuclear Renaissance” and the bright future that lied ahead of us. But the unfortunate series of events after the Tōhoku earthquake in Japan, changed a lot of minds: Germany, as a drastic example, immediately decided to shut down their similar reactors and abandoned the idea of changing their phase-out law. Similar ideas about a possible revival followed in certain European countries. But before looking to the perspectives nuclear power has to offer, let’s further investigate the nuclear power plants of the future: The GEN-IV sustainable reactors.

2.3.1 Generation IV

In early 2000, the US Department of Energy convened representatives from Argentina, Brazil, Canada, France, Japan, South Korea, South Africa and the UK to discuss an international collaboration for the realization of the next generation nuclear systems: the GEN-IV reactors. This led to the Generation IV International Forum, the GIF, in mid 2001. The name Generation IV has been chosen as the participants pointed out that reactors evolved from early prototypes to more advanced systems in approximate discrete steps:

1. The early prototypes in the 50s and 60s that were already mentioned in this chapter: e.g. the Shippingport PWR in the USA, the UNGGs and Phenix in France,...
2. The current operating plants that were constructed from the 60s - 70s and whose design is based on the design of the Westinghouse PWRs, the General Electrics BWR or the Canadian CANDU design.
3. The advanced reactors that have been designed in the 90s and that are under construction or have been constructed mostly in Asia. Some of these designs have never been constructed due to a reduced interest.

For the last Generation of reactors, GEN-III, it is recognized that some more technical evolutions have been introduced and advances are still made. These evolutionary designs are thus termed GEN-III⁺ reactors. These evolutionary designs, which include the EPR, are currently deployed. Some of the advanced reactors that have been designed in the 90s are already outdated relative to these evolutionary reactors and they will most likely never be constructed. It is foreseen that, starting from 2030, the newest generation of nuclear reactors will see the deployment phase. All the evolutions can be found graphically in figure 2.4, which is the latest

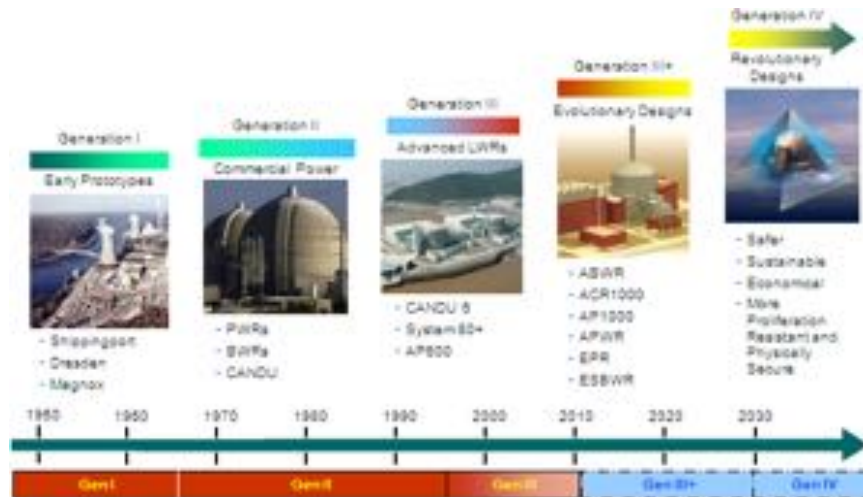


Figure 2.4: The evolution of nuclear power reactors, according to the Generation International Forum [22].

graph published on the GEN-IV website [21, 22].

The goals for the new generation of reactors are quite challenging, the GIF looks for reactor systems that are:

- **Sustainable** GEN-IV systems will provide sustainable energy generation that meets clean air objectives and promotes long-term availability of systems and effective fuel utilization for worldwide energy production. They will minimize and manage their nuclear waste and notably reduce the long-term stewardship burden, thereby improving protection for the public health and the environment
- **Economic** GEN-IV systems will have a clear life-cycle cost advantage over other energy sources. They will have a level of financial risk comparable to other energy projects.
- **Safe and Reliable** GEN-IV systems operations will excel in safety and reliability. They will have a very low likelihood and degree of reactor core damage. They will eliminate the need for offsite emergency response.
- **Proliferation Resistant and Physically Protected** GEN-IV systems will increase the assurance that they are a very unattractive and the least desirable route for diversion or theft of weapons-usable materials, and provide increased physical protection against acts of terrorism.

These goals should help the transition to sustainable nuclear energy generation as described in the previous sections. However, taking into account the trend to evolve to an open deregulated energy market, they should also ensure the deployment of reactors in deregulated energy markets. The safety demands for GEN-IV systems are of course in place to protect the public and to contribute to the sustainability, but they are also there to protect the financial investments. The reliability demand, different from safety and an often used synonym for the availability, reduces the financial risk for investors as they reduce the investment risk and aid to guarantee a good return of investment. The last, but not the least, is to cope with the rising terrorist threat in the world today. But, equally important, is that this latter enables the worldwide distribution of GEN-IV reactor systems without the proliferation of nuclear weapons or the spread of nuclear weapons material.

With these goals in hand, many reactor concepts were screened. Some of these reactor concepts dated back to the early days of nuclear technology development, and there are many concepts that can potentially respond to the GEN-IV criteria. Nonetheless, only six commercially promising systems were retained that have some development overlap and accommodate some national interests. These six systems, with some of their notable advantages and disadvantages, are:

- *The Gas-Cooled Fast Reactor – GFR*
The GFR system is a helium-cooled reactor with a fast neutron spectrum. As such, the GFR systems can work with a relatively high output temperature. This makes them excellent to produce electricity, but also to deliver process heat. The fast spectrum of the GFR also enables actinide management in a closed fuel-cycle. Gas-cooling, and the high temperatures due to inefficient heat transfer, necessitates however very resistant materials.
- *The Lead-Cooled Fast Reactor – LFR*
The LFR system can just like the GFR profit from a fast neutron spectrum, and due to the high boiling point of lead (about 1750 °C) also deliver both process heat and electricity. Differently from GFRs, the excellent capabilities of the lead or lead-alloy coolant reduces material requirements. The LFR also benefits from a possible small size and long refueling intervals. Nonetheless, lead and its alloys have possible radiotoxicity consequences and corrosion issues.
- *The Sodium-Cooled Fast Reactor – SFR*
The SFR is, similar to the LFR, a liquid metal cooled reactor that uses the excellent coolant properties of liquid sodium. Due to the lower boiling point of sodium (about 900 °C), these reactors main purpose is electricity generation and actinide management. Similar to LFRs, they benefit from inherent safety features. And sodium benefits greatly from the large experience

gained over the years. Nonetheless, sodium is a chemically reactive coolant and it has possible dangerous accidental feedbacks.

- *The Supercritical-Water-Cooled Reactor System – SCWR*

The SCWR is actually an evolution of the BWR, but with a possible fast, epithermal or thermal spectrum. The SCWR can as thus participate in actinide management. However, its main design parameter – the use of a supercritical coolant – stems from certain disadvantages from phase change systems and the high thermal efficiencies that can be reached with a supercritical working fluid. The use of high pressures and temperature under irradiation, demands additional material studies. On top of that, the effect of a depressurization and the properties of supercritical water call for further research.

- *The Very-High-Temperature Reactor System – VHTR*

The VHTR is a gas-cooled thermal reactor system that is in principal an evolution of the UNGG. Nonetheless, it features high outlet temperatures and passive safety features. And although the design is both suited for electricity production and process heat, its safety features benefit the latter. But to maintain these safety features, the VHTR's core contains a lot of graphite. This reactor is thus always thermal and thus not suited for actinide management. Additionally, the peculiar pebble fuel design isn't convenient in a closed fuel cycle. And as for the GFR, the VHTR requests additional research on very resistant materials

- *The Molten Salt Reactor System – MSR*

The MSR is an old reactor concept that has been revived with the GEN-IV program. Unlike the previous designs that all contain nuclear fuel in a solid form, the MSR has a molten fuel. The intense mixing of the fuel and the coolant evades the consideration of fuel-coolant heat transfer efficiency. The molten mixture also has a very high boiling point and thus enables high outlet temperatures for process heat or efficient electricity generation. And as the mixture contains both coolant, fuel and fission products; it is possible to do direct chemistry on site for fission product extraction or easy minor actinide management without specific solid fuel production. Nonetheless, the fission products result in a corrosive mixture. The molten state also leads to a high mobility of fission products and tritium.

A graphical representation of these systems is given in figure 2.5. Although the GIF puts a lot of attention on the reactors themselves, the GEN-IV technological roadmap also stipulates that there is a need to collaborate and to direct research efforts on the technologies related to the fuel cycle.

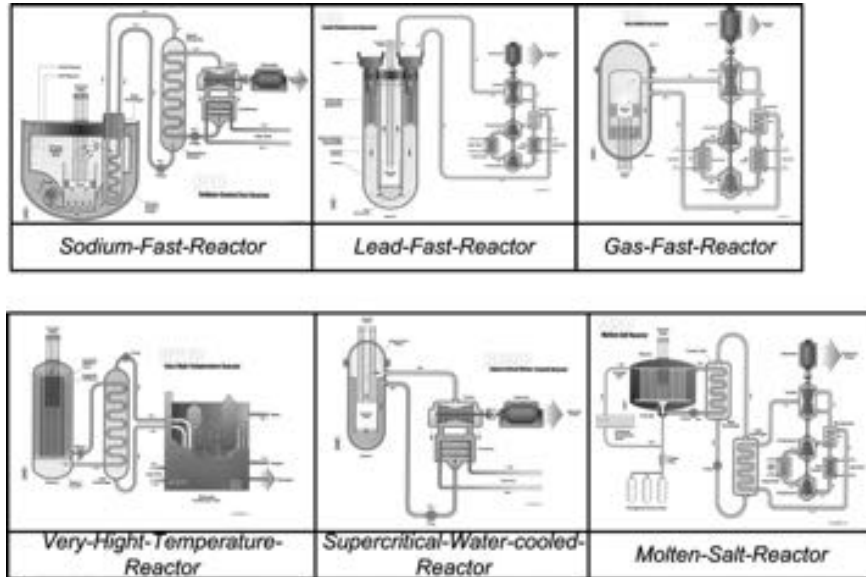


Figure 2.5: The six Generation-IV nuclear reactor systems as illustrated by the Generation-IV International Forum [22].

2.3.2 The future

But even with the attractive perspectives that GEN-IV reactors have to offer, it is unlikely that they'll be deployed significantly on the short and mid-term. One of the reasons is the Fukushima accident that chilled the excitement of the nuclear renaissance. Most research will most likely shift towards nuclear safety and the life extensions of the aging nuclear power plants. Especially the case of the reactor pressure vessel faults in Belgium seems to underline the need to study more in detail the safe life extension. Another reason is the economical crisis that makes the costly investments in nuclear development unlikely, but also unnecessary according to market theories, because there is a reduced power demand. The shift to an open energy market in Europe thus partially inhibits new deployment. Even worse, with the current energy and emission policies, the IEA predicts an increase in the use of coal [5] and mentions in the world energy outlook summary of 2012 that this is the "golden age of gas".

Even though these predictions are rather grim, the growing need for energy and the obvious consequences of polluting energy sources are clear signs that a shift in energy production is necessary. Although the possibilities of the classical renewable energy sources such as solar, wind, . . . shouldn't be underestimated or neglected;

nuclear energy will remain necessary. And it is the author's opinion that it is only a matter of time before nuclear replacement capacity will be considered to replace the aging nuclear plants in the mid- to long term.

References

- [1] J.W. Storm van Leeuwen and P. Smith. *Nuclear Power: the Energy Balance*, August 2005.
- [2] David Bodansky. *Nuclear Energy: Principles, Practices, and Prospects*. Springer, 2004.
- [3] *The Power Reactor Information System*. <http://www.iaea.org/pris/>.
- [4] *The IAEA Research Reactor Database*. <http://nucleus.iaea.org/rrdb/>.
- [5] *Key World Energy Statistics*. International Energy Agency, 2012.
- [6] Paul Reuss. *L'épopée de l'énergie nucléaire: Une histoire scientifique et industrielle*. EDP Sciences – INSTN - Génie Atomique, 2007.
- [7] Gabrielle Hecht. *The Radiance of France: Nuclear Power and National Identity after World War II*. The M.I.T Press, 1998.
- [8] W. Marth. *European Fast Reactor – The Story of the European Fast Reactor Cooperation*. Technical Report KfK 5225, Kernforschungszentrum Karlsruhe, 1993.
- [9] *Loi 2006-739 du 28 juin 2006 de programme relative à la gestion durable des matières et déchets radioactifs*. <http://www.Legifrance.gouv.fr>.
- [10] F. Gauché. *French SFR program and the ASTRID prototype*. In *Fast Reactors and Related Fuel Cycles: Challenges and Opportunities*, Kyoto, Japan, December 7 2009.
- [11] F. Gauché. *French SFR R&D program and Design Activities for SFR Prototype ASTRID*. *Energy Procedia*, 7:314–316, 2011.
- [12] P. Govaerts, A. Jaumotte, and J. Vanderlinden, editors. *Un demi-siècle de nucléaire en Belgique: Témoignages*. Belgian Nuclear Society –Presses Interuniversitaires Européennes, 1994.
- [13] E. Laes, L. Chayapathi, G. Meskens, and G. Eggermont. *Kernenergie en Maatschappelijk Debat*. Technical report, viWTA, November 2004.

- [14] *Belgian Phase-out Law (Wet houdende de geleidelijke uitsap uit kernenergie voor industriële elektriciteitsproducte – Loi sur la sortie progressive de l'énergie nucléaire à des fins de production industrielle d'électricité)*. Belgian Official Journal (Belgisch Staatsblad – Moniteur Belge) p.9879, February 2003.
- [15] M. Vanderhaegen. *CFD modeling of the primary cooling system of MYRRHA*. Master's thesis, Belgian Nuclear Engineering Network – Ghent University, 2008-2009.
- [16] E. Laes. *NUCLEAR ENERGY AND SUSTAINABLE DEVELOPMENT: Theoretical reflections and critical-interpretative research towards a better support for decision making*. PhD thesis, Katholieke Universiteit Leuven, Faculteit Toegepaste Wetenschappen, Departement Werktuigkunde: Toegepaste Mechanica en Energieconversie, 2006.
- [17] David Mosey. *Reactor Accidents: Institutional failure in the nuclear industry*. Number ISBN 1-903-07745-1. Nuclear Engineering International, 2nd edition, 2006.
- [18] M. Drouin. *Feasibility Study for a Risk-Informed and Performance-Based Regulatory Structure for Future Plant Licensing*. Technical Report NUREG-1860, United States Nuclear Regulatory Commission, December 2007.
- [19] John R. Lamarsh and Anthony J. Baratta. *Introduction to Nuclear Engineering*. Number ISBN 0-201-82498-1. Prentice Hall, 3rd edition, 2001.
- [20] Bernard L. Cohen. *The Nuclear Energy Option: An Alternative for the 90s*. Plenum Press, 1990.
- [21] U.S. DOE Nuclear Energy Research Advisory Committee and the Generation IV International Forum. *A Technology Roadmap for Generation IV Nuclear Energy Systems*, December 2002.
- [22] *Generation IV International Forum*. <http://www.gen-4.org>.

3

Sodium Fast Reactors

*“In a cavern, in a canyon, excavating for a mine
Dwelt a miner forty niner, and his daughter Clementine
Oh my darling, oh my darling, oh my darling, Clementine!
Thou are lost and gone forever. Dreadful sorry, Clementine.”*

*Oh My Darling Clementine
19th century American balad*

3.1 Introduction

The Sodium Fast Reactor is a reactor that operates on a fast neutron spectrum and that is cooled by liquid sodium. It is often referred to as the Liquid Metal Fast Breeder Reactor (LMFBR) in earlier works because in the past and especially in the West, liquid metal-cooled reactors almost exclusively used sodium as a coolant. In this chapter we'll focus in particular on the reactor design and design basis accidents. As such we'll take a short look at the development history of these reactors and some lessons learned, discuss the choice of coolant, the peculiarity of the neutronics and the implications for the fuel and coolant system design. This latter is quite important as the fuel assembly design is important for the liquid metal boiling analysis.

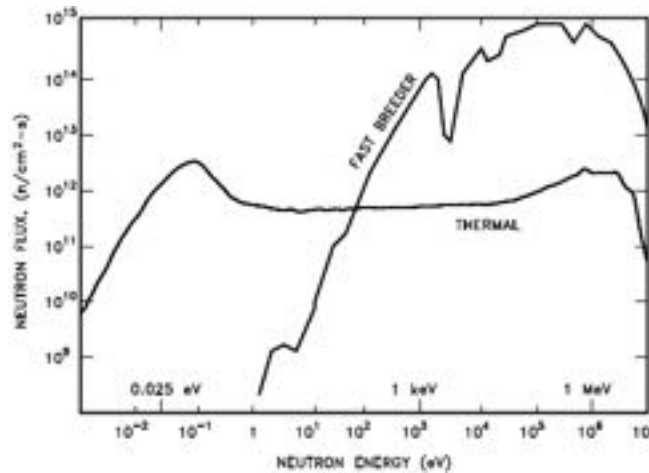


Figure 3.1: A comparison between a thermal neutron spectrum, originating from a moderated fission spectrum, and a fast spectrum originating from an unmoderated fission spectrum typical for a fast reactor [2].

3.2 Fast Reactor Physics

Because the fast neutron spectrum of an SFR is one of its main and most important characteristics for the design of these reactors, and given that it is important for the understanding of fast reactor accidents, we start our discussion with an introductory section on fast reactor physics. As for any reactor, reactor physics deals with the generation, absorption, transport and deceleration of neutrons. In a fast reactor, the high energy neutrons that originate from fission are only slightly or not moderated at all to give a neutron spectrum as given in figure 3.1. Or that is at least the aim.

3.2.1 Elastic Collisions and Energy Loss

In an elastic collision between a neutron and a reactor material, with a collision that is assumed to be isotropic (i.e. in the collision, each scattering angle has equal probability), we can deduce that the neutrons are scattered with equal probability between the initial energy E_0 and a fraction of that initial energy α : $[\alpha E_0, E_0]$. The fraction α can be related to the atomic mass A by:

$$\alpha = \left(\frac{A - 1}{A + 1} \right)^2 \quad (3.1)$$

The energy loss deduced for successive collisions, is however impractical to calculate and it is easier to define an average energy loss by a collision. Even better is

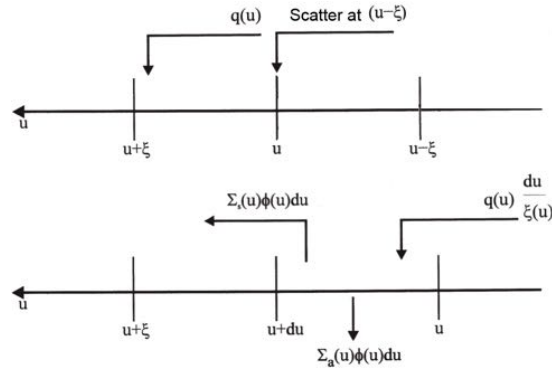


Figure 3.2: The neutrons that scatter at a lethargy $u - \xi$, gain a lethargy ξ and are scattered to a lethargy u . This means that all neutrons that are slowing down at u come from an interval between u and $u - \xi$. Thus the $q(u)$ neutrons slowing down at u can go from u to $u + \xi$. If we divide these neutrons evenly over the interval ξ and look at an infinitely small interval du they are either scattered or absorbed in that interval.

the use of the average loss in logarithmic inverse energy, this logarithmic inverse energy is termed the lethargy. This lethargy increases with a collision and without going into the details, the average lethargy gain ξ for a nuclide with an atomic mass A is approximately given by:

$$\xi \approx \frac{2}{A + \frac{2}{3}} \tag{3.2}$$

With this average energy loss we can define the slowing-down density q , that is the number of neutrons that interact in a unit volume in a unit time and gain a higher lethargy. Because we treat every neutron as average, the average neutron that interacts at a certain lethargy will either be absorbed or scattered to a lethargy ξ higher. Hence in an interval of width ξ , q neutrons arrive. The slowing down density thus is given by (see figure 3.2):

$$q(E) = \xi \cdot (\sigma_a(E) + \sigma_s(E)) \cdot N \cdot \phi(E) \tag{3.3}$$

In this equation N is the material particle density and $\phi(E)$ is the neutron flux. This neutron flux is the product of the neutron density $n(E)$ and the neutron velocity. Together with a microscopic cross-section or the probability $\sigma(E)$ for a nuclear reaction with the neutron (e.g. absorption or scattering) and the particle density, this gives the interaction rate for these nuclear reactions per unit time and per volume at the energy E .

Equation 3.3, although quite simplistic and not containing the global change of

Material	Density (g/cm^{-3})	Molar mass A (g)	ξ	σ_s ($10^{-24} cm^{-2}$)	$\xi\sigma_s N$ (cm^{-1})
$H_2O_{(l)}$	1.00	18.02	0.948	103	3.2631
$H_2O_{(g)}$	0.03	18.02	0.948	103	0.1044
He	0.005	4.00	0.425	0.8	0.0003
Be	1.85	9.01	0.209	7	0.1809
C	1.60	12.01	0.158	4.8	0.0608
Na	0.97	22.99	0.085	4	0.0086
K	0.87	39.10	0.050	1.5	0.0010
Fe	7.86	55.85	0.035	11	0.0331
Zr	6.40	91.22	0.022	8	0.0074
Hg	13.55	200.61	0.001	20	0.0008
Pb	11.35	207.21	0.001	11	0.0004
Bi	9.75	209.00	0.001	9	0.0003

Table 3.1: The slowing down power for several materials. These values were deduced from thermal (low-energy) nuclear properties and are given as an illustrative example to deduce acceptable fast reactor materials. The density of steam and helium are given at 62 bar (900 psi), at saturation or at 600°C.

the slowing down density with lethargy due to absorption, can nonetheless give a good insight on the materials that are compatible with a fast reactor. We recall that in a fast reactor, fast neutrons are desired and we don't want to have much neutrons slowing down. Thus we want a small slowing down density. We can achieve this by:

1. Choosing materials that have a high atomic mass A . This reduces the average lethargy gain in interactions and thus the amount of neutrons that are scattered to higher lethargy (lower energy).
2. Choosing materials that have a low particle density N . This reduces the amount of interactions that can lead to a lower energy.
3. Choosing materials that have a low scattering interaction rate, thus with low $\sigma_s(E)$. This also reduces the amount of interactions.
4. The neutron flux $\phi(E)$ isn't variable as the fission power is proportional to this flux, the fissile material density (enrichment) and the microscopic cross-section for fission.

Thus the product $\xi N \sigma_s(E)$, the slowing down power, should be optimized to be as low as possible. Table 3.1 gives the slowing down power for a small amount of materials. In this table, one can directly identify materials that aren't acceptable in very high quantities in fast reactors, for which water is the most notable. Steam

however, used as a coolant for example, directly becomes somewhat more acceptable due to its lower density. Nonetheless, the presence of hydrogen will result in a fast spectrum with a higher thermal contribution because a single neutron-hydrogen interaction can result in very low energies. Other acceptable materials include lead, bismuth, mercury, sodium, potassium, zirconium or helium.

3.2.2 Inelastic Collisions and Energy Loss

Although there is the tendency to go for materials with a higher atomic mass, these materials however do have a disadvantage with regard to neutron energy loss. Materials with a higher atomic mass, in general, have excited states at energies that are lower compared to lower atomic mass materials (see figure 3.3). This excited states allow for inelastic energy losses. Thus for those elements, there is a spectrum softening component related to the inelastic scattering. This inelastic scattering is also more probable for those materials, i.e. they have a higher microscopic cross-section. We don't go into details of inelastic scattering as it is out of the scope of this chapter.

3.2.3 Fuel Design

The suitable fast reactor materials all have to be put together with the fuel to obtain a coolable geometry. Besides the peculiar fuel pebbles or the fuel plates in certain reactor designs, the uranium and plutonium fuel is often contained inside fuel pins. The best fuel pin arrangement can be deduced from the infinite multiplication factor k_{∞} , which determines the neutron multiplication from one generation to another in an infinite reactor system:

$$k_{\infty} = \frac{n_{t_{i+1}}}{n_{t_i}} \quad (3.4)$$

This infinite multiplication factor can, in a simplified fast reactor approach¹, be determined by the product of the effective neutron utilization f and the neutron production η . The neutron production η gives the amount of neutrons created by fission, per absorption in the fuel. This latter is a function of the chemical state of the fuel (i.e. metallic, oxide, carbide, nitride, ...) and the amount of fissile material present in the fuel and specific fissile isotopes (^{233}U , ^{235}U or ^{239}Pu , ...). In general, we can say that η increases with the fuel enrichment, i.e. the amount of fissile material present in the fuel.

¹The infinite multiplication factor for a fast reactor is deduced from the four-factor formula for a thermal reactor. The four-factor formula is however a two-group formula and in our fast reactor approach we only assume one group. Hence the resonance escape probability, which is the transport from the fast to the thermal group doesn't intervene. The same goes for the fast-fission factor, which gives the surplus of neutrons generated by fission in the fast group before transport to the thermal group.

The effective utilization factor can be represented by the ratio of absorption in the fuel, per absorption in the entire reactor system. The result for an infinite reactor and a fuel lattice cell are equivalent, thus assuming homogeneity along the axis of the fuel we can write:

$$f = \frac{N_{fuel}\sigma_{a,fuel}A_{fuel}}{N_{fuel}\sigma_{a,fuel}A_{fuel} + N_{coolant}\sigma_{a,coolant}A_{coolant} + N_{ssc}\sigma_{a,ssc}A_{ssc}} \quad (3.5)$$

As the fuel cost increases with fuel enrichment, the effective utilization factor should be maximal. This is done by choosing materials with a relatively low microscopic cross-section for neutron absorption. However, fast spectrum parasitic absorption is relatively low in comparison with the absorption of typical fuel constituents such as ^{235}U or ^{239}Pu as can be seen in figure 3.3. When investigating figure 3.3, it should be kept in mind that the neutron flux is high in the 0.1 to 1 MeV region and the cross-sections in equation 3.5 are suitably averaged by the neutron flux. In thermal reactors it is usually the cross-section at 0.025 eV that is important. This is one of the reasons that in fast reactors stainless steel is preferred over the low-absorption expensive zirconium alloys commonly used in thermal reactors. This also explains the inexistent core poisoning transients compared to thermal reactors, allowing a fast reactor to load-follow easier than typical thermal reactors.

Because neutron moderation isn't important in fast reactors, and even unwanted, it is possible to optimize the effective utilization factor as a function of fuel-to-coolant ratio. This latter can not be varied in a thermal reactor as the coolant (or moderator) unit cell fraction is imposed by neutron moderation considerations. It is easily shown that the most optimal fuel-to-coolant ratio is obtained for a triangular lattice (see figure 3.4). Hence most fast reactor's fuel pins and subassemblies are arranged in such a geometry. However, this tight geometry results in an extreme volumetric power density for a reduced coolant area and as such exotic coolants with very good heat removal capacities, such as liquid metals, are considered.

3.2.4 Neutron Production

It is clear that fast reactors present certain advantages towards thermal reactors, nonetheless, these advantages are compensated by cooling difficulties. ~~Nonetheless, it remained worthwhile to continue with the development of fast reactors.~~ This is related to the neutron production per neutron absorption in the fuel η . The neutron production by fission, per neutron absorption by a fissile nuclide is given in figure 3.5 as a function of energy.

To maintain the fission reaction, we need at least one neutron per fission, some margin to compensate for parasitic absorption by the coolant and structural mate-

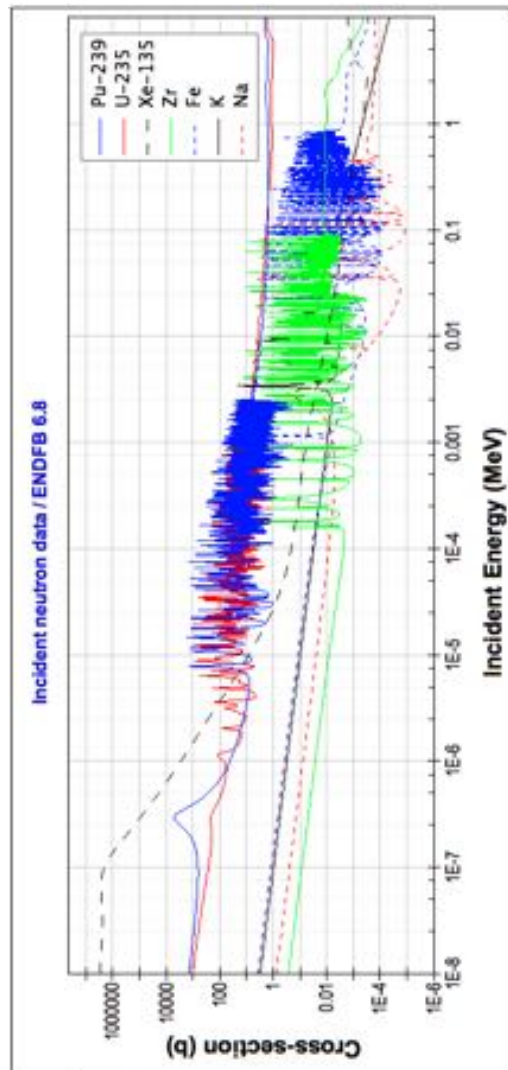


Figure 3.3: The neutron absorption cross-section in units of barn (10^{-24} cm^2) as a function of the incident neutron energy for several structural materials (Fe, Zr), coolants (K, Na), fuel constituents (^{235}U , ^{239}Pu) and the notable thermal neutron poison ^{135}Xe from the ENDFB 6.8 database. Notice the resonance behavior in the cross-section that indicate excited states of the $A + 1$ nuclide.

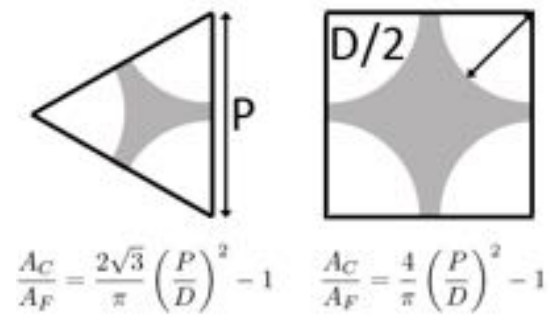


Figure 3.4: The coolant-to-fuel ratio A_C/A_F for a triangular and rectangular lattice as a function of the pin pitch P and the pin diameter D .

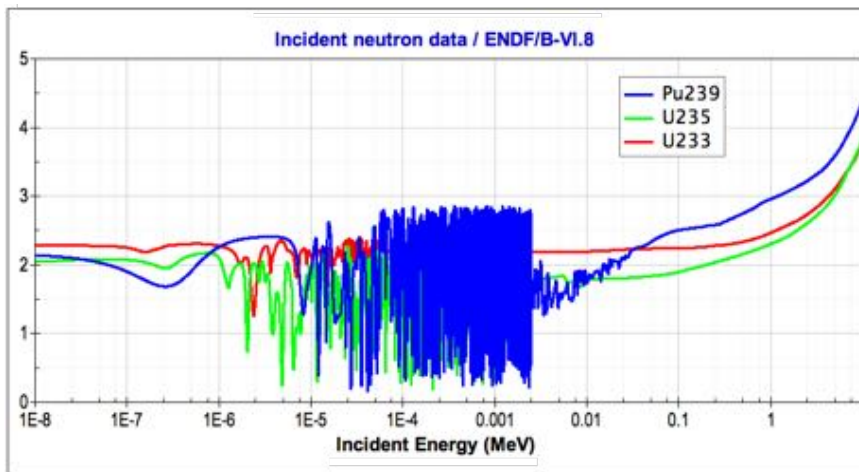


Figure 3.5: The number of neutrons generated by fission, per neutron absorption by ^{233}U , ^{235}U and ^{239}Pu as a function of energy. From the ENDFB 6.8 database

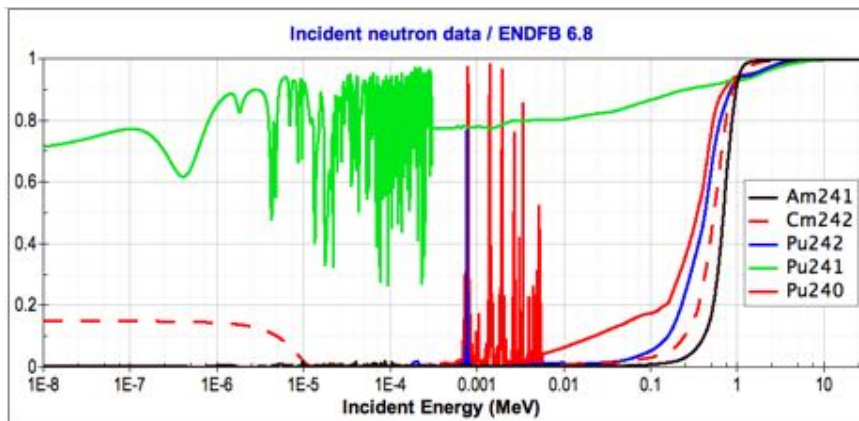


Figure 3.6: The fission-to-absorption ratio for several minor actinides as a function of the incident neutron energy from the ENDFB 6.8 database.

rial and some margin to compensate neutrons that are transported out of the core. However this leaves us still with a neutron surplus. These neutrons can be used for several purposes, most notably for the transmutation or breeding. This explanation and graph 3.5 also shows the interest in the plutonium fuel cycle, as the absorption of a neutron in ^{239}Pu generates more neutrons than any other fuel cycle.

3.2.5 Transmutation and Breeding

Breeding is the process in which more fertile isotopes are converted to fissile isotopes than the amount of fissile isotopes consumed to sustain the fission process. Hence there is one neutron necessary to maintain the fission reaction and one neutron to be absorbed by the fertile isotopes. Hence breeding should be possible for energies where the amount of neutrons per absorption is larger than two. This is true for thermal energies, but we must take into account the parasitic absorption from structural materials too. Again referring to figure 3.3, it is obvious that this parasitic absorption is often too large to obtain any breeding. However, it isn't impossible as the ^{232}Th - ^{233}U allows for thermal breeding at a reduced breeding ratio (i.e. the ratio of fissile material produced to the amount of fissile material consumed).

Another possibility is to use the additional neutrons liberated in the fission process to destroy minor actinides such as ^{241}Am and ^{242}Cm and the higher Pu isotopes (^{240}Pu , ^{241}Pu , ^{242}Pu). This process is termed transmutation. The reason is the fission-to-absorption ratio, given in figure 3.6, which is higher than one half in a

fast spectrum. This leads to a high amount of destruction of the minor actinides and as such they won't accumulate in a fast reactor and its associated fuel cycle. This latter is in contrast with the thermal reactor and their fuel cycle where neutron capture prevails. But because a fast reactor has a high fission-to-absorption ratio, it is possible to destroy the historically accumulated minor actinide waste of the thermal reactor (LWR) fuel cycle. It should be added nonetheless that the introduction of minor actinides in a critical reactor system, that is a reactor system with a continuing fission chain reaction, has some control issues due to certain properties of these minor actinides. More suitable for transmutation are the sub-critical systems, i.e a reactor system without a chain reaction where the fission process act as a neutron amplifier. These subcritical systems are intrinsically more controllable and can tolerate higher minor actinide fuel fraction. Additionally, the neutron producing reactions that are considered at the moment (e.g. a D-T fusion reaction, a spallation source) generate very high energy neutrons that increases the fission to absorption ratio, thus optimizing the transmutation efficiency.

3.2.6 Core Neutron Leakage and Reactor Dynamics

Equation 3.4 defined the infinite multiplication factor, i.e. the multiplication factor for an infinite system. Unfortunately a real core is never infinite in size and hence compensation for the neutron leakage out of the finite core has to be incorporated. This is done by multiplying the infinite multiplication factor k_{∞} with the neutron non-escape probability. The latter is a function of the density, scattering neutron cross-section, the preferred scattering angle, the neutron absorption cross-section and the reactor geometry. Or, in other words, it is a function of nuclear properties, the density and the reactor geometry. We can write the finite multiplication factor for a typical cylindrical core configuration with radius R and height H [1]:

$$k_{eff} = k_{\infty} \exp(-C_1 R^4 - C_2 R^2 H^2) \quad (3.6)$$

Hence any decrease in core radius or core height results in an increased effective multiplication factor. This leads to a rising neutron density, and thus an increased reactor power. The inverse is however also true, a core expansion leads to a multiplication factor less than one. The core goes subcritical and the neutron density decreases slowly. The latter effects are only present in fast reactors because in a thermal reactor there is a feedback by a changed neutron moderation². In general, the multiplication factor is reduced to the core reactivity ρ_{core} :

$$\rho_{core} = \frac{k_{eff} - 1}{k_{eff}} \quad (3.7)$$

²This explains the expression by Prof. F. Vanmassenhove – a former highly respected nuclear engineering professor at the University of Ghent, Belgium – A fast reactor is neutronically unstable (i.e. not in its optimal, most reactive, state.)

This core reactivity is easily related to the change of neutron density and power in time t by $\exp(\rho_{core}t)$. But this is a simplified model and even with an infinite negative core reactivity, the reactor power doesn't decrease immediately. There is a specific reactor time constant that hinders the power to decrease faster. And even after the neutron density has reached a negligible value, a residual power of about 7 % remains present due to the decay of fission products. This residual power also decreases, much more slowly than the neutron power, with a certain time constant.

Core anti-reactivity can be introduced by increasing neutron leakage, or by decreasing the effective utilization factor of equation 3.5. Whereas leakage is shown to increase by a change in dimension, the effective utilization factor is insensitive to such changes due to the fact that they annihilate in the ratio (for a constant mass system). Hence control rods with neutron absorbers are introduced in the core, increasing the denominator in equation 3.5 and resulting in a negative core reactivity.

3.3 Historical Development and Operating Experience

Having discussed the basic necessary fast reactor physics, a small historical discussion is mandatory even in this chapter. It is as such already just for the sake of the citation given at the beginning of this chapter. It's not the aim to discuss all the reactor programs, or their aim, but a simple overview of reactor operating experience and technology can be seen as enlightening for the discussion that will follow.

3.3.1 Clementine

The initial development is often cited in an atoms for peace framework [3] in order to use uranium at its full potential. In this case the breeding potential of fast reactor is often mentioned, which stimulated past research due to a fear of a lack of fissile material. However, other sources mention the dual nuclear weapons objectives associated with the earliest design [4]. This is an unfortunate and always returning observation for any nuclear technology³. As such, the first, fast and plutonium fueled reactor was used to obtain nuclear data at the higher neutron energies. But the use of the mercury liquid metal in Clementine⁴, as a first of a kind operating LMFBR in 1949, led to significant advances in liquid metal cooling technology

³In this context it should be mentioned that the second nuclear submarine, the USS Seawolf, was indeed powered by a sodium-cooled reactor. But this reactor operated on an epithermal neutron spectrum. As thus it can't be classified as an SFR

⁴Hence the citation of "Oh My Darling, Clementine" at the beginning of this chapter

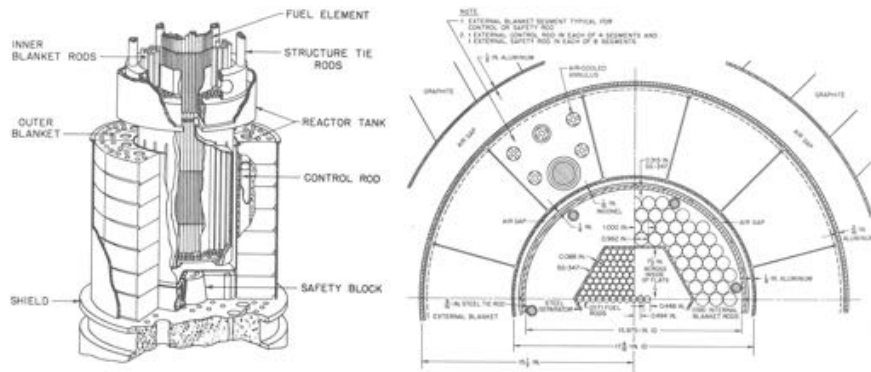


Figure 3.7: The EBR-I Mark II core showing the loading pattern. Each fuel and blanket rod was placed separately in the bottom plate. [5].

and proved the feasibility to control a fast reactor system. It was eventually shut down after the low-carbon steel cladding ruptured and Pu-metal dissolved in the Hg coolant.

3.3.2 The Experimental Breeder Reactor

The next reactor system, EBR-I in 1951, profited from these advances and opted for a potassium-sodium eutectic alloy (NaK, 22 wt% Na, 78 wt% K). However, EBR-I was more aimed at demonstrating the technical feasibility of nuclear electricity generation. As such, it isn't surprising that EBR-I generated the first nuclear electricity in 1951. The first core of EBR-I also gave physical proof of breeding: more fissile material was produced than consumed. However, EBR-I is also the first fast reactor to have a significant accident. In the first EBR-I cores, the fuel rods were inserted in a bottom plate as given in figure 3.7. The core shown in figure 3.7 had a positive reactivity feedback during certain transients, i.e. an increase in reactivity when positive reactivity was inserted. During a test to understand the positive reactivity feedback, a power excursion led to a partial core melt. This led the EBR-I team to redesign the core: the Mark III core that is given in figure 3.8. The fuel and blanket rods were placed inside subassemblies, increasing the mechanical stability of the core during heat-up. As such, rod bowing and the resultant core compactation by fuel rod nearing was prevented. This design approach has been included in all the following fast reactor designs.

To further prevent the fuel rods from nearing each other, whilst maintaining a tight configuration, several grids and fuel rod configurations were proposed and tested. This led to strange nested fuel rod configurations with a star-like assembly

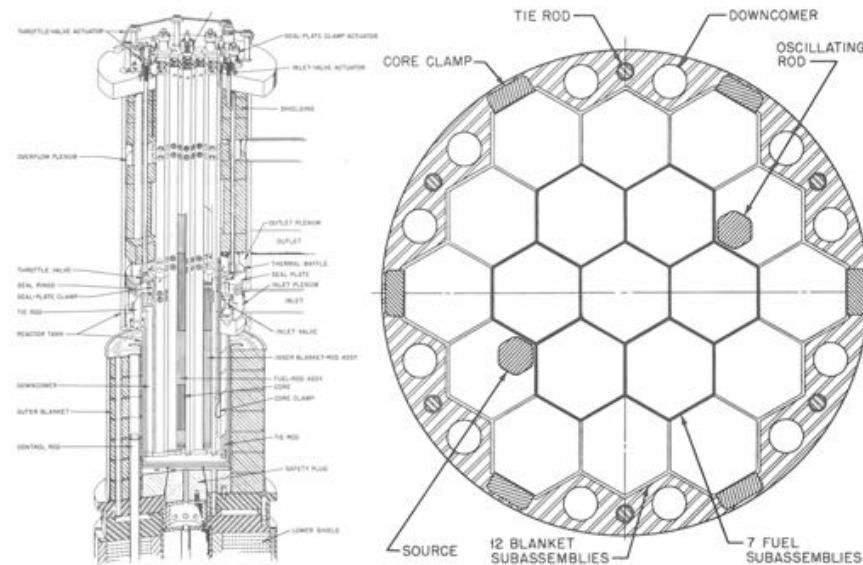


Figure 3.8: The EBR-I Mark III core showing the loading pattern. This core was characterized by fuel and blanket assemblies as we know them today. [5].

such as in Britain's Dounray Fast Reactor. However, the design that is used most frequently at the moment, seems to have found its origin in Russia. Russia's first SFR power reactor BR-5 started operation in 1959 with a wire spacer to maintain the fuel rods, as can be seen in figure 3.9. This design approach has been implemented in many of the following fast reactor designs. Nonetheless, the alternative option of spacer grids has been retained in several designs.

3.3.3 Fermi

Last but not least is the Fermi reactor accident, which significantly influenced the fuel assembly design. Officially Fermi-I was the Enrico Fermi Atomic Power Plant, the first commercial fast reactor project and aimed at producing electricity at an industrial scale. The reactor power was thus quite high and corresponded to a normally fueled unit of that time (156 MW_e). The fact that they succeeded during the 1960's, admitting that it was only partially, in this mission is quite astonishing. The reason that they succeeded only partially was related to some steam generator problems, but more importantly to the subassembly melting accident in 1966. Let's take a look at the accident progression [6]:

- During initial tests, the operators found high outlet temperatures that deviated about 20°C from the expected values. However this readings tended to

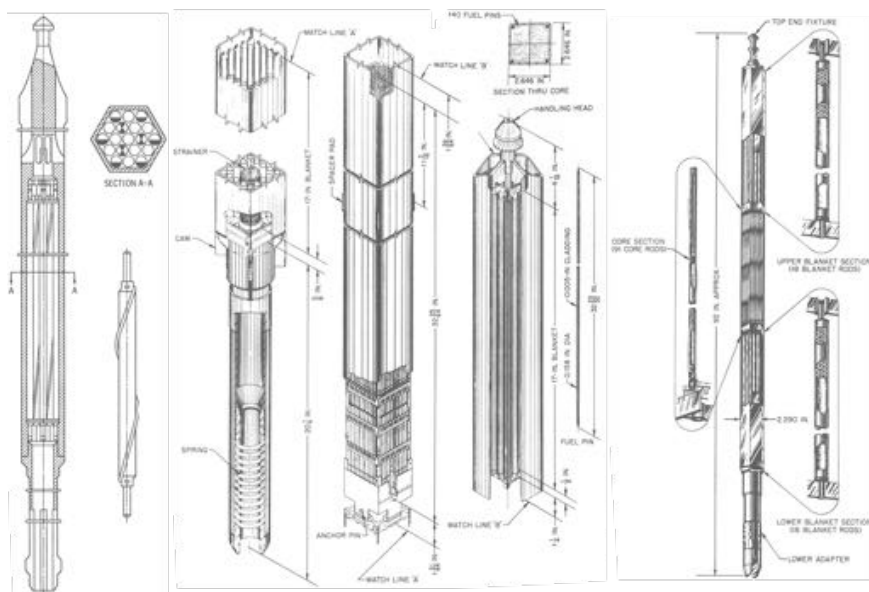


Figure 3.9: Left: The BR-5 fuel assembly design showing the spacing of the fuel pins by means of a wire spacer. Middle: The Fermi fuel design showing the unprotected coolant inlet. Right: The EBR-II fuel assembly design, incorporating both a wire spacer and inlet ports. [5].

oscillate between test and were well within the design margins. Hence the deviations were found to be acceptable, but required more investigation.

- To understand these readings a core-reshuffle was performed. During power-up, the operators found that the reactimeter⁵ indicated a negative reactivity. Because negative reactivity can also be caused by core disassembly, increased neutron leakage, . . . reactor alarms were triggered. However the reactimeter had previously been found to be sensitive to noise and thus the power was further increased.
- It was noticed that an intermediate power level was attained with more reactivity insertion than during other test, as thus measurements were performed to verify the core state. Before these measurement results were analyzed, radiation alarms were triggered in the reactor building. This clearly indicated that there was a serious problem and the reactor was scrammed, i.e. a high amount of negative reactivity was introduced.
- An analysis of the primary reactor gas systems, revealed the presence of typical fission products. The typical metallic fuel used in these reactors could only release these products if a fuel melt occurred. Hence core damage was confirmed.

It is clear that several errors were made, or better imprudent operations were performed, by the reactor operators during the power-up. However, it should be taken into account that the experience with reactors of such a size were inexistent in 1966, hence Mosey's conclusion on institutional failure [7] is perhaps a bit too exaggerated. However, the accident should be considered as very serious. The core state and the extent of core degradation was unknown. Given that the core isn't in its optimal state, any core collapse due to a faulty movement could result in further damage. Therefore, further gas analysis was performed to assess the extent of the core damage. This revealed that only one fuel assembly equivalent did melt and hence the core would be in a stable state. Several more tests were nonetheless undertaken to verify. Once a recriticality was practically excluded, operation started to discharge the entire core. During this discharge, the forces necessary to remove some elements were very high. Two subassemblies were stuck and couldn't be removed directly. The core melt was localized! After all elements were discharged, the sodium was drained and a structural element was found to have broken loose. This element was able to block the inlet of several subassemblies and led to a partial to almost total instantaneous blockage during the power-up. The cause for the oscillatory temperature behavior and the final meltdown was found!

In total 3 years, 9 months and thirteen days of identification, recovery and repairs

⁵An instrument that gives the reactor period related to equation 3.7 and thus directly the reactivity.

followed the incident. Furthermore an entire core of elements that might have been damaged due to overheating were discarded and full operation resumed on a entire new set of elements. The accident was clearly a loss of investment, that contributed to the halt of the program when new fuel had to be rented, fabricated and validated. Nonetheless this reactor program most likely contributed significantly to reactor safety as afterwards flow guards and inlet ports were implemented in many reactor programs. These inlet ports are common in fast reactors nowadays. Additionally many instruments were designed to detect fuel damage as early as possible.

3.3.4 SuperPhenix Blockage Incident

Rahmani et al. [8] describe the abnormal heating of a subassembly in the core of SuperPhenix during power-up in January 1985. It was noticed that one subassembly had higher outlet temperature than the others. The particular subassembly had also been remachined and thus the hypothesis of a forgotten rubber protection plug emerged quickly. It was shown afterwards that the plug was indeed forgotten, partially plugging the fuel assembly during pyrolysis with the sodium. The incident was detected during power-up by the core instrumentation even though no particular alarms were triggered. Unlike the Fermi case, corrective actions were immediately taken that prevented any reactor damage. The specific assembly was removed, analyzed and new inspections were implemented to guarantee the conformity of the subassemblies.

3.3.5 The Prototype Fast Reactor Oil Spill

During operation of the Prototype Fast Reactor in Scotland, it was noticed that many components had black, tarry deposits [9]. It was concluded that those black deposits came from pump oil losses to the coolant, as several liters of oil had been lost from the pump oil system. Nonetheless, between 1974 and 1990 no particular problems were encountered that could be contributed to the oil spill. However starting from 1990, the pumps showed irregular behavior. After some time it was clear that oil did in fact enter into the coolant once again. This time, it had more markable consequences as the outlet temperature of subassemblies did increase. It is believed that tarry carbon debris in the pumps did detach and blocked the fuel subassemblies, as was confirmed by analysis of the affected subassemblies. The researches from the United Kingdom concluded that oil bearings are best avoided for rotating parts of an SFR.

3.4 The Reactor System

SFR nuclear reactors are quite different from typical water-cooled nuclear reactors due to the specifics of the coolant. Liquid metal coolants have a low vapor-pressure, for example, that eliminates the need for high pressure vessels such as in PWRs (operating pressure of 155 *bar*) or BWRs (operating pressure of 72 *bar*) and a totally different design strategy is the result of this. But let us first discuss the choice of this peculiar coolant, before looking at the design consequences for the reactor system.

3.4.1 The Sodium Coolant

Sodium, liquid from about 98°C up to its boiling point of 880°C, is used as a coolant in many applications where an excellent heat removal rate is desired. Although its use in nuclear reactors is best known, sodium has also been used for solar energy applications (e.g. the ALMERIA single-tower, central receiver design [10]), aircraft engine cooling (during World War II) [11],... In fast reactors it is especially chosen because it has an acceptable slowing down power, but it is a relatively light nuclide such that the inelastic scattering is less significant. The absorption cross-section (see figure 3.3) of pure sodium is also sufficiently low. This latter means less neutron losses due to absorption, which is good for the effective utilization factor. It also means that typical activation products such as the nuclide that results from neutron capture of $^{23}\text{Na} - ^{24}\text{Na}$ – is created in a lesser extent. Furthermore, this typical activation product ^{24}Na has a half-life of about 15 hours, hence radiating intensely but for a short while. The sodium is thus termed a high activity-coolant [5]. ^{24}Na decays by β^- emission, which is well shielded by the sodium coolant. However after this β -decay the resulting ^{24}Mg nucleus is still in an excited state and additional γ -decay follows. Hence there is a need for shielding. But operating on a fast spectrum, the neutron multiplication reaction $^{23}\text{Na} (n, 2n') ^{22}\text{Na}$ is also possible. ^{22}Na is a nuclide with a half-life of 2.6 years and decays by β^+ emission and associated γ -decay of the daughter nuclide. The multiplication reaction occurs however much less than the absorption reaction and the amount of ^{22}Na is less important. However, together with the activation products of the corrosion products (^{60}Co) and possible contaminants from fuel failure (^{137}Cs), it has a high contribution to the dose rate after shutdown as those nuclides have a long half-life [12]. Nonetheless the typical radiation doses for operators are less than the operation doses for typical PWRs.

The latter brings us to the general corrosion behavior of sodium. This generally acceptable corrosion behavior is one of sodium's advantages because sodium is quite compatible with stainless steel, a preferred fuel cladding material. In general, several compounds dissolve in the hot liquid sodium and are deposited in

C	11-27	N	4
Be	0.3	Mg	3
Al	10	K	1000
Ca	10	Ti	10
V	10	Cr	10
Mn	1	Fe	20
Co	10	Ni	10
Cu	3	Zn	100
Sr	10	Mo	10
Ag	1	Cd	1
Sn	20	Ba	30
Pb	10	Bi	10

Table 3.2: Typical impurity content (in ppm gram) of nuclear grade sodium [13].

the colder regions (or vice-versa). This concentration difference leads to a mass transport through the core that must be limited as much as possible to increase the design lifetime of the components and to decrease the activity of the coolant and the components due to deposition of activated products. To prevent corrosion and the associated mass transport, the control of a low oxygen content is very important. On top of that, a high oxygen content can lead to possible plugging of cold parts. It is thus highly advised against operation at high oxygen content and systems for online sodium purification are added as a consequence. Similar conclusions are valid for high hydrogen content as this can also lead to plugging by NaH . Additionally, impurities such as calcium should be prevented for plugging purposes. These plugging considerations lead to the definition of nuclear grade sodium that is of exceptional quality as can be observed in table 3.2. The document by Hinze [14] details that the content of boron and lithium should be limited too for neutron economy considerations. Nonetheless no additional specifications arise because any commercial grade sodium appears to be sufficiently free of neutron poisons that prevents excessive absorption cross-sections.

The excellent heat removal rate of sodium has already been cited in this section, this excellent heat removal rate is mainly related to the high thermal conductivity of liquid metals, and sodium in particular. Table 3.3 gives a short overview of some of the important liquid sodium properties at 450°C at typical reactor pressures. The temperature dependent properties can be found in appendix B. Table 3.3 also indicates that the sodium hydraulic properties such as density and kinematic viscosity are similar to those of water, which leads to a similar hydraulic behavior. This latter also explains our interest. But whilst the hydraulic nature is similar to that of water, the chemical nature of sodium is very different. This was already revealed by the general corrosion behavior, but becomes even clearer

Properties for	Sodium (450°C)	Water (100°C)
Density (kg/m^3)	846	958
Dynamic Viscosity ($10^{-4} Pa.s$)	2.5	2.8
Kinematic Viscosity ($10^{-7} m^2/s$)	3	3
Thermal Conductivity (W/mK)	67	0.68
Heat Capacity (kJ/kgK)	1.3	4.2

Table 3.3: The sodium saturated properties at 450°C from the correlations of Fink and Leibowitz [15], compared to the saturated properties of water at 100°C from the XSteam library [16].

when looking to the reactivity of liquid sodium. Sodium as an alkali metal will react, often exothermically, with many working fluids, non-metallic components, lubricants, . . . and even air. This reactive nature of sodium has an important influence on the reactor design.

Last but not least, as a personal opinion, it should be stated that the choice of any coolant is subjective in nature and depends on subjective priorities. Although an excellent point is made in a recent article, by Garnier and Raoult together with other international sodium researchers [17], in favor of sodium cooling, an equally valid case can be made for liquid lead.

3.4.2 Structures, Systems and Components

Although the atmospheric boiling point of liquid sodium is 880°C, a temperature never passed in nominal conditions, typical SFR reactor building resemble PWR reactor buildings as can be seen in figure 3.10. The reactor building of a PWR has a relatively high volume to limit the containments pressure rise in the event of a pipe break. This latter isn't a concern because the sodium coolant isn't pressurized. However pressurization of the containment is still possible due to sodium fires (i.e. sodium air interactions) and energetic events caused by a fuel meltdown [5]. Hence the containment is designed appropriately for such events, but also to accommodate the giant reactor components.

In general an SFR reactor is composed out of several systems:

- A Primary loop heat transfer systems that contains the activated core coolant, the core and the intermediate heat exchangers.
- A Secondary loop system that contains an intermediate heat exchanger and a not or slightly activated/contaminated coolant that transports the heat generated in the core to the working fluid.

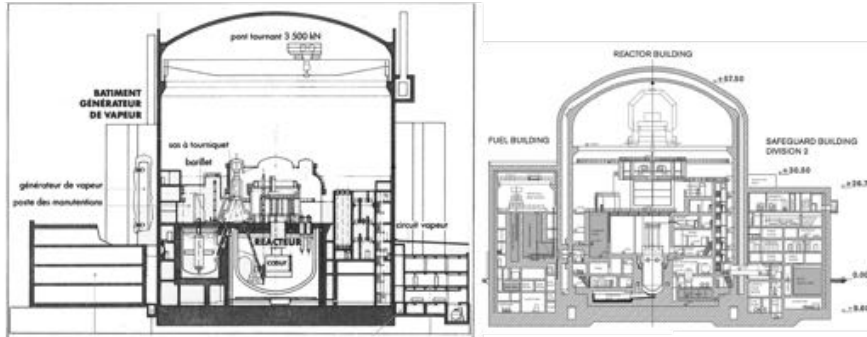


Figure 3.10: A comparison between an SFR and a PWR containment building, the comparison is to scale. Left: The SuperPhenix reactor building which is about 85 m in length [18]. Right: The EPR containment building which is about 67 m in length according to the image of the EPR brochure

- An energy-conversion system in which the heat transferred to the working fluid is used to generate work and electricity. This system is cooled by a cold source – often a river, a lake or the sea – as no thermodynamic cycle is perfect and residual heat has to be rejected.
- Additionally there are auxiliary systems such as systems responsible for emergency cooling, for gas control and sodium purification.

An entire discussion of each system is out of the scope of this work, thus only the primary loop will be described in detail. However, we'll limit the in-depth discussion to the components for which knowledge is important for the analysis of the liquid metal boiling and the associated boiling noise.

3.4.2.1 The Primary Loop

For the configuration of the primary loop there exist two possible options as given in figure 3.11, each with their advantages and disadvantages:

- **The Loop Design**

The loop-type design is by far the most used design in nuclear reactors because it is implemented in the commonly used PWR design. The loop design has significant advantages when it comes to maintenance and leakage control because of the easy access to all the different components. However the system is susceptible to a break in the primary system loops, resulting in a loss of coolant. This is even more serious for liquid metal cooled reactors, as it is less obvious to have safety injection systems to recompensate for the lost coolant. On the other hand the loop type design facilitates the creation

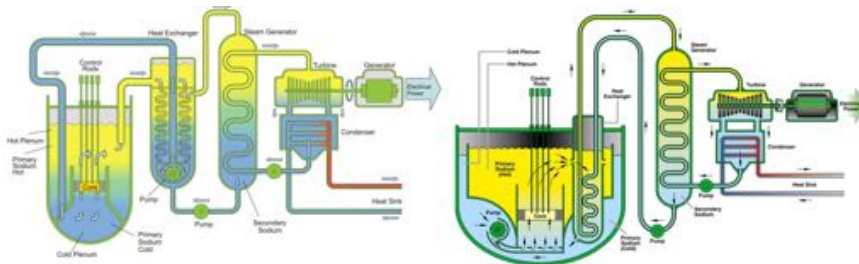


Figure 3.11: A Schematic comparison between a typical loop and pool type SFR. Left: Loop type. Right: Pool type.

of a natural circulation driving pressure. The latter is simplified given by the density difference (intrinsically controlled by the core power and flow) $\Delta\rho$ and the height difference between the hot and cold part ΔL :

$$\Delta p_{buoyancy} = g \cdot \Delta L \cdot \Delta\rho \quad (3.8)$$

The latter height difference can be easily varied, hence it is theoretically possible to increase the buoyancy driving force. The loop type design also reduces the coolant mass available, hence thermal transients are much faster. This latter is advantageous for load-following purposes in which the reactor power is changed rapidly.

- **The Pool Design**

In the pool type design all the components are immersed in a pool that contains the coolant. This reduces the loss of coolant probability as component failure doesn't result in an actual loss of coolant. On the one hand this complicates maintenance operations, whilst on the other hand the coolant mass is much higher. This latter dampens thermal transients, which is important for off-normal events. The pool type design can also result in one free surface, which also has advantages. But for a pool type design, it is difficult to increase the height difference in equation 3.8. This is due to the fact that any increase in height difference results in a larger vessel, which becomes less economic.

For SFRs both designs have been used in the past, but the more commercially sized reactor almost all opted for the pool type design, with the exception of the Japanese design. The Japanese designers take into account the higher seismic resistance of the loop-type design.

A typical pool-type vessel layout is given in figure 3.12. The first notable aspect in

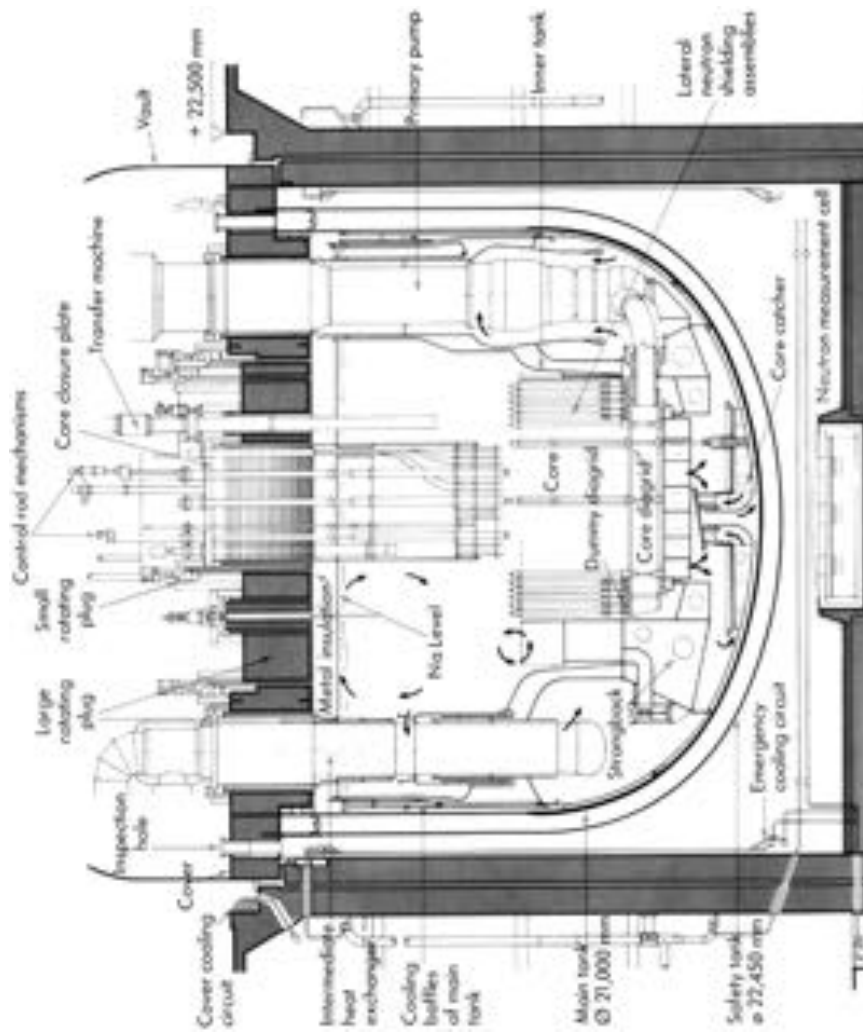


Figure 3.12: A representation of the pool-type reactor vessel of Superphenix, indicating the main components. The region above the core is the hot plenum whereas the region below the core is the cold plenum, referring to the temperature rise as the liquid sodium flows upwards through the core.

this detailed SFR design, which is also noticeable in figure 3.11, is that the liquid metal doesn't directly contact the metal insulation of the reactor cover. Between the free surface and the reactor cover's insulation is a cover gas. This cover gas is slightly pressurized (0.1-0.2 bar) as to prevent air ingress and thus sodium fires. On the other hand the cover gas also take the role of the PWR pressurizer: During heat up, the specific volume of sodium increases (i.e. the density decreases). The cover gas thus takes up this volume change. Due to the reactive nature of sodium, only inert gasses are acceptable for use as cover gas. Cover gasses that have been considered are nitrogen, helium and argon. Although nitrogen is very attractive as a cover gas, the nitridization of the steel structures at high temperature and the possible precipitation of calcium impurities in the form of Ca_3N_2 (which can cause plugging) limit the use of nitrogen as a cover gas in reactor systems. And basically only argon is used as a reactor cover gas because of the higher leakage rate of helium.

To describe the reactor vessel more in detail, we begin a virtual tour in the reactor vessel at the core outlet:

1. At the core outlet of a typical SFR the sodium temperature is around 550 °C. This hot sodium flows as a jet in the upper plenum, often referred to as the hot plenum, inside/above the inner tank.
2. The jet that flows out of the subassembly outlet, first encounters the above core structure. This structure, although very important as it contains the control rod drive mechanism and guides the control rods, hinders the jet that gives the typical above core flow a flowering pattern.
3. This flowering behavior creates a good mixing of the jets of the different subassemblies, resulting in a relatively uniform upper plenum temperature [19, 20]. This hot sodium flows inside the intermediate heat exchanger (IHX).
4. Inside the IHX the hot primary sodium flow is cooled down by a counter-current cold secondary sodium flow, heating the secondary fluid and cooling the primary fluid to around 400 °C.
5. The cold liquid flows out of the IHX inside the lower plenum or cold plenum, which is below/outside of the inner tank. The cold liquid flow from this lower plenum to the pump inlets.
6. The pump pressurizes the liquid so that it flows inside the strongback and the diagrid. Inside this diagrid, the flow is distributed among the fuel subassemblies of the core. A small fraction of the flow, the by-pass flow, doesn't

pass through the subassemblies, but still passes through the core in the small spaces between the subassemblies.

7. Inside the core's subassemblies the cold liquid is heated, restarting our tour. The temperature rise in the subassemblies is about $\pm 150^\circ\text{C}$, which is about four times the temperature increase over a PWR-core of the same power rating and mass-flow. The latter is easy to understand from table 3.3, because the difference in heat capacity is about a factor four.

Although our virtual tour followed the main flow inside the vessel, there are many intensional leakage paths that are for instant used to cool the baffles of the inner tank or to prevent selfwelding⁶. Outside of the reactor vessel there is also a remarkable structure, this is the safety vessel. The reactor vessel is placed inside this safety vessel to prevent a loss of coolant. The small gap between the reactor and the safety vessel assures that the sodium level never decreases below the IHX inlet. Hence ensuring a cooling flow in the event the reactor vessel is breached. To prevent any energetic chemical reaction, this safety vessel is also maintained under an inert atmosphere.

3.4.2.2 The Reactor Core

Now that we've described the primary system, we can go down a level and have a closer look at the reactor core. Although the core is one of the most important structures in a nuclear reactor, its volume is only small compared to the reactor vessel. As is clear from the previous discussion, the core is assembled out of several subassemblies through which sodium flows and through which the sodium is heated by nuclear fission. The hexagonal subassemblies are, similar to the fuel pins, arranged in a triangular lattice to increase the effective utilization factor in equation 3.5 as can be seen in figure 3.13. The core given in figure 3.13 shows a transversal homogeneous core, while it is axially heterogeneous. This is the new low void core concept of CEA. During sodium boiling, with a reduced sodium density and thus reduced neutron absorption by the sodium due to a decrease of the product

$$N_{coolant}\sigma_{a,coolant}A_{coolant} \quad (3.9)$$

in equation 3.5, the effective utilization factor increases. This is the basis of the infamous positive reactivity feedback in an SFR core. In the new void core concept of CEA, these changes are offset by an increased neutron leakage towards the upper plenum. For small cores such a leakage offset occurs naturally. However for a large core such as the CFV-core, some design modifications have to be considered.

⁶Selfwelding is a typical liquid metal corrosion mechanism in static coolant between small gaps. The metal dissolves in static liquid and creates a new alloy-bond between the structures, as described by Miller in Chapter 4 of the Liquid-Metals Handbook [11].

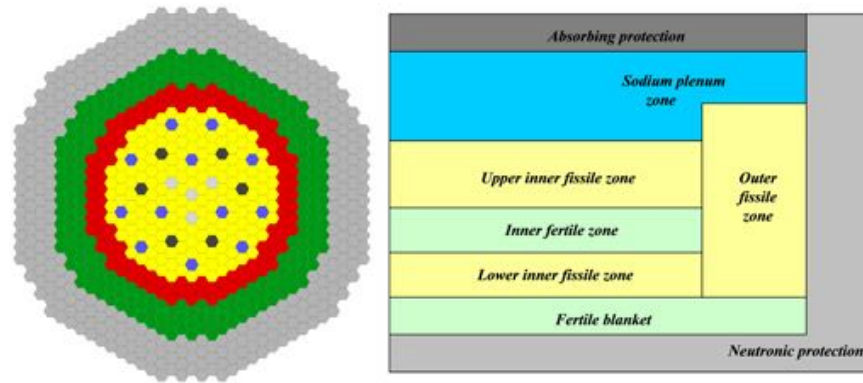


Figure 3.13: The Low void core - CFV - concept of CEA [21]. Left: Transversal cross-section of the core (Grey - Steel shielding assemblies. Green - Steel reflector assemblies. Red - Outer core assemblies. Yellow - Inner core assemblies. Blue - Control rod assemblies. Black - Shutdown rod assemblies.). Right: Axial cross-section of the core in an r - z representation.

of all, there is the pancake form of the core i.e. the dimensions don't respect the optimal ratio of radius R and height H :

$$\frac{R}{H} \approx 0.541 \quad (3.10)$$

Further neutron leakage to the upper plenum result during sodium voiding in the sodium plenum at the top of the core as explained by Wensch in a book on fast reactor technology of 1966 [5]. Secondly, the axial heterogeneity enforces the previously mentioned axial leakage in the case of voiding. However, this type of core results in a higher enrichment and lower breeding gain. The latter was highly undesirable in the past and thus rarely or not completely implemented. And although the concepts of heterogeneity, a sodium plenum and the pancake form were known in the past; the axial heterogeneity has never been implemented. The advantage of this axial pattern is that voiding will progress axially, whereas transversal voiding in all the subassemblies is less likely [1].

3.4.2.3 The Fuel Assembly

Going down one level, we find the fuel assemblies that constitute the core. These fuel assemblies have commonly a hexagonal form to retain the triangular grid. The deviation of this form in the Fermi reactor (see figure 3.9) is attributed to possible economic fuel developments that privileged a square form. These fuel assemblies have a steel wrapper to increase the mechanical stability of the core and to prevent compactation. Inside these hexagonal tubes, the fuel pins are maintained. These

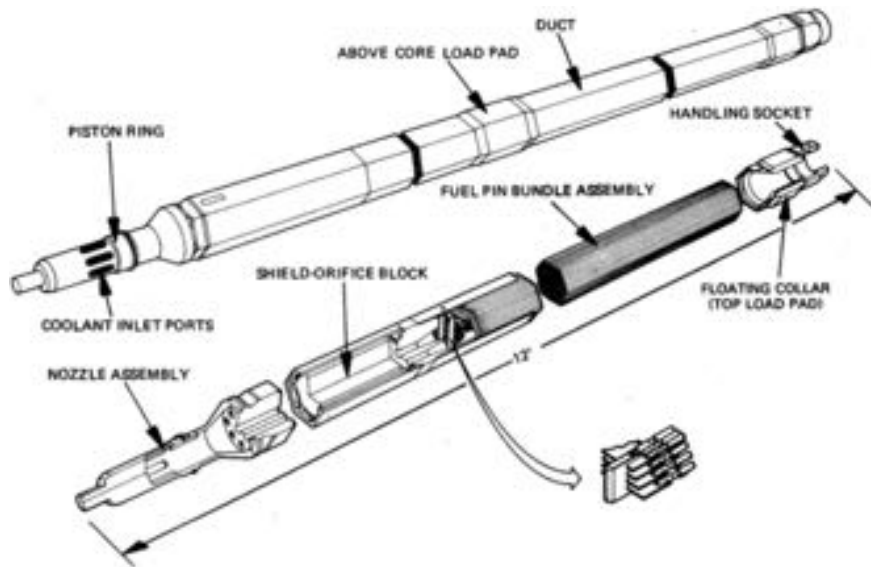


Figure 3.14: The typical fuel assembly structure.

fuel pins are attached to a spacer grid by a keyway in the bottom end cap of the fuel pins as can be seen in figure 3.14 of a typical SFR subassembly. The pins aren't fixed at the top to allow for axial expansion and to prevent core compaction by rod bowing. The spacing between the fuel pins and the wrapper tube is maintained by a wire spacer or a spacer grid. But to better understand the flow inside these fuel assemblies, we embark on another virtual tour.

1. We start our tour at the diagrid of figure 3.12. In this diagrid, there is a network of cylindrical holes in which the lower adapter of a fuel subassembly is positioned. The sodium flows inside the fuel assemblies by the inlet ports. These inlet ports prevent any total and sudden blockage. A small fraction of the flow, i.e. the by-pass flow, doesn't pass these inlet ports and flows from the diagrid in the small space between the steel wrapper tube of two neighboring subassemblies.
2. Once the flow passed these inlet ports, the coolant enters in a cylindrical tube that is connected to a divergent part. In this divergent part, the coolant passes from the small cylindrical tube into the wider hexagonal part that contains the fuel pins.
3. The flow isn't distributed equivalently between all the fuel pins. In general, we can say that more coolant passes the external fuel pins (those closest to

the wrapper duct) than the  al fuel pins. Hence the external fuel pins are overcooled, whereas the ~~external~~ fuel pins are “undercooled”

4. Once passed the fuel pins and/or reflector rods, the heated coolant is mixed either in the sodium plenum (as in the CFV concept), in the assemblies convergent or the at the outlet. Hence the assemblies outlet temperature is more or less homogeneous.
5. From this outlet, the coolant flows into the upper plenum. In case this outlet is blocked by a heavy object, the collar contains small holes to permit coolant flow through the assembly.

Hence it is clear that a practically complete blockage incident is taken into account by the assembly design. Nonetheless blockages can still occur due to fabrication errors as became clear in the case of SuperPhenix, but careful inspections before loading should eliminate this risk. Other small blockage can occur due to agglomerates that can pass the inlet ports, but that are capable to block the flow at the spacer grid that holds the fuel pins. Hence operating with a very pure sodium composition is important, as well as preventing any degradation of this purity! From figure 3.14 it also becomes clear that most of the volume in the active part of the core⁷ is taken up by the fuel pins.

3.4.2.4 The Fuel Pin

Last, but not least, we discuss the fuel pins that take up the major part of the volume of a fuel assembly. These fuel pins contain the fissile material in the form of oxides, nitrides, carbides or simply a metal alloy. Although the metallic fuel has been considered frequently in the past and especially in the USA, we will focus on the oxide fuel because it is generally preferred in Europe.

The typical fuel pin is given in figure 3.15. Inside the cylindrical pin, which forms the fuel cladding, small porous pellets of PuO_2-UO_2 are stacked. Because there is initially a small gap between the cladding and the pellets, the fuel pins are pressurized with helium to enhance the heat transfer between the two solid surfaces. Fission products will be created during irradiation, thus increasing the specific volume of the fuel-fission product mixture. On top of that fission gasses are created that have a large specific volume. These fission consequences lead to swelling of the pellet and after a while the pellet and the cladding inner surface contact. Additionally, the fuel swelling creates stresses in the pellets that leads to pellet cracking. The thermal gradient in the fuel also leads to material restructuring, thermally induced stresses and deformations,... Hence it can be said that these fuel pins are

⁷The active part is the part of the core that contributes to the fission reaction and thus most of the heat generation.

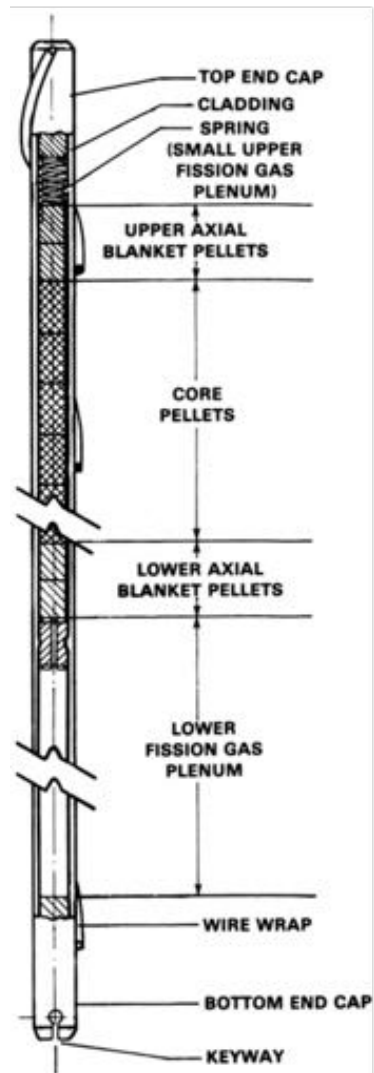


Figure 3.15: The typical fuel pin structure (SuperPhenix fuel pin) from Reynolds and Waltar [1].

operated under extreme conditions while they generate power. Because fission gasses are released inevitably from these pellets, a gas plenum is foreseen such that the pressure rise inside the fuel pin remains acceptable.

3.4.2.5 Defense-In-Depth

It may be noted that we reviewed the structure of an SFR from the containment to the fuel pellet. In fact we looked at an SFR from the outside to the inside. We might also have followed the containment barrier order. SFRs, like any other reactor, respect the defense-in-depth principle with several containment barriers to the release of fission products:

- Fission products are created inside the fuel pellets. Their migration is prevented by the fuel matrix.
- Around the fuel matrix is the cladding creating an additional migration barrier.
- The fuel pins, inside a fuel assembly, inside the core, are part of the primary system and contained in the reactor vessel. This present an additional boundary to fission product dispersal.
- Last but not least is the final containment structure: the reactor building.

3.4.2.6 Examples

To finish this section, we give some dimensional details in table 3.4 of the fuel assemblies for some notable reactors that will often recur in this text: Rapsodie, Phenix and SuperPhenix.

3.5 SFR and GEN-IV

It is clear that SFRs, with their capability to breed fissile material or to transmute the minor actinide nuclear waste, comply with the sustainability requirement of the Generation IV International Forum. From all GEN-IV reactor designs it is also the nearest-term actinide management design. This is mainly related to the large amount of experience that has been accumulated in the past for this specific reactor design. On a personal note, SFR systems enjoy this preference over other GEN-IV designs due to the fact that this operational experience also includes many accidents⁸. In our historical scope we addressed several of these accidents, at the level of the core and the primary loop. Most of these accidents led to many developments and improvements to protect against reactor accidents. However,

⁸A similar conclusion is true for LWRs.

Properties for	Rapsodie	Phenix	Superphenix
Nominal reactor power (MW_{th})	40	563	2990
# Core assemblies	73	103	364
Subassembly duct width (mm)	49.8	124	173
Subassembly length (mm)	1661.5	4300	5400
Subassembly pitch (mm)	50.8	127	179
# Pins/subassembly	61	217	271
Pin outer diameter (mm)	5.1	6.6	8.5
Pin pitch/Diameter	1.16	1.18	1.15
Pin Length (mm)	320	850	2700
Maximal pin linear power (kW/m)	43	45	48
Average pin linear power (kW/m)	31	27	30

Table 3.4: Fast Reactor Data for Rapsodie, Phenix and SuperPhenix from the IAEA Fast Reactor Database [22]. The number of core assemblies is the total number of inner and outer core assemblies. The subassembly duct width is measured from flat-to-flat. The pin pitch diameter ratio comes from the data of Waltar and Reynolds [1]

there remain quite a few technological gaps to be solved for the other GEN-IV requirements.

- There is the additional fuel cycle cost due to reprocessing of the spent fuel. However fuel cost are more or less unimportant for reactor operation compared to the initial investment and cost reductions can be foreseen for the waste disposal. But the higher capital cost of the SFR reactors due their complexity and size compared to traditional LWR designs, threaten the economic competitiveness of SFRs. Therefore a reduction of the capital cost, i.e. design simplification, is very important.
- The specific neutronicly unstable nature of fast reactors, i.e. they aren't in their most reactive state, calls for a thorough demonstration that any bounding event can be handled in a passive manure, which is the preferred safety response. A safe accident response is necessary to comply with the safety and reliability requirement of the GIF.

3.6 Accident Analysis

3.6.1 Introduction

It is this last GIF requirement that leads us to a small reactor accident analysis, again limiting us to the primary system and in particular the core. Because of the importance given to the Fukushima accident, we set the tone with a small

analysis of such a Protected Loss Of Heat Sink (PLOHS) combined with a total station blackout (loss of on-site and off-site power). This also allows us to explain the definition of a protected and unprotected accident as given by Reynolds and Waltar [1]:

- Protected Accident:

For protected accidents, the plant protective system is supposed to operate. Hence a significant amount of negative reactivity is inserted in the core, reducing the power level to the decay heat fraction. Hence the accident analysis initiates at the decay heat power levels. This doesn't mean that protected accidents won't have recriticality issues that bring the core again to higher power levels.

- Unprotected Accident:

For unprotected accidents, the plant protective system is postulated to fail e.g. control rod blockage, no control rod action because an initial anomaly isn't detected, . . . Hence the accidents initiate at full power. Again this doesn't result always in an accident progression at full power levels, as reactivity feedback mechanism may result in an increase or decrease of the core power.

So for our SFR equivalent Fukushima accident, we postulate that the plant protective systems do not fail. However because a loss of on-site and off-site power all pumps stop, and core cooling is lost. Furthermore, due to a lack of a heat sink, the natural circulation in the primary loop can not be initiated. We also postulate that back-up heat removal systems can not be started as was the case for the BWR plant in Fukushima. We try to determine the margin for coolant boiling for an SFR and BWR of equivalent thermal power. In the BWR-case the coolant boiling will lead to a pressurization of the primary system, which is a danger for one of the confinement structures. In the SFR-case this is also true, however we also have to take into account the possible reactivity risk. It is tempting to take the BWR and SFR reactor volumes, the subcooling margin and a decay heat fraction (e.g. 1%) of the thermal power. This results in a time margin, a response-time, before boiling sets in:

Property	BWR	SFR
Primary Fluid Mass (metric ton)	300	3300
Fluid Specific Heat Capacity (J/kgK)	5200	1265
Primary Reactor Structure Mass (metric ton)	1700	3000
Structure Specific Heat Capacity (J/kgK)	650	650
Total Heat Capacity (MJ/K)	2700	6100
Boiling Margin (K)	30	300
Time Constant (hours)	~ 1	~ 18

Table 3.5: Simplified thermal time constant assessment for the decay heat fraction for a BWR and an SFR of about 3 GW_{th} power, deduced from order of magnitude assessments of their core inventory.

Although these results are attractive and are often used to make the case for the excellent safety characteristics of SFRs, they overlook many details and do injustice to the considerations that went into the BWR design (see the book on BWR technology by Lahey and Moody [23]). In a BWR, the approximation is more or less accurate because the coolant volume (i.e. the primary system volume) and the core volume are more or less equivalent. However, a simple look at figure 3.12 already demonstrates that this isn't the case for a pool-type SFR. Furthermore, the heated length in an SFR is only a small fraction of the fuel assembly length. Hence only a limited volume can be considered and boiling starts early in the fuel assemblies⁹. If no positive reactivity feedback results due to the in-core boiling, heat will likely be transported between the fuel pins and the hot plenum because boiling-condensation is one of the most effective heat transfer mechanisms. If local boiling heat transfer deterioration related to dry-out can be prevented, an SFR will likely have a significant response time. Albeit that the margins will most likely be given by boiling natural circulation consideration and dry-out limits, because the loss of efficient fuel cooling can lead to fuel failure and increased reactivity. This is of course a qualitative analysis to demonstrate that an SFR reactor can effectively be designed against conditions that often control the debate in this post-Fukushima era. Now it's time to look more in detail to core accidents and their role in licensing.

3.6.2 Core Disruptive Accidents

The specific nature of SFRs, i.e. the reactivity increase with core compactation, led to special attention and the study of so-called Hypothetical Core Disruptive Accidents (HCDA, CDA or even Severe Accident¹⁰) in the past. This is the type

⁹The results of this analysis are confirmed by the remark of Waltar and Reynolds that the thermal time constant are smaller in an SFR in comparison with an LWR, which is incompatible with the results given in table 3.5.

¹⁰Often a confusing terminology is used in literature.



Figure 3.16: A schematic representation of the Bethe-Tait Hypothetical Core Disruptive Accident scenario from Reynolds and Waltar [1].

of accident that can be postulated to be possible, yet to be of an extremely low probability. During such an HCDA the core is assumed to melt. In its degraded state, the core is assumed to collapse under its own weight. This compaction leads to a power excursion and a final energetic disassembly scenario as depicted in figure 3.16 from the book of Waltar and Reynolds [1]. This accident was first analyzed by Bethe and Tait in the 1950s with assumptions that provided an analytical solution and an order of magnitude estimate for the maximum work-energy delivered to the reactor environment, independent of the actual initiating accident. It is this work-energy (pdV) delivered to the reactor environment that can cause containment loading. This type of accident is only possible for fast reactors, and it is on this point that SFR and LWR safety differentiates¹¹. In the past this HCDA has even been considered as a Design Basis Accident (DBA) and was thus treated for the actual reactor design and licensing [24]. This said, we might look at the specifics of a DBA.

3.6.3 Design Basis Accidents

A Design Basis Accident is, according to Waltar and Reynolds [1], an accident that leads to the most severe consequences of all considered credible. In fact the DBA accidents considered for accident evaluation are the most severe of a family of representative accidents associated to initiating events. These families of initiating events are used to verify the effectiveness of the plant protective system.

Each initiating event has been historically related to a power/flow imbalance and can thus be classified as a Transient OverPower accident (TOP) or a Transient UnderCooling accident (TUC), i.e. they are related to an accident in which the

¹¹In LWR core compaction leads to a shut-down due to a loss of moderation. On the other hand the typical depressurization accidents in LWRs don't have to be considered for SFRs

power increases for a constant cooling rate or the cooling decreases for a constant power rate. For example, one of the DBA accidents for SPX was a typical but conservative unprotected loss of flow (ULOF). In this ULOF accident an unprotected pump coastdown was assumed, followed by sodium boiling and a power excursion, finally leading towards a HCDA. Due to this DBA, significant mitigating structures had to be in place to withstand the release of mechanical energy during the disassembly phase. This is clearly a severe TUC accident leading to a HCDA, that as a DBA protects against many lesser accidental scenarios and thus reduced the need to analyze them in detail. Nonetheless it results in a system that isn't risk-optimized (i.e. the reactor is optimized against a very unlikely accident, while more likely accident paths receive less attention). For the safety approach for the European Fast Reactor (EFR) project, that followed the SPX project but was never constructed, the importance of the latter accident has been reduced by improvements in the shutdown systems. Hence the failure of the plant protective system could be almost excluded. However, the unlikely event was still evaluated to assess the consequences and the possible risk posed by these consequences. Although the accident received much less attention, fuel melting could and can not be ruled out. Especially local blockages were seen as a possible fuel melt initiators¹². As an envelope of smaller blockage accidents the Total Instantaneous Blockage at full power was introduced and studied as a Beyond Design Basis Accident (BDBA) [25]. No special mitigating features had to be implemented, however it had to be demonstrated that the melt wouldn't propagate beyond limits given by thermal and neutronic considerations [26].

For the new generation of SFRs, it is difficult to assess the accident evaluation and the DBAs of the future. On the one hand there is the United States Nuclear Regulatory Commission that presented a regulatory structure for a risk-informed and performance based licensing approach that is almost independent of the reactor type [27]. On the other hand there is a recent article by French researchers [28] that might give an indication of the new strategy that will be taken in the current French SFR reactor project. This strategy is based on the experience gained with the EPR reactor and it mentions the consideration of local blockages. However they don't attribute any particular different importance to the TIB accident. They mention however that an improved early and reliable detection of the TIB accident is important to avoid the risk of core melt propagation and thus important to prevent a full core disruptive accident. Hence, the actual importance of the TIB accident in the licensing approach is still unclear in the open literature. But given the particular importance of the TIB accident's detection and the central position of blockage accidents detection in this PhD, we'll have a closer look to this particular

¹²Not unlikely the importance of these initiators was related to the experience with SPX and the Prototype Fast Reactor oil spill.

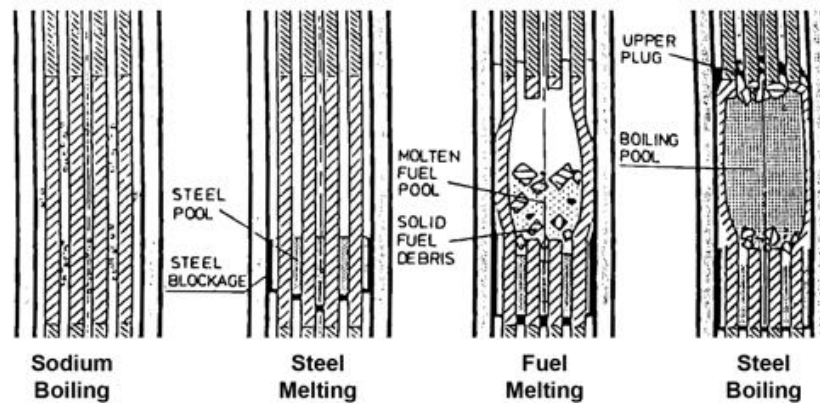


Figure 3.17: A schematic evolution of the Total Instantaneous Blockage accidental scenario [26].

accident.

3.6.4 The Total Instantaneous Blockage Accident

The Total Instantaneous Blockage (TIB) has been introduced because it is difficult to define and to evaluate all possible dangerous blockage accidents that can lead to melt propagation. Yet, as an envelope accident the TIB contains all smaller blockages that, if undetected, evolve to a full blockage by fuel melt propagation. The typical accident scenario is:

1. The fuel subassembly is completely blocked at the inlet during full power operation. There is no more coolant flow through the assemblies as the wrapper tube prevents mass exchange between two neighboring subassemblies.
2. The fuel subassembly is undercooled as no flow passes through it, while the power still has its nominal value. The sodium thus starts to heat up.
3. The sodium inside the fuel assembly starts to boil due to the heat up and the assembly eventually boils dry.
4. The fuel cladding starts to melt due to a total loss of cooling capacity in the assembly, eventually leading to fuel melting and even steel boiling.

This scenario is given in figure 3.17. It must be stressed that a TIB scenario is highly hypothetical due to the presence of coolant inlet ports at the subassemblies.

This is an important lesson learned from the Fermi-accident, that was actually a TIB-scenario at low power or a Total Initial Blockage. In this low power case, natural circulation regimes can be created inside the subassembly. These natural circulation regimes permit a transfer of the heat generated inside the assembly by condensation-evaporation mechanisms and they reduced the damage done to the Fermi-reactor. Thus the initiating event is practically eliminated. On top of that, there is no realistic cause to assume that a local blockage that leads to local fuel melting will quickly evolve to a larger part of the subassembly. In fact, the MOL-7C in-pile fuel melt experiments¹³ demonstrated that the propagation time in a subassembly is less than, but in the order of a minute.

The initial thermalhydraulic information of the TIB phenomena have been deduced from an out-of-pile loop experiment GR19BP (“Grappe à 19 aiguilles, bouchage en pied” or 19-pin assembly with an inlet blockage). However to simulate the fuel melt and possible propagation, an integral test with realistic nuclear heating and thus with a real fuel assembly is necessary. These experiments were part of the SCARABEE experimental program with its dedicated SCARABEE reactor. In fact the SCARABEE reactor was a light-water moderated open pool-type experimental reactor that contained the experimental loop. The driver core delivered the neutrons to the experimental loop’s test assembly and thus the nuclear power generated inside the test assembly. Inside the experimental loop, liquid sodium evacuated the heat generated by the fission reaction. For the TIB experiments, the flow was rapidly canceled by closing a valve at the inlet that started the accidental scenario. The reactor was obviously scrammed the moment the experimental objectives were attained or when certain safety issues arose.

The main lessons of the SCARABEE experimental program, extrapolated to a large power reactor like SPX, are:

- Sodium boiling set in very quickly.  After the blockage initiation, there are only about 2.5 seconds ~~between the onset of boiling and flow annulation.~~
- Not much later, about 2 seconds after boiling started, dryout occurs. In other words, the assembly boils dry at a specific location, leading to heat transfer degradation
- The fuel pin cladding starts to melt about 6 seconds after accident initiation, followed by fuel melting almost 5 seconds later.
- In the molten steel-fuel mixture heat is still being generated due to a continuing fission reaction in the molten fuel. This is possible because the neighboring fuel assemblies in the reactor still provide neutrons. As this mixture

¹³i.e. experiments in the pile, or the core, of a reactor

heats up, it eventually begins to boil at about 13 seconds from the accident's initiation.

- Due to the aggressive environment inside the fuel assembly, the steel wall of the fuel assembly (the hexcan) is attacked and eventually the boiling mixture melts through the hexcan about 2-3 seconds after the mixture starts to boil. The melt penetrates the neighboring bundle's hexcan and thus about 16-17 seconds after the initiating event, the accident propagates to the neighboring subassemblies.

Although these values are orders of magnitude taken from the work of Kayser and coworkers [26, 29] and their exact value depends more or less on a correct representation of the heat transfer between the blocked assembly and the by-pass flow in the inter-wrapper space. Yet, it is without question that the accident progression during a TIB is very fast. For a SPX-type reactor, the neutronic and thermal propagation limits were set at the second row of neighboring assemblies. This limit is reached about 30 seconds after accident initiation. Hence the plant protective system, assumed to remain operational due to its high reliability, should intervene before sufficiently early to stop the reactor before the second row of neighboring subassemblies is affected by the accident. A scram, i.e. an activation of the plant protective system¹⁴, is most likely to be triggered by the detection of a specific class of short-lived fission products that emit neutrons. Extrapolation of the detection time of this specific class of fission products, from the SCARABEE test with fresh fuel to a reactor system, should allow to attain a safe shutdown.

3.7 Conclusion

Sodium Fast Reactors that fission heavy metals with a fast neutron spectrum and that use sodium coolant to transport the heat generated in the core, can build upon a historical operating experience that resulted in great improvements relative to safety. Those improvements are of great benefit for this reactor type that can be deployed on the short term to consume a certain part of the nuclear waste created so far by the current reactor fleet. Fast reactor physics can however not exclude an energetic energy release during fuel melting, nor can fuel melting be excluded. Hence a set of accidental scenarios is used to evaluate and verify the protective systems put in place. One of those accidental scenarios demands for a good and reliable detection method to assure that it won't develop into an energetic release

¹⁴Actually SCRAM is the abbreviation of Shutdown Control Rod Axe Man, this is the person that had to cut a rope to drop a shutdown control rod inside the core of Chicago Pile-I (the first man-made critical mock-up). The abbreviation has however become a common used term for an emergency control rod drop.

scenario caused by a whole core melt. If this specific hypothetical accidental scenario is retained, such a detection method is important to comply with the requirements for the newest generation of nuclear reactors.

References

- [1] Alan Edward Waltar and Albert Barnett Reynolds. *Fast Breeder Reactors*. Pergamon Press, 1981.
- [2] DOE *Fundamentals Handbook: Nuclear Physics And Reactor Theory*. Number DOE-HDBK-1019/1-93. U.S. Department of energy, 1993.
- [3] R.R. Smith and D.W. Cissel. *Fast Reactor Operation in the United States*. In International Symposium on Design, Construction and Operating Experience of Demonstration LMFBR's, Bologna, Italy, April 10-14 1978.
- [4] Merle E. Bunker. *Early Reactors – From Fermi's Water Boiler to Novel Power Prototypes*, 1983.
- [5] J. G. Yevick and A. Amorosi, editors. *Fast Reactor Technology: Plant Design*. The M.I.T Press, 1966.
- [6] E.P. Alexanderson. *Fermi-I: New age for nuclear Power*. American Nuclear Society, 1979.
- [7] David Mosey. *Reactor Accidents: Institutional failure in the nuclear industry*. Number ISBN 1-903-07745-1. Nuclear Engineering International, 2nd edition, 2006.
- [8] L. Rahmani, S. Dechelette, and C. Bandini. *Unusual occurrences during LMFR Operation*, chapter SPX significant events and whether it would have happened on EFR. Number IAEA-TECDOC-1180. IAEA, October 2000.
- [9] A. Cruickshank and A.M. Judd. *Unusual occurrences during LMFR Operation*, chapter Problems Experienced during operation of the Prototype Fast Reactor, Dounreay, 1974-1994. Number IAEA-TECDOC-1180. IAEA, October 2000.
- [10] D. Mills. *Advances in solar thermal electricity technology*. Solar Energy, 76:19–31, 2004.
- [11] D.L. Katz, R.R. Miller, C.B. Jackson, R.M. Adams, E.C. Miller, H.F. Poppendiek, T. Trocki, I.R. Kramer, and R.N. Lyon. *Liquid-Metal Handbook*. Office of Naval Research, Department of the Navy, 2nd edition, January 1954.

- [12] *Liquid Metal Coolants for Fast Reactors Cooled by Sodium, Lead and Lead-Bismuth Eutectic*. Number NP-T-1.6. IAEA, 2012.
- [13] K. Künstler, H.-J. Lang, H. Heyne, V.D. Ananiev, E.B. Kirpikov, and Ju.V. Kulpin. *Monitoring and Control of impurities in the primary circuit of the IBR-2 reactor*. Journal of Nuclear Materials, 200:169–176, 1993.
- [14] R.B. Hinze. *Sodium Purity Requirements (A Review and Evaluation)*. Technical report, Liquid Metal Engineering Center, 1967.
- [15] J.K. Fink and L. Leibowitz. *Thermodynamic and Transport Properties of Sodium Liquid and Vapor*. Technical Report ANL/RE-95/2, Argonne National Laboratory, Reactor Engineering Division, January 1995.
- [16] Magnus Holmgren, *Matlab X Steam, Thermodynamic properties of water and steam, 2007*.
- [17] Yoshihiko Sakamotoa, Jean-Claude Garnier, Jacques Rouault, Christopher Grandy, Thomas Fanning, Robert Hill, Yoshitaka Chikazawa, and Shoji Kotake. *Selection of sodium coolant for fast reactors in the US, France and Japan*. Nuclear Engineering and Design, 254:194–217, 2014.
- [18] *La Centrale de Creys-Malville*. NERSA, 1984.
- [19] D. Tenchine. *Some Thermal Hydraulic Challenges in Sodium Cooled Fast Reactors*. Nuclear Engineering and Design, 240:1195–1217, 2010.
- [20] D. Tenchine, V. Barthel, U. Bieder, F. Ducros, G. Fauchet, C. Fournier, B. Mathieu, F. Perdu, P. Quemere, and S. Vandroux. *Status of TRIO_U code for sodium cooled fast reactors*. Nuclear Engineering and Design, 242:307–315, 2012.
- [21] Manuel Saez, Bernard Riou, and Michel Buchwalder. *The pre-conceptual design of the nuclear island of ASTRID*. In International Congress on Advances in Nuclear Power Plants (ICAPP 2012), Chicago, USA, June 24-28 2012.
- [22] *Fast Reactor Database*. IAEA, 2006.
- [23] R.T. Lahey and F.J. Moody. *The Thermal-Hydraulics of A Boiling Water Reactor*. American Nuclear Society, 2nd edition, 1993.
- [24] Hans K. Fauske. *The Role of Core-Disruptive Accidents in Design and Licensing of LMFBRs*. Nuclear Safety, 17(5):550–563, September-October 1976.

- [25] Gaston Kayser, Jean Charpenel, Claude Jamond, Georges Berthoud, and Karl Schleisiek. *Main SCARABEE lessons and most likely Issue of the sub-assembly blockage accident*. In International Meeting on Sodium Cooled Fast Reactor Safety, Obninks, October 1994.
- [26] G. Kayser, J. Charpenel, and C. Jamons. *Summary of the SCARABEE-N Subassembly Melting and Propagation Test with an Application to a Hypothetical Total Instantaneous Blockage in a Reactor*. Nuclear Science and Engineering, 128:144–185, 1998.
- [27] M. Drouin. *Feasibility Study for a Risk-Informed and Performance-Based Regulatory Structure for Future Plant Licensing*. Technical Report NUREG-1860, United States Nuclear Regulatory Commission, December 2007.
- [28] Stephane Beils, Bernard Carlucc, Nicolas Devictor, Gian Luigi Fiorini, and Jean François Sauvage. *Safety Approach and R&D Program for Future French Sodium-Cooled Fast Reactors*. Journal of Nuclear Science and Technology, 48(4):510–515, 2011.
- [29] G. Kayser and J. Papin. *The Reactivity Risk in Fast Reactors and the related international programmes CABRI and SCARABEE*. Progress in Nuclear Energy, 32(3/4):631–638, 1998.

4

Liquid Metal Boiling

*“There I found the souls of lords who had served my father and my brothers; some plunged in up to the hair of their heads, others to their chins, others with half their bodies immersed. These yelling, cried to me, ‘It is for inflaming discontents with your father, and our brothers, and yourself, to make war and spread murder and rapine, eager for earthly spoils, that we now suffer these torments in these rivers of boiling metal.’ ” **On the Origin of Dante’s Inferno, Curiosities of Literature***

*Isaac Disraeli
1835*

4.1 Introduction

Liquid metals are best known for their use in nuclear reactors, however they have also been used for solar energy applications (e.g. the ALMERIA single-tower, central receiver design [1]), aircraft engine cooling (during World War II) [2],... In all these applications an excellent heat removal rate is desired for extreme heat loads such that even peculiar coolants such as liquid metals are preferred over more common refrigerants. Nonetheless, it would seem that only in nuclear reactors the conditions for liquid metal boiling could be reached, as liquid metals boil commonly at temperatures as hot as hell. Thus with this reasoning it can be concluded that liquid metal boiling research started the moment liquid metal-cooled fast breeder

reactors were considered and that is was especially considered for accidental analysis.

Although this reasoning is completely logic, the liquid metal handbook [2] mentions that liquid mercury boilers were in commercial use in the United States since 1922. The Russian liquid metal boiling heat transfer textbook also mentions the study of mercury boiling in pre-war Soviet Russia [3], thus before the discovery of nuclear fission. Although it is difficult to imagine mercury boilers today due to its toxicity, but the use of mercury in power generation is actually quite rational. Today, a Combined Cycle Gas Turbine is a common high efficiency heat engine in which a Brayton-cycle¹ gas turbine is combined with a Rankine-cycle² that extracts heat from the exhaust gasses of the gas turbine. While experience with gas turbines is today well established, it wasn't so in 1922. Hence engineers looked at other means to design a high efficiency heat engine: a Rankine-Rankine Combined Cycle:

1. Liquid mercury absorbs the energy of the hot source and is evaporated. The resulting mercury vapor is expanded over a turbine and the vapor is condensed in the mercury condenser.
2. The mercury condenser is cooled by pressurized water and the water evaporated. The resulting water vapor is expanded over a turbine and the vapor is condensed.

Also Addison mentions the use of liquid metal (in this case potassium) boiling for a heat engine's topping cycle [4]. However, besides this historical introduction, we'll mainly focus on liquid metal boiling inside reactor systems after a small boiling fundamentals discussion that is of course applicable to any fluid.

4.2 Boiling Fundamentals

4.2.1 Nucleation

4.2.1.1 The Origin of Superheat

One of the most important microscopic phenomena during boiling is nucleation and it corresponds to the formation of a small vapor bubble and its growth under

¹In the ideal Brayton cycle, a pressurized non-condensable gas is heated under constant pressure after which it is expanded over a turbine. Under adiabatic work generation conditions this results in a temperature and pressure decrease.

²In the ideal Rankine cycle, a pressurized liquid is evaporated under constant pressure after which the vapor is expanded over a turbine. Under adiabatic work generation conditions this results in a temperature and pressure decrease. Under the adiabatic conditions a part of the vapor condenses, while the remaining vapor is condensed in a condenser section.

the influence of liquid superheat, i.e. the value of the liquid temperature above the liquid saturation temperature. This liquid superheat is necessary for the phase-change to occur, as can be deduced from the equilibrium formulation of a vapor bubble in an infinite liquid. Under an equilibrium formulation [5], the system that contains the vapor and the liquid have to attain a minimal Gibbs free energy G :

$$G = H - TS \quad (4.1)$$

that is the difference between the enthalpy H and the product of entropy S and temperature T . For the vapor-liquid system this Gibbs free energy can be written in term of specific quantities: specific Gibbs free energy (g_v, g_l) and the mass of vapor and liquid (m_v, m_l):

$$G = m_v g_v + m_l g_l \quad (4.2a)$$

$$dG = g_v dm_v + m_v dg_v + g_l dm_l + m_l dg_l \quad (4.2b)$$

Because of the conservation of mass ($dm_v = -dm_l$) the change in Gibbs free energy can be written as:

$$dG = (g_v - g_l) dm_v + m_v dg_v + m_l dg_l \quad (4.2c)$$

The change in Gibbs free energy of each phase can be written as:

$$dg_i = dh_i - T ds_i - s_i dT \quad (4.2d)$$

$$= -s_i dT_i + v_i dp_i \quad (4.2e)$$

where s_i is the specific entropy, h_i the specific enthalpy, v_i the specific volume and the pressure. These changes in specific Gibbs free energy are zero for an equilibrium given in figure 4.1. Because mechanical and thermal equilibrium demand an equal temperature and pressure, the equilibrium condition is easily satisfied:

$$g_v = g_l \quad (4.2f)$$

The latter conditions for this state can be summarized in the simple expression:

$$p_{v,\infty}(T) = p_{sat}(T_{sat}) \quad (4.3)$$

the liquid pressure equals the vapor saturation pressure for the phase equilibrium. However it becomes much more complicated for a curved surface. In this case, mechanical equilibrium demands that the curvature is taken into account in the force balance between the vapor and the liquid (see figure 4.1):

$$p_v \pi R^2 = p_l \pi R^2 + 2\pi R \sigma$$

where σ is the surface tension that represents the energy needed to form a unit surface between the liquid and its vapor. This unit surface is highly imaginary as in

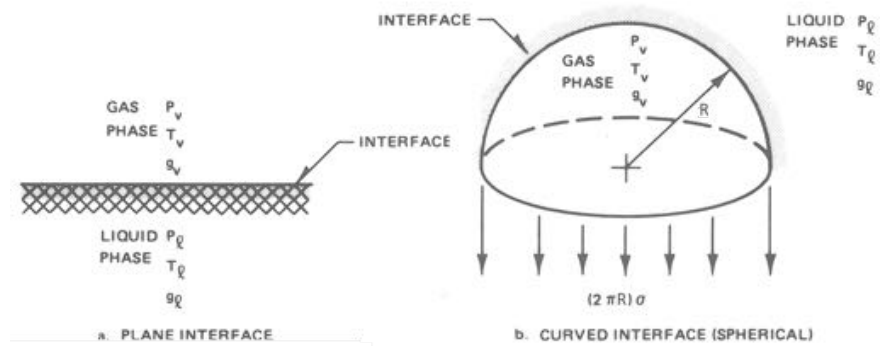


Figure 4.1: A Representation of the surface conditions for a plane and a spherical interface [5].

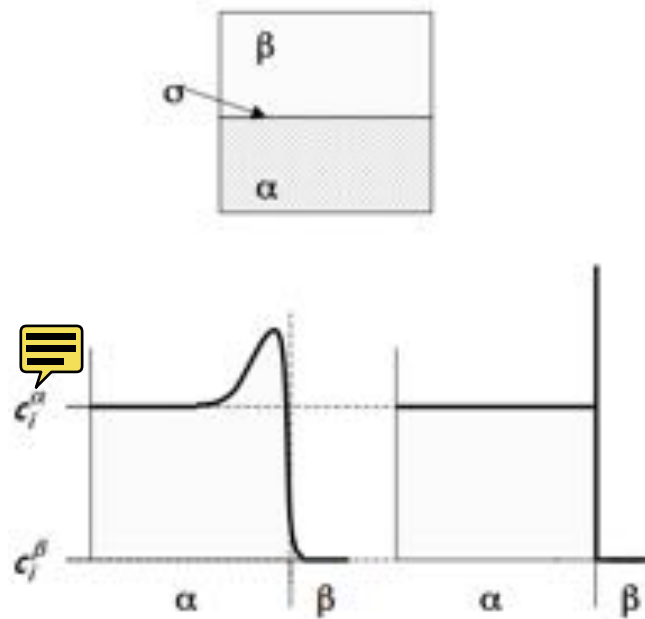


Figure 4.2: Left: realistic representation of the phase boundary. Right mathematical/thermophysical model of a phase boundary. [6].

reality there will be a molecular transition between vapor and liquid as represented in figure 4.2. Nonetheless, for a spherical surface, this surface tension leads to the Laplace equation for the mechanical equilibrium:

$$p_v = p_l + \frac{2\sigma}{R} \quad (4.4)$$

Hence the bubble's content is pressurized compared to the liquid. The thermal equilibrium still demands that the temperature is equal in the liquid and the vapor. The equilibrium in Gibbs free energy has also to be taken into account, which is less evidently satisfied due to the pressure difference:

$$g_v = g_l \quad (4.5a)$$

Or when taking the derivative:

$$dg_v = dg_l \quad (4.5b)$$

$$-s_v dT + v_v dp_v = -s_l dT + v_l dp_l \quad (4.5c)$$

And because dT is zero under equilibrium conditions: Taking into account the Laplace equation, one thus obtains;

$$v_v dp_v = v_l dp_v - v_l d\left(\frac{2\sigma}{R}\right) \quad (4.5d)$$

With the Laplace equation this becomes:

$$(v_l - v_v) dp_v = v_l d\left(\frac{2\sigma}{R}\right) \quad (4.5e)$$

With the assumption of a negligible specific liquid volume v_l compared to the vapor specific volume³, and by using the perfect gas law for one of specific gas-volumes:

$$p_{v,\infty} v_v = \mathcal{R}T$$

with \mathcal{R} the specific gas-constant (i.e. the molar gas constant divided by the molar mass):

$$-\frac{dp_v}{p_v} = \frac{v_l}{\mathcal{R}T} d\left(\frac{2\sigma}{R}\right) \quad (4.5f)$$

Thus the relation for the vapor pressure for a perfectly flat surface ($p_{v,\infty}$), and the vapor pressure above a spherical interface $p_{v,r}$ becomes:

$$p_{v,r} = p_{v,\infty} \exp\left(-\frac{2\sigma v_l}{\mathcal{R}RT}\right) \quad (4.5g)$$

³This approximation becomes invalid for pressures close to the critical pressure. Because the emphasis is on liquid metal boiling at typical reactor conditions, the approximation is acceptable.

This latter equation is often referred to as the Thomson equation in literature [7] and this finally leads to the difference between the flat interface equilibrium pressure and the liquid pool pressure p_l :

$$\begin{aligned}
 p_{v,\infty} - p_l &= (p_{v,\infty} - p_{v,r}) + (p_{v,r} - p_l) \\
 &= p_{v,r} \left(\exp \left[\frac{2\sigma v_l}{RR\bar{T}} \right] - 1 \right) + \frac{2\sigma}{R} \\
 &= \left(p_l + \frac{2\sigma}{R} \right) \left(\exp \left[\frac{2\sigma v_l}{RR\bar{T}} \right] - 1 \right) + \frac{2\sigma}{R} \\
 \text{☺} \quad p_{v,\infty} &= \left(p_l + \frac{2\sigma}{R} \right) \exp \left[\frac{2\sigma v_l}{RR\bar{T}} \right] \quad (4.6)
 \end{aligned}$$

It is directly clear that the temperature in the liquid has to be higher than the saturation temperature (T_{sat}) for a plane interface because $p_{v,\infty} > p_l$. To deduce this liquid superheating (T_{sup}) the Clausius-Clapeyron relation, with h_{lv} the latent heat of vaporization, is used:

$$\begin{aligned}
 \frac{dp}{dT} &= \frac{h_{lv}}{T(v_v - v_l)} \\
 \frac{h_{lv}}{T} dT &= \frac{\mathcal{R}T}{p} dp \\
 \int_{T_{sat}}^{T_{sup}} \frac{h_{lv}}{\mathcal{R}T^2} dT &= \int_{p_l}^{p_{v,\infty}} \frac{dp}{p}
 \end{aligned}$$

This has been solved in a two-step process by Kottowski and Grass [8]:

$$\int_{T_{sat}}^{T_i} + \int_{T_i}^{T_{sup}} \frac{h_{lv}}{\mathcal{R}T^2} dT = \int_{p_l}^{p_l + \frac{2\sigma}{R}} + \int_{p_l + \frac{2\sigma}{R}}^{p_{v,\infty}} \frac{dp}{p}$$

This leads to:

$$\Delta T_{sup} = \left(\frac{2\sigma}{R} \frac{v_l}{v_v} + \left(p_l + \frac{2\sigma}{R} \right) \frac{T_{sat}}{T_{sup}} \log \left(1 + \frac{2\sigma}{Rp_l} \right) \right) \frac{T_{sup}(v_v - v_l)}{h_{lv}} \quad (4.7)$$

☺ The first term is related to the increase of the boiling temperature due to a reduction of the vapor pressure by the curved interface. The second term is related to an increase of the boiling temperature by the capillary forces, i.e. the surface tension. Often the first term is negligible because of the small value of the specific liquid-to-vapor volume ratio (Kottowski [7] mentions that it is only important for superheats exceeding 250°C). The second term is often given by a simplified popular expression [3, 9]:

$$\Delta T_{sup} = \frac{2\sigma T_{sat} v_v}{R h_{lv}} \quad (4.8)$$

Properties	Sodium	Potassium	Mercury	Water
Approximate T_{sat} ($^{\circ}\text{C}$)	900	800	366	100
Vapor density (kg/m^3)	0.33	0.69	3.77	0.60
Surface Tension (N/m)	0.13	0.07	0.04	0.06
Heat of Vaporization (kJ/kg)	3736	1933	296	2256
Superheat ΔT_{sup} ($^{\circ}\text{C}$)	24.7	11.3	4.6	3.3

Table 4.1: The Superheat properties for liquid metals compared to water, for a bubble with a size of $10\ \mu\text{m}$ at atmospheric pressure. The liquid metal properties were taken from the appendix in the book by Subbotin et al. [3]. The saturated properties of water at 100°C are taken from the XSteam library [11].

This expression can only be considered for a relatively large initial bubble of radius r , and only then, as otherwise the exact expression of equation 4.7 can not be approximated by $\log(1+x) \approx x$ (an important point put forward by Giot [10]). Nonetheless for the general conclusions, equation 4.8 is more intuitive and this expression is used to evaluate the superheat dependencies:

- The superheat increases with:
 - The saturation temperature T_{sat} .
 - The surface tension between the vapor and the liquid σ
 - The specific vapor volume v_v
- The superheat decreases with:
 - The bubble radius R .
 - The latent heat of vaporization h_{lv} .

To put this in perspective, table 4.1 gives these properties and the resulting superheat for a $10\ \mu\text{m}$ bubble for different liquid metals and water. It is clear that liquid metals have the tendency for a higher liquid superheat in comparison to water at atmospheric pressures. This is in particular due to their higher saturation temperature.

4.2.1.2 Homogeneous vs. Heterogeneous Nucleation

In the previous section it was assumed that the initial bubble is already present. However, this isn't always the case and the first bubble has to be created. This is possible by spontaneous formation of a nucleation site by means of energy fluctuations in the liquid. This often leads to very high superheats as the fluctuation energy needed to form a void-nucleus with radius r_k , corresponding to a certain

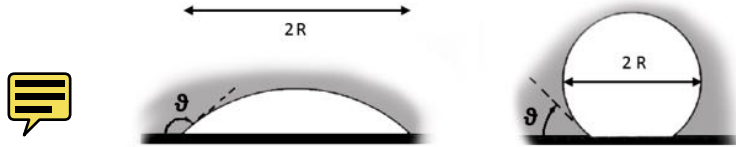


Figure 4.3: Typical conditions at a flat solid interface with an attached bubble. Left: Non-wetted surface ($90^\circ < \theta < 180^\circ$). Right: Wetted surface ($0^\circ < \theta < 90^\circ$).

superheat:

$$E_b = \frac{4}{3}\pi\sigma r_k^2$$

$$\propto \frac{1}{\Delta T_{sup}^2}$$

increases with the critical radius r_k and thus decreases with superheat when substituting equation 4.8. Because very high superheats aren't present for the boiling behavior of e.g. water, the homogeneous superheat is quite unlikely. Due to the fact that liquids are often contained between surfaces, the effect of the surface has to be taken into account for the superheat. For a completely flat surface, we can identify two conditions, as given in figure 4.3:

- For poor wetting ($90^\circ < \theta < 180^\circ$) behavior the condition in equation 4.8 becomes:

$$p_v \pi R^2 = p_l \pi R^2 + 2\pi\sigma R \sin(\theta)$$

$$\Delta T_{sup} = \frac{2\sigma T_{sat} v_v \sin(\theta)}{R h_{lv}}$$

Hence for a poor wetted surfaces the superheat could be reduced significantly.

- For well wetted surfaces ($0^\circ < \theta < 90^\circ$) the condition in equation 4.8 becomes:

$$(p_v - p_l) 2\pi R^2 \int_0^{\pi-\theta} \sin(\theta) d\theta = \frac{2\sigma}{R} 2\pi R^2 \int_0^{\pi-\theta} \sin(\theta) d\theta$$

$$\Rightarrow \Delta T_{sup} = \frac{2\sigma T_{sat} v_v}{R h_{lv}}$$

This thus doesn't result in a reduction in superheat as for a poor wetted surface.

A flat surface is of course an approximation of the reality as the surface of any structures contains defects that form small cavities of conical, cylindrical or slotted shape that can reduce the superheat even for well wetted surfaces. Thus the

presence of a surface with small imperfections already explains partially the reduced superheats observed for actual boiling. Due to the nucleation at a surface, the phenomenon is termed heterogeneous nucleation.

Another possible heterogeneous superheat reduction comes from the non-condensable gasses in the liquid. Due to the presence of dissolved gasses in the liquid, the law of Henry implies that at any surface there must be a partial gas pressure (p_g) corresponding to the mole fraction of dissolved gas (x_g), or with Henry's law:

$$p_g \propto x_g$$

This is also valid at the bubble surface and changes the mechanical equilibrium equation 4.4 to:

$$p_v + p_g = p_l + \frac{2\sigma}{R} \quad (4.9)$$

Hence condition 4.8 can be reduced to:

$$\Delta T_{sup} = \frac{T_{sat} v_v}{h_{lv}} \left(\frac{2\sigma}{R} - p_g \right) \quad (4.10)$$

Of course interaction between the possible heterogeneous nucleation phenomena is possible, e.g. nucleation at a flat surface or cavity in the presence of non-condensable gasses.

The previous developments are valid for any liquid. But whilst it is common knowledge that water starts to boil with insignificant superheat, this observation can not directly be extrapolated to liquid metals. The best example is mercury. Mercury unlike water doesn't wet metallic surfaces, thus reducing the superheat at a heating surface. For the mercury boilers, alloying elements were necessary to obtain a better initial liquid-solid contact and associated heat exchange. Nonetheless, the moment boiling started, the preference of the vapor to attach to the wall led to typical unstable film boiling behavior i.e. a non-stable vaporous film separated the liquid and the solid [12].

4.2.1.3 Nucleation of Liquid Sodium

Although mercury is a good example for the difference in microscopic behavior, mercury isn't the coolant of interest in this study. It is sodium and its properties under typical reactor operation that are most important.

The Superheat Problem We have already seen in table 4.1 that the liquid sodium has a tendency for rather high superheats for homogeneous nucleation. To determine which nucleation mechanism is dominant, we should look at the wetting behavior on typical reactor materials. Figure 4.3 show the equilibrium wetting angle

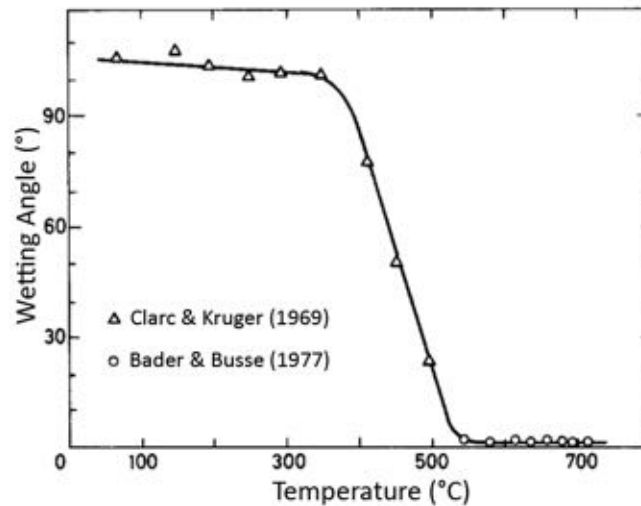
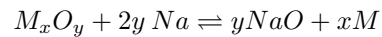


Figure 4.4: Typical equilibrium wetting angle on a 304L stainless steel surface for liquid sodium [13].

on a stainless steel surface. Although this equilibrium wetting angle is for 304L Stainless Steel, this behavior is typical for sodium: for a certain temperature the wetting angle drops to zero. This phenomenon is related to the sodium-protective oxide layer interaction at the steel surface:



In general the metal M is reduced by the reactive sodium. This reaction has an equilibrium concentration, hence explaining the use of an equilibrium contact angle. Because the equilibrium contact angle is reached when the chemical reaction attains an equilibrium, sodium wetting is time-dependent (typical time constants of several hours intervene). Nonetheless for sodium-cooled fast reactors, the typical heating surfaces are at temperatures above 500°C and the residence time is sufficient to assume a zero wetting angle with flooded cavities. This would indicate that homogeneous nucleation is the dominant nucleation phenomenon.

This tendency for homogeneous nucleation and the tendency for high superheats led to the conclusion that high superheats occur at the onset of boiling [14]. This was furthermore confirmed by early experimental results of small and relatively simple boiling experiments. This led to intensive studies to deduce the bubble growth rate at the onset of boiling. Or better, the slug growth rate at the onset of boiling. This slug growth determined the vapor volume fraction in the reactor core as a function of time. Because early large reactor cores had a positive (and often

relatively large) void reactivity coefficient, this gave the rate of reactivity increase in the reactor system. This reactivity insertion rate translates in a power ramp rate. Because slug growth and superheat are related, it was important to determine the superheat and the associated power ramp rate to determine boiling accident consequences. Due to the random nature of superheat, as it depends among others on the energy fluctuations in the liquid, this led sometimes to confusing and often conflicting experimental conclusions. Nonetheless Kottowski [7] mentions that parameters such as pretest history, the wall material, the heat flux, the temperature ramp rate, the liquid metal purity, . . . influence the boiling inception superheat.

Due to the importance of the superheat and the maximal ramp rate associated to it, theoretical studies were initiated on the subject. One of the most interesting theoretical studies is given by Claxton [15]. Claxton considered the energy necessary to form the void-nucleus and to fill that void-nucleus with vapor, leading to a stable nucleus. The energy required is thus the formation energy of the void (first term) and the evaporation energy of the mass inside the bubble (the second term):

$$E_b = \frac{4}{3}\pi r_k^2 \sigma + \frac{4}{3}\pi r_k^3 \rho_v h_{lv}$$

The neutrons in a nuclear reactor will transfer a part of their energy to the coolant. If this transferred energy over a path of the order of magnitude of an equivalent bubble diameter ($2r_k$) equals the energy necessary for vapor nucleus formation, nucleation and boiling will follow. Radiation is thus a limiting factor for the superheat in nuclear reactor systems. Although Claxton concluded that it was unlikely that nucleation would initiate by radiation before surface cavities activated, it is important to know that even for perfect wetting behavior a limiting mechanism exists. Without going into the details of Claxton's analysis, it is clear that only radiation that loses its energy over a limited distance can be considered or the linear energy loss:

$$-\frac{dE}{dx}$$

should be high. This is exactly the definition of high LET (Linear Energy Transfer)-radiation: High energy neutrons (of which there are plenty in fast reactor systems), α -particles, energetic fission fragments⁴, . . .

During the development of fast reactors, more sophisticated experimental devices were designed. These devices led to the surprising result of practically inexistent superheat [16].

⁴The energy of the fission reaction, about 200MeV, is distributed between a discrete number of neutrons and a discrete number of fission fragments. The highest fraction of the energy is carried by the fission fragments.

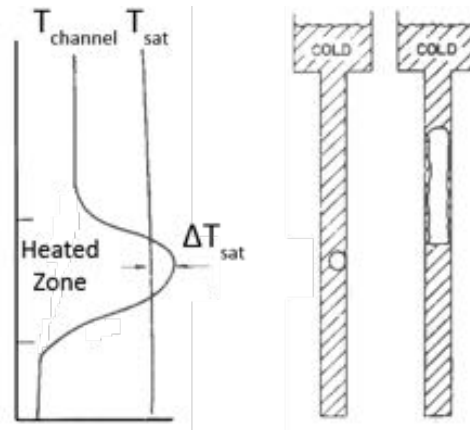


Figure 4.5: The typical expulsion behavior with a small fraction of the channel superheated as given in the temperature graph on the left. On the right side, the nucleation of a bubble is given that rapidly grows to a slug in the channel and forces the liquid out. From Van Erp [21].

Beyond the Superheat Recent sources still mention the superheat as being factual [17, 18], research is still conducted on the subject of superheat [19] and even at a very recent conference a superheat study was presented [20]. The tendency to mention the superheat at boiling inception is not surprising, most sodium boiling literature is dedicated to the subject. However, fewer articles like that of Seiler [16] mention very explicitly that high superheat has never been observed for relatively slow heating experiments in convective boiling loops. The reference to slow transients must be seen in comparison to experiments that simulated TOP-accidents with a very high ramp rate. Although there is no reason to question these observations, a clear and sound demonstration is necessary before a conclusion can be formulated with confidence. This confidence is necessary as the slug-like expulsion (given in figure 4.5) generates high pressure waves that are relevant to the acoustic noise generated during boiling. A first hint to the nucleation and inexistent superheat is given by Fauske [14], referring to a study of Thormeier [22]: the presence of a pre-existing gas phase.

Thormeier (and Veleckis [23]) deduced the solubility of non-condensable gasses like argon or helium in liquid sodium. The results can be summarized in a Henry law, with a temperature dependent Henry constant k_H as given in appendix B:



$$\begin{aligned}
 x_g &= p_g k_H \\
 &= p_g \cdot 5.49 \cdot 10^{-3} \exp(-10055 K/T)
 \end{aligned}
 \tag{B.8}$$

Hence any cavity at a heated wall, **thus** with a wall temperature T_w higher than the bulk temperature T_b , $T_w > T_b$, will have a wall equilibrium dissolved gas concentration corresponding to the gas pressure at the cavity and the local temperature (neglecting any equilibrium gas pressure decrease at a curved surface):

$$\begin{aligned} x_w &= \left(p_l + \frac{2\sigma}{r^*} - p_v(T_w) \right) 5.49 \cdot 10^{-3} \exp(-10055 K/T_w) \\ &> (p_l - p_v(T_b)) 5.49 \cdot 10^{-3} \exp(-10055 K/T_b) \\ &= x_b \end{aligned}$$

The cavities equivalent radius r^* is introduced to take into account the reduction in the capillary pressure at a cavity, without specifying the cavity. It is evident that for low vapor pressures, the wall concentration (x_w) is higher than the bulk (x_b) and by means of diffusion the gas in the cavity will go into solution, decreasing the gas pocket's size and the entire wall will thus be wetted by the liquid sodium. Thus even this observation tends to argument in favor of homogeneous nucleation theory as the sodium will tend to clean the surface of initially trapped gas pockets.

However, if gas bubbles were to exist continuously in liquid sodium, the superheat wouldn't be an issue. And it is just this that is mentioned by Thormeier. In a reactor or even a hydraulic sodium loop, a cover gas is present:

- At this cover gas the sodium is at its highest temperature  his high temperature corresponds to a high equilibrium concentration.
- The hot sodium always passes through a heat exchanger in thermalhydraulic loops, thus decreasing the temperature and decreasing the equilibrium concentration.
- The cold sodium is thus supersaturated in dissolved gas, resulting in the nucleation of small non-condensable bubbles.
- The non-condensable bubbles dissolve again due to the increase in temperature.

As an image says more than words, this process is conceptually visualized in figure 4.6. Additionally, there are several bubble entrainment processes in forced convection loops and reactor systems that create additional bubbles: vortices at the cover gas liquid free surface, small helium leaks from the control and fuel pins, . . . To verify the continued presence of bubbles, the non-condensable lifetime is analyzed.

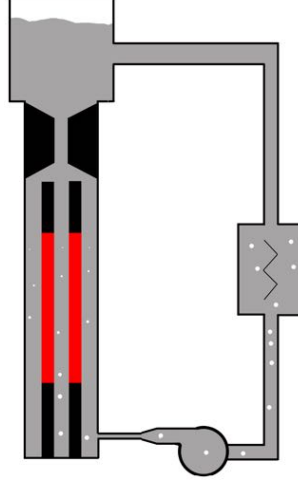


Figure 4.6: A conceptual visualization of the non-condensable behavior in a thermal hydraulic sodium loop.

Non-Condensable behavior It is interesting to note that a free bubble in liquid sodium is thermodynamically unstable due to the capillary pressure, again assuming that no differences in the equilibrium occur due to a curved surface:

$$p_{g,b} = p_l + \frac{2\sigma}{R} > p_l > \frac{x_g}{k_H}$$

It should thus normally dissolve spontaneously. For simplicity, we assume a stationary bubble and the diffusion process can be easily written in the form of Fick's law (with the diffusion coefficient D given by the liquid viscosity η_l , the Boltzmann constant k_b and the atomic radius of argon r_{Ar} : $\frac{k_b T}{6\pi\eta_l r_{Ar}}$) for spherical coordinates:

$$\frac{\partial x_g}{\partial t} = D \left(\frac{\partial^2 x_g}{\partial r^2} + \frac{2}{r} \frac{\partial x_g}{\partial r} \right) \quad (4.11a)$$

with an initial mole fraction at the bubble surface of x_r^0 and a constant mole fraction far away from the bubble x_b , this leads to an equation for $\Delta x_g = x_g - x_b$:

$$\frac{\partial(r \Delta x_g)}{\partial t} = D \frac{\partial^2(r \Delta x_g)}{\partial r^2} \quad (4.11b)$$

this is a typical one-dimensional equation for which the solution can be found in classical text books for idealized temperature and/or mass diffusion problems [24, 25]:

$$r \Delta x_g = r_b (x_r^0 - x_b) \left(1 - \operatorname{erf} \left(\frac{r - r_b}{2\sqrt{Dt}} \right) \right) \quad (4.11c)$$

or

$$x_g(r) = x_b + \frac{r_b}{r}(x_r^0 - x_b) \left(1 - \operatorname{erf} \left(\frac{r - r_b}{2\sqrt{Dt}} \right) \right) \quad (4.11d)$$

This equation is still in units of moles of gas per mole mixture. As the dissolved gas doesn't actually contribute to the volume, we can easily deduce the concentration:

$$c_g = x_g \frac{\rho_l}{M_{Na}}$$

where M_{Na} is the molar mass of sodium. The concentration defined as such is given in units of moles per unit of liquid volume. The outflow in units of mole/s is thus given by:

$$\frac{\partial n_g}{\partial t} = -4\pi r_b^2 D \left. \frac{\partial c_g}{\partial r} \right|_{r=r_b} \quad (4.11e)$$

$$= 4 \left(\left. \frac{k_H \rho_l}{M_{Na}} \right|_b p_g - \left. \frac{k_H \rho_l}{M_{Na}} \right|_l p_l \right) \left(\pi D r_b + \sqrt{\pi D/t} r_b^2 \right) \quad (4.11f)$$

$$\approx 4 \left. \frac{k_H \rho_l}{M_{Na}} \right|_b p_g \left(\pi D r_b + \sqrt{\pi D/t} r_b^2 \right) \quad (4.11g)$$

The approximation is justified because the pressure $p_l < p_g$ and because Henry's constant k_H will be much smaller for the temperature far away from the bubble due to its exponential dependency (see equation B.8). Assuming that the perfect gas law is valid inside the bubble, a bubble radius can be associated to the amount of gas in the bubble. This leads, after integration, to:

$$r_b(t_{i+1}) = \left(1 - \frac{\Delta n_g}{n_g(t_i)} \right)^{1/3} \left(\frac{T(t_{i+1})}{T(t_i)} \right)^{1/3} \left(\frac{p_l + \frac{2\sigma(T(t))}{R} - p_v(T) \Big|_{t_i}}{p_l + \frac{2\sigma(T(t))}{R} - p_v(T) \Big|_{t_{i+1}}} \right)^{1/3} r_b(t_i) \quad (4.11h)$$

Thormeier used these equations to determine the non-condensable behavior for several initial bubble sizes, with either argon or helium, as a function of a defined temperature ramp rate. From this he concluded that helium is better to be avoided as a cover gas, because helium bubbles dissolved independent of the initial radius.

Nowadays, we know that bubbles between 10 and 100 μm are present inside the liquid sodium [26]. We take the maximum bubble radius as an initial bubble radius and evaluate its response to different heating transients. This then results in bubble behavior as given in figure 4.7 for heating transients with different ramp rates associated to a thermal time constant:

$$T = T_0 + \frac{T_b - T_0}{\tau_{th}} t$$

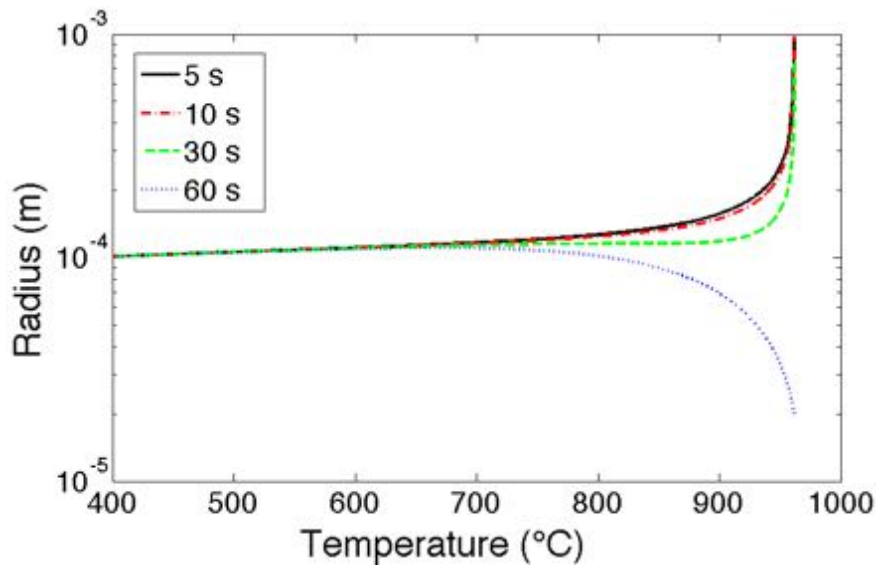


Figure 4.7: The non-condensable bubble behavior in liquid sodium as a function of temperature and the heat-up rate to the boiling point at atmospheric pressure, for an initial bubble of $100\ \mu\text{m}$ at 380°C , according to the model of Thormeier.



One of that major assumptions of Thormeier's model is the use of the normal diffusion equation. Hence the bubble's transient is calculated by a quasi-steady-state approach with a negligible interface velocity and associated fluid flow. To verify this hypothesis, the bubble's interface velocity $\frac{dR}{dt}$ is given in figure 4.8. This figure clearly shows that the quasi-steady-state approach is valid, at least as long as boiling nucleation doesn't intervene.

The annihilation of superheat and the stabilization of boiling by non-condensable gas is also identified in a solar system alkali-metal pool-boiler. Although the use of a liquid metal boiler seems strange for solar systems, the excellent heat transfer characteristics of liquid metals reduces thermal non-uniformities, pressures, . . . hence increasing the lifetime and cost efficiency of solar boilers. Moreno [27] mentions that xenon gas reduced the temperature oscillations during boiling and increased the hot-standby restart reliability (especially important for a solar boiler when a cloud passes that temporarily reduces the heat load). Hence nucleation sites were present to prevent large superheat and temperature oscillations between two superheating events. Moreno also mentions that xenon is especially effective to do so, as helium for example will not be entrained because of buoyancy issues.

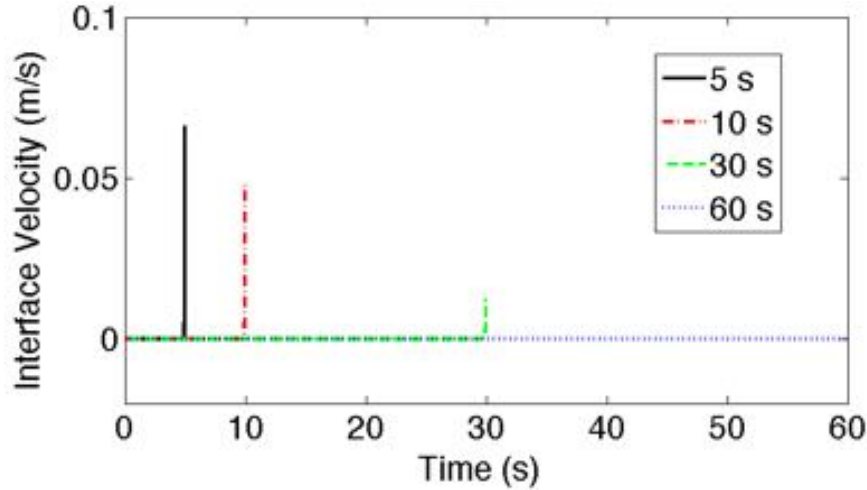


Figure 4.8: The non-condensable bubble's interface speed in liquid sodium as a function of time and the heat-up rate to the boiling point at atmospheric pressure, for an initial bubble of $100\ \mu\text{m}$ at 380°C , according to the model of Thormeier.

Nucleation Conclusions The theory of Thormeier, although approximate, clearly shows that all initially present bubbles will dissolve for very slow heating transients and high boiling inception superheats will most likely follow. Such slow heating transients can be imagined for the early simple experiments. This explains the occurrence of high superheats for the earlier experiments, whereas more modern experimental loops are reported not to show this behavior. We can however not verify this theory experimentally as there are no liquid metal boiling loops operational at the time of writing. We can only rely, with a critical attitude, on the literature and the knowledge of former liquid metal boiling experts.

4 Condensation-Evaporation Heat Transfer

The evaporation heat transfer for liquid sodium at the microscopic level has often been described by non-equilibrium formulations [28, 29]. These formulations are able to capture the rapid heat and  transfer processes that are associated with the high superheat incipient boiling, and as such they were useful to deduce a best estimate for the bubble expulsion behavior. One of the simplest and most often encountered formulation in literature is the classic Hertz-Knudsen formula for the mass flux (\dot{G} - units of $\text{kg}/(\text{m}^2\ \text{s})$) at a plane vapor-liquid interface:

$$\dot{G} = \frac{\beta}{\sqrt{2\pi\mathcal{R}}} \left[\frac{p_{sat}}{\sqrt{T_{sat}}} - \frac{p_v}{\sqrt{T_v}} \right] \quad (4.12)$$

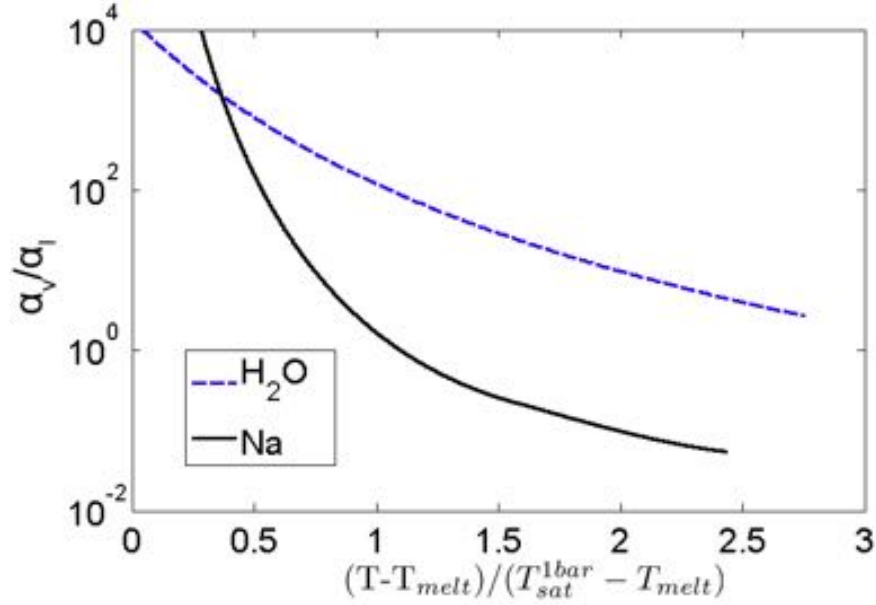


Figure 4.9: The thermal diffusivity ratio of the vapor and liquid of saturated water and sodium as a function of a dimensionless temperature: $(T - T_{melt})/(T_{sat}^{1bar} - T_{melt})$, with T_{melt} the reference melting temperature.

with \mathcal{R} the specific gas constant, p_{sat} the saturation vapor pressure (and associated saturation temperature T_{sat}) at the plane interface, β the so called evaporation/condensation/accomodation coefficient from kinetic theory [30]. p_v and T_v represent the actual vapor pressure and vapor temperature. With this formulation $\dot{G} > 0$ represents a mass transfer from the liquid to the vapor.

Equation 4.12 can also be seen as an additional heat transfer resistance that is associated with the liquid-vapor interface. In this regard non-equilibrium formulations become especially important for the condensation of liquid metals. This latter is mainly related to the similar thermal diffusivity of the vapor and the liquid, which is typical for liquid metals (see figure 4.9). This can be easily understood by considering the definition of the thermal diffusivity α as defined by Lienhard and son [25]:

The thermal diffusivity is a measure of how quickly a material can carry heat away from a hot source. Since material does not just transmit heat but must be warmed by it as well. The thermal diffusivity involves both the thermal conductivity and the volumetric heat capac-

ity.

And although this definition gives a vague qualitative idea, we take a look to the dimensionless unsteady heat transfer analysis included in many standard textbooks on heat transfer to get a more a qualitative understanding. The dimensionless unsteady heat diffusion equation can be written as:

$$\frac{\partial \Theta}{\partial \chi} = \frac{\partial \Theta}{\partial Fo} \quad Fo = \frac{\alpha t}{L} \quad (4.13)$$

Where Θ is a dimensionless temperature, χ is a dimensionless length and Fo is the Fourier number that takes the form of a dimensionless time-scale. Hence for a stationary vapor bubble in liquid sodium, when there is no real coolant flow during the earliest phases of the collapse, the system could be solved by a unique diffusion equation (the diffusivity of vapor and liquid is as good as equal for atmospheric pressures). For a steam bubble in water, the superior heat diffusivity of the vapor will lead to a higher Fourier number in the vapor. The temperature will thus faster diffuse through the vapor, and its temperature can be assumed to be constant on time-scales necessary for the heat to diffuse through the liquid.

The high and almost equal thermal diffusivity of the vapor and the liquid can also lead to a temperature drop at the vapor-liquid interface greater than the temperature drop in the liquid and vapor [31, 32]. The resistance due to the liquid-vapor interface was first hypothesized after researchers found a condensing heat transfer rate for liquid metals, which was significantly lower than the classical Nusselt result [33], even with the low Prandtl-number corrections (that apply to liquid metals) as calculated by Sparrow and Gregg [34]. This can be seen in figure 4.10 that was reconstructed from Misra and Bonilla's sodium condensation data [35] and from the correlation deduced by Shu [36] for the Sparrow and Gregg data. From such observations, it was possible to deduce the value of the β coefficient. For liquid metals, numerous sources [30, 37, 38] mention that this coefficient should be equal to one. Any deviation from one would be caused by vapor subcooling [38], measurement errors [37] or trace non-condensables [39]. Kochurova gives another theory [40]: Sodium, as a pure metal should have a β coefficient of one. However, even nuclear grade sodium contains impurities that might change the surface tension ($\Delta\sigma$). Hence an activation energy for condensation/evaporation is introduced. This activation energy translates into a reduction of the β coefficient that can be modeled by:

$$\beta = \exp\left(-\frac{\Delta\sigma M_{Na}^{2/3}}{\rho_l^{2/3} N_{av}^{2/3} k_b T}\right) \quad (4.14)$$

with N_{av} the avogadro number, M_{Na} the molar mass and k_b the Boltzmann constant. This formulation can also explain that significant deviations from unity only

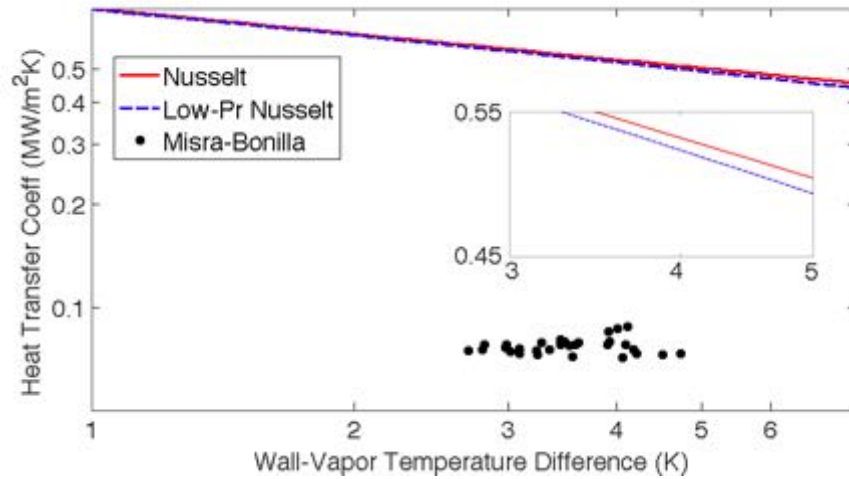


Figure 4.10: The experimental data of Misra and Bonilla for condensing sodium [35] compared to the original Nusselt theory and the low Prandtl number corrections. Notice the small corrections for the small temperature differences under consideration.

occur at higher vapor pressures. But taking into account that we can only expect deviations of the order of a few percents for the surface tension, we can calculate the variation of the β coefficient similar to Kochurova. The following has to be taken into account to obtain similar results:

- If all properties are taken temperature dependent, the β coefficient would increase with increasing vapor pressure.
- The surface tension ($\Delta\sigma$) and the temperature (T) are taken at the condenser temperature, for our calculations: 1153 K. These values are therefore fixed, which is logical because the thermal resistance of the liquid metal can be neglected.
- The vapor pressure only influences the condensate molecular surface:

$$\left(\frac{M_{Na}}{\rho_l N_{av}} \right)^{2/3} \quad (4.15)$$

The result is given in figure 4.11. But given the possible variation of the surface tension (see appendix B), it is reasonable to conclude that the β coefficient can be taken equal to 1.

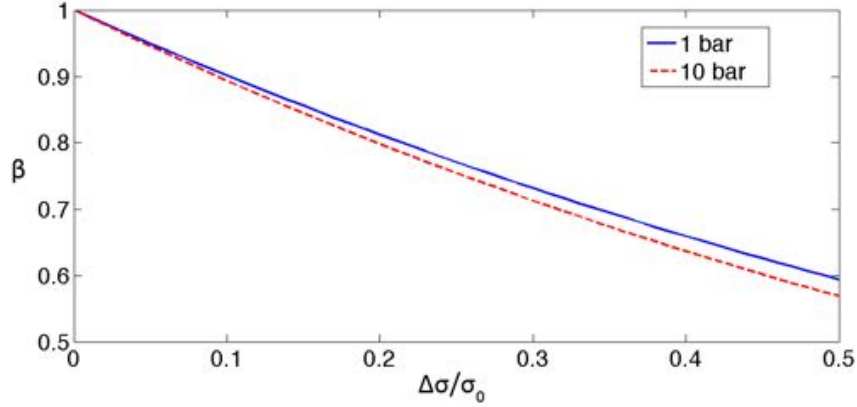


Figure 4.11: The β condensation coefficient calculated according to the model of Kochurova as a function of vapor pressure and relative surface tension change at the 1153.2K (the saturation temperature at 1 bar).

The interface heat transfer resistance can also be written as an interphase heat transfer coefficient (h_i) given by:

$$h_i = \frac{2\beta}{2-\beta} \sqrt{\frac{1}{2\pi\mathcal{R}} \frac{h_{lv}^2 p_{sat}}{T_{sat}^{2.5} \mathcal{R}}} \quad (4.16)$$

This formula, derived from Schrage's theory, becomes:

$$h_i = \sqrt{\frac{2}{\pi\mathcal{R}} \frac{h_{lv}^2 p_{sat}}{T_{sat}^{2.5} \mathcal{R}}} \quad (4.17)$$

when taking into account the previous discussion. An important fact is that it is this interface resistance that has been retained as a constitutive equation in the computer analysis code SABENA [41], as it should from the theoretical point of view.

4.3 Subassembly Boiling

4.3.1 Introduction

The standard works on liquid metal boiling [3, 12] include a discussion on the typical pool boiling curve, discovered in 1934 by Nukiyama, i.e. the curve that describes the boiling phenomena of stagnant liquid in contact with a heated surface. Although the phenomena inside a subassembly differ due to the flow and the constraint geometry, as can be seen in figure 4.12, it is interesting to explain

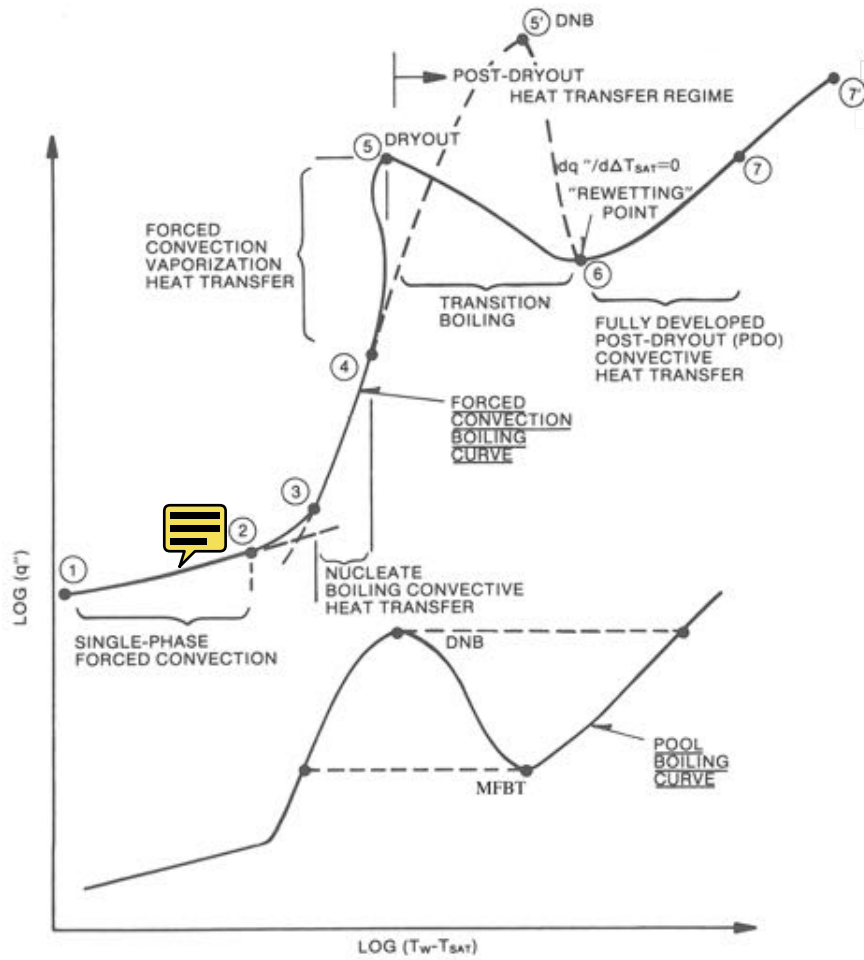


Figure 4.12: The boiling heat transfer curve from Lahey and Moody [5].

and quantify certain phenomena: the Critical Heat Flux (CHF) or departure from nucleate boiling transition; and the minimum film boiling temperature (MFBT).

4.3.1.1 Departure of Nucleate Boiling Heat Flux

The Departure of Nucleate Boiling (DNB) Transitions is given in figure 4.12 and is a heat flux imposed transition i.e. for a certain heater power, nuclear reactor neutron density, ... The phenomenon is an important limiting factor for LWRs as the heat transfer changes from nucleate boiling at the wall to film boiling at the heated wall. During film boiling a thin vapor layer separates the heated wall from the liquid and heat transfer is severely degraded as can be seen by an increase of the wall temperature due to this transition in figure 4.12.

Subbotin [3] discusses this phenomenon and gives some quantitative information on the basis of correlations based on experimental data. The experimental data was obtained from boiling experiments without the presence of argon, and the results are thus prone to superheat phenomena and unstable boiling, it can nonetheless be concluded that very high heat flux values can be obtained at atmospheric pressure: a value of $3.58 MW/m^2$ can be deduced with Subbotin's correlation that gives the most accurate results for atmospheric pressure according to Ishii [42]:

$$q''_{cr} = 0.14 \left[1 + \frac{C}{p_{cr}} \left(\frac{p}{p_{cr}} \right)^{-0.4} \right] \rho_v h_{lv} \left[\frac{\sigma g \Delta \rho_{lv}}{\rho_v^2} \right]^{1/4} \quad (4.18)$$

where the values of $C = 45 atm$ and $p_{cr} = 357 atm^5$ have been used by Subbotin to correlate the experimental data to the typical Kutateladze expression for q''_{cr} . This correlation is only for steady boiling: unsteady boiling has a lower C-value that results in a reduced critical heat flux ($2.36 MW/m^2$).

4.3.1.2 Minimum Film Boiling Temperature

The minimum film-boiling temperature T_{min} corresponds to the wall temperature at which the transition boiling regime changes into a stable film boiling regime. It is thus for an imposed heated surface temperature. An imposed heater temperature occurs during the quench of forged metal, the quench of heated fuel assemblies after a loss of cooling and the interaction between molten fuel and the coolant. The film boiling has been characterized by several authors:

- Farahat et al. [43] immersed pre-heated tantalum spheres in a pool of liquid sodium. Although his results are of a transient nature, they can be qualitatively applied to a steady state. From his experimental data, the following

⁵This was the value for the critical pressure available to Subbotin



correlation was deduced for the MFBT:

$$T_{min} = 1593.6K + 12.2(T_{sat} - T_{Na}) \quad (4.19)$$

- Zimmer et al. [44] performed a similar experiment with molten alumina (Al_2O_3) and found the following correlation for the MFBT:

$$T_{min} = 1600K + 7.2(T_{sat} - T_{Na}) \quad (4.20)$$

Although these correlations are simple in use, they can not necessarily be extended to other liquid metals or other solid/molten contact surfaces. A first analytical hydrodynamic approach to the MFBT has been given by Berenson [45]:

$$T_{min}^I - T_{sat} = 0.127 \frac{\rho_v h_{lv}}{k_v} \left[\frac{g(\rho_l - \rho_v)}{(\rho_l + \rho_v)} \right]^{2/3} \left[\frac{\sigma}{g(\rho_l - \rho_v)} \right]^{1/2} \left[\frac{\mu_v}{(\rho_l - \rho_v)} \right]^{1/3} \quad (4.21)$$

However at the minimal film boiling temperature local perturbations might cause vapor collapse and thus generate cold spots due to local cooling, invalidating the isothermal surface hypothesis for the Berenson correlation. To give an estimate of the importance of these local cold spots, Henry [46] proposed an analytical expression to evaluate the temperature drop during the cold liquid-hot surface contact:

$$\frac{T_{min} - T_{min}^I}{T_{min}^I - T_l} = 0.42 \left[\sqrt{\frac{k_l \rho_l c_l}{k_w \rho_w c_w}} \frac{h_{lv}}{c_w (T_{min}^I - T_{sat})} \right]^{0.6} \quad (4.22)$$

where T_{min}^I corresponds to the MFBT by the Berenson correlation and the sub-
 w to the properties of the hot contact surface.

4.3.1.3 Hydraulic Diameter

The hydraulic diameter of a subchannel of an SFR is an important property for the remainder of our discussion on sodium boiling thermal-hydraulics. It is to that end that we repeat some of the properties given in table 3.4 in table 4.2. The hydraulic diameter is given by the ratio of the flow area and the wetted perimeter:

$$D_h = \frac{4A_C}{P_w} \quad (4.23)$$

for an interior triangular subchannel, as given in figure 3.4, these are given as a function of the fuel pin outer diameter (D_{pin}) and the pin pitch-to-diameter ratio

Properties for	Rapsodie	Phenix	Superphenix
Pin outer diameter (<i>mm</i>)	5.1	6.6	8.5
Pin pitch/Diameter	1.16	1.18	1.15
Hydraulic Diameter (<i>mm</i>)	2.5	3.5	3.9
Confinement number C_o	1.64	1.15	1.04
Maximal pin linear power (<i>kW/m</i>)	43	45	48
Average pin linear power (<i>kW/m</i>)	31	27	30
Subchannel hydraulic diameter (<i>mm</i>)	2.5	3.5	3.9
Maximal heat flux (<i>MW/m²</i>)	2.7	2.2	1.8
Average heat flux (<i>MW/m²</i>)	1.9	1.3	1.1

Table 4.2: Subassembly subchannel hydraulic diameter and heat fluxes. The properties for the calculation of the Confinement number were taken at the atmospheric saturation temperature.

(P/D_{pin}) when neglecting the effect of the wire spacer:

$$A_C = \frac{D_{pin}^2}{4} \left[\sqrt{3} \left(\frac{P}{D_{pin}} \right)^2 - \frac{\pi}{2} \right] \quad (4.24)$$

$$P_w = \frac{\pi D_{pin}}{2} \quad (4.25)$$

The hydraulic diameter is thus given by:

$$D_h = \frac{2D_{pin}}{\pi} \left[\sqrt{3} \left(\frac{P}{D} \right)^2 - \frac{\pi}{2} \right] \quad (4.26)$$

The result of this equation is given in table 4.2. Also mentioned in the table, are the maximum heat flux (i.e. the ratio of the maximum pin linear power and the pin perimeter – q''_{max}) and the average heat flux (i.e. the ratio of the maximum pin linear power and the pin perimeter – q''_{av}).

Besides being an important parameter for the flow and heat transfer calculations, i.e. we can imagine that a tube of the same hydraulic diameter has more or less similar properties, it can already be used to determine some geometric properties of the subchannel. This is of course assuming that subchannels are independent from one to another. This isn't necessarily true as the wire-space doesn't close the channels entirely, but allows for some cross-flow. However, assuming subchannel independency reduces the complexity of the analysis.

Kandlikar [47] for example mentions that the dimensional limit between conventional and minichannels is given by a diameter of 3 *mm*. Although this is an easy-to-use criterion, Kandlikar's paper only mentions water and typical refrigerants

such as Freon, it is not necessarily applicable to sodium. This latter is especially important as the hydraulic diameter of a subchannel approaches these values. A more universal criterion is described by Tome [48] on the basis of Kew and Cornwall's analysis in his review article. They defined a confinement number Co that is the ratio of an order of magnitude estimate for the vapor bubble diameter upon detachment (D_v) and the channel hydraulic diameter:

$$D_v \sim \left(\frac{\sigma}{g\Delta\rho_{lv}} \right)^{1/2} \quad (4.27)$$

$$Co = \left(\frac{\sigma}{g\Delta\rho_{lv}D_h^2} \right)^{1/2} \quad (4.28)$$

Equation 4.27 contains the basis of the typical Fritz correlation for the bubble detachment diameter during steady⁶ boiling on a horizontal plate [49], deduced from buoyant and adhesion forces (see figure 4.3):

$$\frac{\pi D_v^3}{6} \Delta\rho_{lv}g = f(\theta)\pi D_v\sigma$$

where $f(\theta)$ is a function that takes into account the influence of the wetting angle. The confinement number basically indicates that a reduction of the hydraulic diameter confines the detached bubble and changes the bubble dynamics and conventional two-phase flow characteristics. The limit chosen by Kew and Cornwall was a confinement value higher than 0.5.

Assuming that this reasoning can be extrapolated to sodium boiling, we can conclude that general two-phase flow characteristics don't apply to sodium boiling inside subassemblies as their confinement number is higher than 0.5. Thus we have to look to data that applies to small diameter channels. That is of course if we can more or less justify the extrapolation of equation 4.27 to sodium boiling. The experimental verification of this extrapolation was impossible. However the data in the book of Subbotin et al. [3, page 141], deduced from X-ray photography of alkali metal pool boiling⁷ of sodium and potassium, was judged to be in satisfactory agreement. This criterion is of course for saturated boiling, thus we turn away from the geometrical problem to explore the thermal-hydraulic problem more in detail.

⁶Zuber's PhD nor any other references define in detail the definition of steady boiling. However the fact that this correlation is deduced from a static analysis, the bubble has to be stable at the wall. Hence the region close to the wall should at least be at saturation. This equation thus doesn't apply to subcooled nucleate boiling with a narrow (in comparison to the bubble detachment diameter) saturated layer.

⁷There is thus always the risk that the data is deduced from superheated sodium.

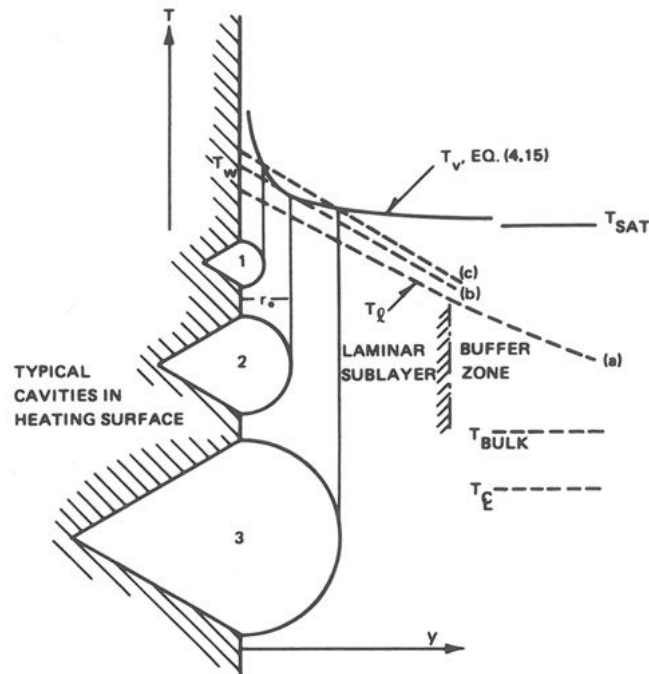


Figure 4.13: The typical conditions for a bubble nucleating at a surface (from Lahey and Moody [5]).

4.3.2 Wall Superheat

To determine the onset of nucleate boiling, the well-known Hsu criterion can be used. This criterion that gives the superheat at the wall at the onset of boiling is relatively easily deduced when combining equation 4.8 for the homogeneous nucleation superheat with the heat transfer at a heated surface: assuming a laminar liquid sublayer close to the wall, the heat flux at the wall can be written as:

$$q''_w = -k_l \frac{\partial T}{\partial y} \quad (4.29a)$$

The homogeneous nucleation superheat expressed by equation 4.8 can be considered as the vapor temperature close to the wall for a bubble to exist:

$$T(y) = T_l + \frac{2\sigma T_{sat} v_v}{y h_{lv}} \quad (4.29b)$$

Combining equation 4.29a and 4.29b gives the point where the local liquid temperature is tangent to the condition for bubble growth (see figure 4.13):

$$q''_w = -k_l \left. \frac{\partial T}{\partial y} \right|_{y=r_b} = \frac{2k_l \sigma T_{sat} v_v}{r_b^2 h_{lv}} \quad (4.29c)$$

this point is the critical radius r_k that is thus given by:

$$r_k = \left(\frac{2\sigma T_{sat} v_v k_l}{h_{lv} q_w''} \right)^{1/2} \quad (4.29d)$$

This critical cavity radius corresponds to the first nucleation site that can produce vapor. As such we can calculate the wall superheat, assuming a linear temperature gradient in the the laminar sublayer:

$$T_w - T_l = \frac{q_w'' r_k}{k_l} \quad (4.29e)$$

$$= T_w - T_v \quad (4.29f)$$

 latter expression is possible because the liquid temperature is tangent to the vapor temperature for a stable vapor cavity (see figure 4.13). We can thus write (neglecting superheat reduction by incondensable gasses and wetting effects):

$$T_w - T_{sat} = (T_w - T_v) - (T_{sat} - T_v) \quad (4.29g)$$

$$= \frac{q_w'' r_k}{k_l} - \frac{2\sigma T_{sat} v_v}{r_k h_{lv}} \quad (4.29h)$$

When substituting the result for the critical radius given in equation 4.29d, we obtain an expression for the wall superheat at the onset of boiling as a function of the heat flux:

$$T_w - T_{sat} = \sqrt{\frac{8\sigma T_{sat} v_v}{h_{lv} k_l}} q_w'' \quad (4.29i)$$

Lahey and Moody mention quite explicitly that this relation assumes that a distribution with all sizes of nucleation centers are present at the wall. As such, like Chen mentions [50] for its application to liquid metals, Hsu's criterion imposes a necessary condition for the onset of nucleate boiling, but not a sufficient condition.

If we apply this criterion to the average and maximum heat flux values in table 4.2, we obtain the wall superheat and corresponding critical radii as given in table 4.3. Due to the high thermal conductivity of liquid sodium, the typical critical radius for boiling inception is relatively large. Chen observed this and arguments that for the very well-wetting liquids, such as alkali metals, the cavities corresponding to the critical radius r_{cr} are most likely flooded.

There exist many extension to the model of Hsu. For example, there is the model of Bankoff and Fauske [51] that is especially useful as it was constructed specifically for sodium boiling at lower heat fluxes with the influence of gas entrainment. Besides the mathematical and small physical differences of Hsu's and Bankoff and Fauske's model, the main assumption is that there are bubbles or nucleation sites

Properties for	Rapsodie	Phenix	Superphenix
Maximal heat flux (MW/m^2)	2.7	2.2	1.8
Corresponding Superheat (K)	7.63	6.86	6.24
Corresponding Critical radius (μm)	69	77	85
Average heat flux (MW/m^2)	1.9	1.3	1.1
Corresponding Superheat (K)	6.48	5.31	4.94
Corresponding Critical radius (μm)	82	100	107

Table 4.3: Subassembly subchannel hydraulic diameter and heat fluxes. The properties for the calculation of the Confinement number were taken at the atmospheric saturation temperature.

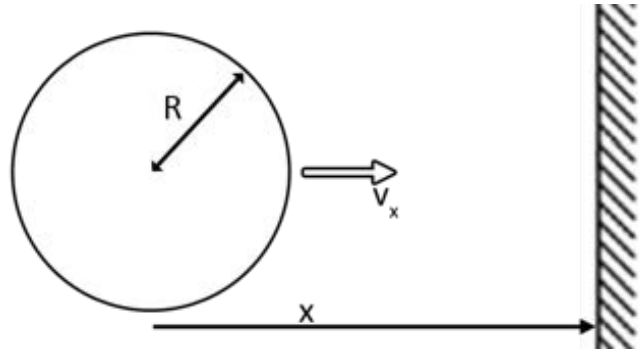


Figure 4.14: The bubble's reference frame close to a wall boundary. To be used to deduce the forces acting on the bubble as defined in equation 4.30a.

present at the wall. Bankoff and Fauske (and other authors who take into account the entrained bubbles [12]) assume that bubbles present in the circulating fluid diffuse to the wall. We have already established that non-condensable bubbles are present in a reactor system, but any detailed information of the bubble motion with respect to the cladding of the fuel pins are lacking. Yet, we can formulate a number of hypotheses concerning this bubble motion:

- The bubble's diameter generally increases when crossing the core region, which can be explained due to the pressure losses in the core and the temperature rise (the relatively rapid passing of the bubbles makes it possible to eliminate bubble dissolution from this discussion). With a formula given in Brennen's book on Bubble dynamics [52], we can deduce the force (relative to the frame of reference given in figure 4.14) acting on the bubble:

$$F_x = -\frac{2\pi}{3} \left[\frac{d}{dt}(v_x R^3) + \frac{3}{4} \frac{R^2}{x^2} \frac{d}{dt} \left(R^3 \frac{dR}{dt} \right) \right] \quad (4.30a)$$

Assuming a bubble with a non-existent translational velocity and a constant

bubble growth rate $R(t) = R_0 + a t$ gives:

$$F_x = -\frac{2\pi}{3} \left[R^3 \frac{dv_x}{dt} + \frac{9}{4} \frac{R^4}{x^2} a^2 \right] \quad (4.30b)$$

If the force on the bubble is zero, then the bubble growth is a repulsive action that pushes the bubble away from the wall. However, the linear growth of the bubble radius might be a too simplistic approach. On top of that,  ton [53] writes that a bubble oscillation close to the boundary tends to result in an attractive force.

- The transversal temperature gradient between the wall and the bulk liquid, i.e. the temperature decrease between the wall and the bulk liquid, also result in a force on the bubble. This is related to the decrease of the surface tension from the wall to the bulk liquid, that leads to a Marangoni force towards the hot liquid [52]:

$$F_x = -2\pi R^2 \frac{d\sigma}{dT} \frac{dT}{dx} \quad (4.31)$$

It is clear that not all forces acting on the bubble have been studied nor the resulting bubble motion relative to the fuel pin's cladding, as this was not our goal. But it can be hypothesized that bubbles might have the tendency to diffuse to the wall. Nonetheless, it is clear that the exact non-condensable bubble motion in the small subchannels of an SFR is an unknown but important phenomenon to understand the wall superheat and detailed nucleation phenomena.

We nonetheless have to repeat that Seiler [16] mentions, based upon the experimental knowledge gained from boiling loops with an argon cover gas at CEA Grenoble, that boiling inception superheat does not seem important for Liquid Metal Fast Breeder Reactor safety and that it has not been observed during the slow heat-up transients that are representative for reactor conditions. The latter is supported with the measurements of Le Guillou et al [54], who write that boiling appears when the wall temperature becomes equal to the saturation temperature⁸. Superheat estimates, perhaps overestimates, based on Hsu's criterion - that may be used because of the presence of 100 μm bubbles - confirm this observation.

4.3.3 Subchannel Temperature Profile

Next to the actual value of the wall temperature at boiling inception, it is as important to know the temperature profile inside the subassembly to understand the boiling regime and the possible two-phase flow phenomena. The best way to acquire

⁸It must also be added that the small superheat values given in table 4.3 must be seen in comparison to the high saturation temperature. They could have been seen as a possible measurement error.

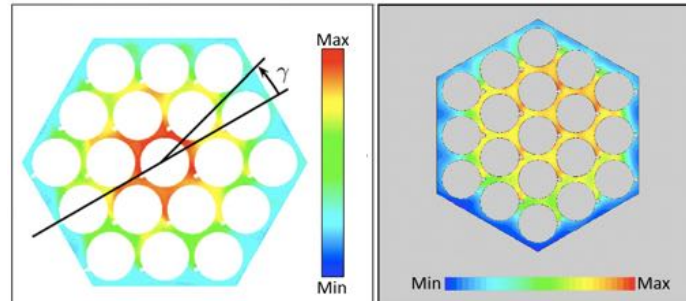


Figure 4.15: The temperature profile inside a 19-pin subassembly during normal operating conditions, as simulated by Rolfo and Péniguel [56] (left) and Hamman and Berry [56] (right). Due to the fact that the profile is intended for qualitative purposes, the temperature scales have been deleted.

so, would have been a high resolution Computational Fluid Dynamics (CFD) simulation. This has been done by Hamman and Berry [55] and Rolfo and Péniguel [56] for nominal operation condition. These profiles are given, qualitatively, in figure 4.15. These profiles reveal a strong radial temperature gradient inside a subassembly due to the overcooling of the subchannels close to the hexcan. However in between the fuel pins the temperature profile is qualitatively smooth.

However the exact resolution of the extremely small boundary layer between the wall and the turbulent core of the flow is often resolved by means of wall functions, that need special care for liquid metals (or low-Prandtl number) simulations. Additionally, CFD simulations are grid-sensitive and relatively expensive⁹. Hence we take our refuge to established thermal-hydraulic analyses that can be resolved relatively easily to obtain more quantitative information inside a subchannel at the onset of boiling.

In the field of liquid metal thermal-hydraulics and low-Prandtl number fluids, the heat transfer theory of Martinelli for a turbulent flow inside a heated tube is a well recognized evaluation of the temperature profile. Although it is well recognized and quoted numerously e.g. by Waltar and Reynolds [57], Todreas and Kazimi [58] or in the LBE handbook [59], it is difficult to find a clear description of his analysis. Due to the importance of this theory to the field of liquid metals, and the difficulty to obtain the original article of 1947 [60], his analysis for the temperature field in a tube is summarized here.

The Reynolds-averaged flow equation, thus for the mean flow variables with the

⁹The expenses are not only related to the possible license fee, the computational expenses related to computing power are also important as they are the limiting factor of the simulation's precision.

oscillating turbulent component written in terms of a turbulent eddy diffusivity for momentum ϵ_M and heat ϵ_H , in a cylindrical tube with a fully developed flow¹⁰ becomes:

$$\frac{1}{\rho} \frac{\partial p}{\partial z} = \frac{1}{r} \frac{\partial}{\partial r} \left[r(\epsilon_M + \nu) \frac{\partial v_z}{\partial r} \right] \quad (4.32a)$$

with a corresponding heat transport equation:

$$v_z \frac{\partial T}{\partial z} = \frac{1}{r} \frac{\partial}{\partial r} \left[r(\epsilon_H + \alpha_l) \frac{\partial T}{\partial r} \right] \quad (4.32b)$$

By expressing the pressure gradient in equation 4.32a in function of the wall shear stress (the wall shear stress acts on the cylinder boundary $\tau_w 2\pi r_0$, while the pressure acts on the cross section $\pi r_0^2 \Delta p$),

$$\frac{1}{\rho} \frac{\partial p}{\partial z} = \frac{2\tau_w}{\rho r_0}$$

a simplification of equation 4.32a is possible:

$$\frac{\tau_w}{\rho} \left(1 - \frac{r_0 - r}{r_0} \right) = -(\epsilon_M + \nu) \frac{dv_z}{dr} \quad (4.32c)$$

A similar simplification can be applied for equation 4.32b by applying a heat balance in the cross-section ($q_w'' 2\pi r_0 = c_p \rho \Delta T$) and assuming that the average temperature increase and the local temperature increase are equal (i.e. a thermally developed flow with a constant heat flux):

$$\frac{q_w''}{c_p \rho} \left(1 - \frac{r_0 - r}{r_0} \right) = -(\epsilon_H + \alpha_l) \frac{dT}{dr} \quad (4.32d)$$

Thus knowing the velocity profile and the ratio of the heat and momentum eddy diffusivity, the temperature profile can be determined for a thermally developed flow with a constant heat flux.

For a pipe-flow or a flow on top of a flat plate, the velocity profile is well known and often expressed as a function of the dimensionless wall coordinate y^+ , which for a pipe becomes:

$$y^+ = \frac{\sqrt{\tau_w/\rho} (r_0 - r)}{\nu}$$

The definition of the wall shear has already been introduced in equation 4.32a and 4.32c. This expression, although relating to many physical parameters, can give the impression to be somewhat artificial, it is further developed into an expression

¹⁰The condition of a fully developed flow implies that the velocity profile in the tube can be treated as a constant in the axial direction

with somewhat more sensible engineering variables. We start with the wall shear stress:

$$\tau_w = \frac{\partial p}{\partial z} \frac{r_0}{2}$$

The pressure losses can be written in terms of a pressure loss coefficient f_{loss} and a mean velocity $v_{z,av}$:

$$\tau_w = f_{loss} \frac{\rho}{2r_0} \frac{v_{z,av}^2}{2} \frac{r_0}{2}$$

Thus the dimensionless wall coordinate in function of engineering variables becomes:

$$\begin{aligned} y^+ &= \sqrt{\frac{f_{loss}}{8}} v_{z,av} \frac{(r_0 - r)}{\nu} \\ &= \sqrt{\frac{f_{loss}}{8}} \frac{Re}{2r_0} (r_0 - r) \end{aligned}$$

with Re , the Reynolds number given by:

$$Re = \frac{v_{z,av} 2r_0}{\nu}$$

The dimensionless velocity profile v_z^+ given by

$$v_z^+ = \frac{v_z}{\sqrt{\tau_w/\rho}}$$

then becomes:

$$\begin{cases} y^+ & y^+ < 5 & \text{Laminar sublayer} \\ -3.06 + 5 \log y^+ & 5 < y^+ < 30 & \text{Buffer layer} \\ 5.5 + 2.5 \log y^+ & y^+ > 30 & \text{Turbulent core} \end{cases}$$

Laminar sublayer The name of the sublayer already clarifies that turbulence is absent in the layer, hence the turbulent diffusivities ϵ_M and ϵ_H are zero. Equation 4.32d thus becomes:

$$\begin{aligned} \frac{dT}{dr} &= -\frac{q_w''}{c_p \rho} \frac{1}{\alpha_l} \left(1 - \frac{r_0 - r}{r_0} \right) \\ &= -\frac{q_w''}{c_p \rho} \frac{Pr}{\nu} \left(1 - \frac{r_0 - r}{r_0} \right) \end{aligned} \quad (4.33a)$$

with Pr the ratio of the momentum (ν) to thermal (α_l) diffusivity. A further simplification can be made in the laminar sublayer as this layer is relatively small compared to the tube dimensions:

$$\begin{aligned}\frac{dT}{dr} &= -\frac{q_w''}{c_p \rho} \frac{Pr}{\nu} \left(1 - \frac{r_0 - r}{r_0}\right) \\ &\approx -\frac{q_w''}{c_p \rho} \frac{Pr}{\nu}\end{aligned}\quad (4.33b)$$

$$T_w - T(r) = \frac{q_w''}{c_p \rho} \frac{Pr}{\nu} (r_0 - r) \quad (4.33c)$$

Buffer layer In the buffer layer, both the molecular thermal diffusivity α_l and the turbulent thermal diffusivity are important. They should thus both be taken into account. Whilst the molecular thermal diffusivity is a material property that can be found (or easily deduced from $\alpha_l = k_l / \rho_l c_{p,l}$) with material tables, the turbulent thermal diffusivity ϵ_H must be deduced from the turbulent momentum diffusivity and their ratio.

We define the ratio of the turbulent momentum diffusivity and the eddy thermal diffusivity as the turbulent Prandtl-number:

$$Pr_t = \frac{\epsilon_M}{\epsilon_H} \quad (4.33d)$$

as for now this turbulent Prandtl number is treated as a constant parameter. The momentum eddy diffusivity in the buffer layer is then the only parameter needed to obtain a solution for the temperature profile. From the velocity profile and equation 4.32c, we obtain:

$$\frac{dv_z}{dr} = -\frac{5\sqrt{\tau_w/\rho}}{r_0 - r} \quad (4.33e)$$

$$\epsilon_M = -\frac{\tau_w/\rho}{dv_z/dr} \left(1 - \frac{r_0 - r}{r_0}\right) - \nu \quad (4.33f)$$

The moment diffusivity can thus be calculated, for which a similar simplification can be done as for the buffer layer:

$$\begin{aligned}\epsilon_M &= \frac{\sqrt{\tau_w/\rho}}{5} \left(1 - \frac{r_0 - r}{r_0}\right) (r_0 - r) - \nu \\ &\approx \frac{\sqrt{\tau_w/\rho}}{5} (r_0 - r) - \nu\end{aligned}\quad (4.33g)$$

With this data, equation 4.32d becomes:

$$\frac{q_w''}{\rho c_p} \left(1 - \frac{r_0 - r}{r_0}\right) = -\left(\frac{\sqrt{\tau_w/\rho}}{5 Pr_t} (r_0 - r) - \frac{\nu}{Pr_t} + \alpha_l\right) \frac{dT}{dr}$$

or after some rearrangement:

$$\frac{q_w''}{\rho c_p} \frac{5/\nu Pr_t}{\frac{\sqrt{\tau_w/\rho}(r_0-r)}{\nu} + 5\left(\frac{Pr}{Pr_t} - 1\right)} = -\frac{dT}{dr} \quad (4.33h)$$

Although the integration was simple for the laminar sublayer, the dimensionless wall coordinate y^+ has to be reintroduced to simplify the integration in the sublayer:

$$\begin{aligned} T_{buffer} - T &= \frac{q_w''}{\rho c_p} \int_{y^+=5}^{y^+} \frac{5/\nu Pr_t}{\frac{\sqrt{\tau_w/\rho}(r_0-r)}{\nu} + 5\left(\frac{Pr}{Pr_t} - 1\right)} dy \\ &= \frac{q_w''}{\rho c_p \sqrt{\tau_w/\rho}} \int_{y^+=5}^{y^+} \frac{5 Pr_t}{y^+ + 5\left(\frac{Pr}{Pr_t} - 1\right)} d(\sqrt{\tau_w/\rho} y/\nu) \\ &= \frac{q_w''}{\rho c_p \sqrt{\tau_w/\rho}} \int_{y^+=5}^{y^+} \frac{5 Pr_t}{y^+ + 5\left(\frac{Pr}{Pr_t} - 1\right)} dy^+ \end{aligned}$$

The temperature in the buffer layer thus becomes:

$$T_{buffer} - T = 5 \frac{q_w'' Pr_t}{c_p \rho \sqrt{\tau_w/\rho}} \log \left[1 + \frac{Pr}{Pr_t} \left(\frac{\sqrt{\tau_w/\rho}(r_0-r)}{5\nu} - 1 \right) \right] \quad (4.33i)$$

where T_{buffer} is the temperature at the boundary of the buffer layer and the laminar sublayer.

Turbulent core In the turbulent core the turbulent diffusivity becomes normally so large that any molecular heat transfer effects can be neglected. It is however at this point that normal and low-Prandtl liquids (such as liquid metals) differ. The high thermal diffusivity of liquid sodium (see figure B.12) can not always be neglected in comparison with the thermal turbulent diffusivity. Furthermore, a turbulent eddy tends to loose or gain heat during its travel due to the high thermal diffusivity of the liquid sodium. The latter leads to a reduction on the enhancement of turbulent heat diffusivity, i.e. the turbulent eddy can't carry heat that far away from a heated source as compared to a normal liquid. The turbulent Prandtl number can be higher than one, whereas it is close to one for common fluids [58, 59]. Nonetheless, Martinelli assumed a turbulent Prandtl number equal to one and this value will be retained as a means to not complicate this section more than necessary.

In the turbulent core, we obtain from the velocity profile and equation 4.32c:

$$\frac{dv_z}{dr} = -\frac{2.5\sqrt{\tau_w/\rho}}{r_0 - r} \quad (4.33j)$$

$$\begin{aligned} \epsilon_M &= \frac{\sqrt{\tau_w/\rho}}{2.5} \left(1 - \frac{r_0 - r}{r_0}\right) (r_0 - r) - \nu \\ &\approx \frac{\sqrt{\tau_w/\rho}}{2.5} \left(1 - \frac{r_0 - r}{r_0}\right) (r_0 - r) \end{aligned} \quad (4.33k)$$

The latter approximation is justified because the kinematic viscosity, i.e. molecular viscosity, can be neglected in comparison with the momentum diffusivity caused by turbulence. With this data, equation 4.32d becomes:

$$\frac{q_w''}{\rho c_p} \left(1 - \frac{r_0 - r}{r_0}\right) = - \left(\frac{\sqrt{\tau_w/\rho}}{2.5 Pr_t} \left(1 - \frac{r_0 - r}{r_0}\right) (r_0 - r) + \alpha_l \right) \frac{dT}{dr}$$

or after some rearrangement:

$$\frac{q_w''}{\rho c_p} \frac{2.5/\nu Pr_t (1 - \frac{r_0 - r}{r_0})}{\frac{\sqrt{\tau_w/\rho}(r_0 - r)}{\nu} \left(1 - \frac{r_0 - r}{r_0}\right) + 2.5 \frac{Pr}{Pr_t}} = -\frac{dT}{dr} \quad (4.33l)$$

To integrate this equation, we again reintroduce the dimensionless wall distance y^+ :

$$\begin{aligned} T_{core} - T &= \frac{q_w''}{\rho c_p} \int_{y^+=20}^{y^+} \frac{2.5/\nu Pr_t (1 - \frac{y}{r_0})}{y^+ \left(1 - \frac{y}{r_0}\right) + 2.5 \frac{Pr}{Pr_t}} dy \\ &= \frac{q_w''}{\rho c_p \sqrt{\tau_w/\rho}} \int_{y^+=30}^{y^+} \frac{2.5/\nu Pr_t (1 - \frac{y}{r_0})}{y^+ \left(1 - \frac{y}{r_0}\right) + 2.5 \frac{Pr}{Pr_t}} dy^+ \end{aligned}$$

The resulting temperature profile obtained after a non-trivial integration becomes (as a function of the wall coordinate y and y_2 , with $y_2^+ = 30$):

$$\begin{aligned} T_{core} - T &= 1.25 \frac{q_w'' Pr_t}{\rho c_p \sqrt{\tau_w/\rho}} \log \left[\frac{5\lambda + \frac{y}{r_0} \left(1 - \frac{y}{r_0}\right)}{5\lambda + \frac{y_2}{r_0} \left(1 - \frac{y_2}{r_0}\right)} \right] + \frac{1.25}{\sqrt{1 + 20\lambda}} \frac{q_w'' Pr_t}{\rho c_p \sqrt{\tau_w/\rho}} \\ &\log \left[\frac{\left(\frac{2y}{r_0} - 1\right) + \sqrt{1 + 20\lambda} \left(\frac{2y_2}{r_0} - 1\right) - \sqrt{1 + 20\lambda}}{\left(\frac{2y}{r_0} - 1\right) - \sqrt{1 + 20\lambda} \left(\frac{2y_2}{r_0} - 1\right) + \sqrt{1 + 20\lambda}} \right] \end{aligned} \quad (4.33m)$$

$$\lambda = \frac{Pr_t}{Pr Re \sqrt{f/8}}$$

Total Profile The equations constructed in the previous paragraph can be used in two ways:

- With a given heat flux and a reference temperature, the temperature profile is calculated directly. This approach will be taken in this text.
- With a given heat flux, the bulk-to-wall temperature difference can be calculated. With this bulk-to-wall temperature difference and a value for the wall temperature, the temperature profile can be constructed. This is because the equations can be rewritten in the form:

$$\frac{T_w - T(r)}{T_w - T(r=0)} = f(r)$$

This latter approach has been taken in a review article on sodium boiling [9]. Although the bulk and centerline temperature are normally not very different, in liquid metals they can deviate significantly as described in Martinelli's paper [60]. This nonetheless doesn't influence the conclusions of the review article.

4.3.3.1 Reduced Flow

In a situation with a reduced flow induced by an inlet blockage, we can imagine that the heat transfer is degraded and boiling conditions can occur inside a subassembly. As a subchannel can not be analyzed by Martinelli's relations, we analyze the same question inside a tube with an equivalent hydraulic diameter of 3 mm. This value is close to the hydraulic diameter of an SFR subassembly subchannel (see table 4.2). Furthermore we assume that:

- The flow inside the tube is liquid, single phase.
- The flow inside the tube is fully developed turbulent i.e. $Re \geq 10000$.
- The simple Blasius pressure loss correlation $f_{loss} = 0.316 Re^{-0.25}$ is used for a Reynolds number below 30 000, whereas for higher Reynolds values the McAdams relation $f_{loss} = 0.184 Re^{-0.2}$ is used.
- The flow inside the tube is pure sodium, or the presence of argon bubbles doesn't influence the heat transfer properties of the flowing sodium.
- The temperature at the wall corresponds to the wall superheat of $2 MW/m^2$, i.e. 6.6 K.

These assumptions lead to a temperature profile as given in figure 4.16. In the same figure, the temperature profile for water corresponding for the same boiling inception wall superheat is given. To have a wall superheat of 6.6 K in the case

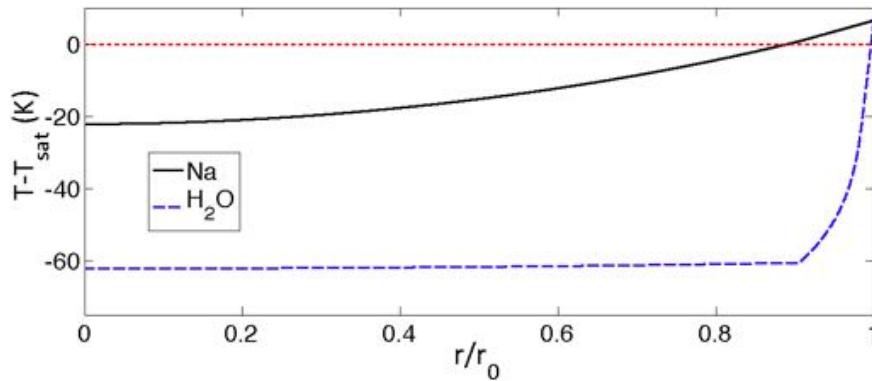


Figure 4.16: The temperature profile at boiling inception for water and sodium in a 3 mm diameter tube with a Reynolds number of 10^4 . The heat flux for water is 0.83 MW/m^2 , while the heat flux for sodium is 2 MW/m^2 , both resulting in a wall superheat of 6.6 K.

of water, equation 4.29i yields a wall heat flux of 0.83 MW/m^2 . In the figure it is clearly visible that the superheated region for sodium is much larger than the superheated layer in the case of water. Additionally, the temperature profile changes much more gradually for sodium than water. The latter doesn't change with an increase in Reynolds number or a change in wall heat flux, as can be observed in figure 4.17.

4.3.3.2 Local Blockages

Local blockages inside the subassembly can also not be resolved by the Martinelli theory, nor can we represent the general behavior inside a subchannel by a representative tube. In general, special subassembly codes or CFD codes have to be applied to these cases. Because no CFD results of a local, partially blocked subassembly are available in open literature, we present the qualitative behavior predicted by the subassembly codes that is discussed by Huber and Peppeler in the Liquid Metal Thermalhydraulics handbook [7]. The typical flow and temperature field during such a subassembly blockage is given in figure 4.18. And although the blockage induces a typical recirculation flow, it should be taken into account that the figure represents the flow and temperature field inside the entire subassembly. Hence the peak temperature will spread over a fraction of a subchannel.

For very small blockages inside a subchannel, e.g. the small flow obstruction caused by the wire spacer or wall deposits, such a small recirculation zone inside the (mini-) subchannel can be postulated.

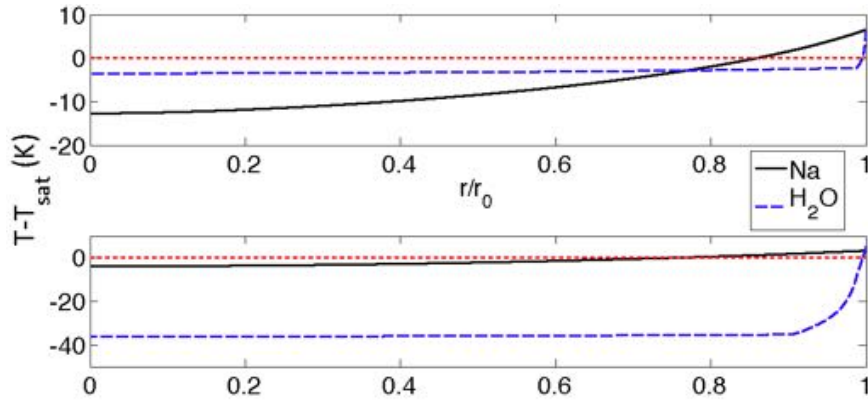


Figure 4.17: The temperature profile at boiling inception for water and sodium in a 3 mm diameter tube. Top: Reynolds number of 10^5 . The heat flux for water is 0.83 MW/m^2 , while the heat flux for sodium is 2 MW/m^2 , both resulting in a wall superheat of 6.6 K. Bottom: Reynolds number of 10^4 . The heat flux for both water and sodium is 0.5 MW/m^2

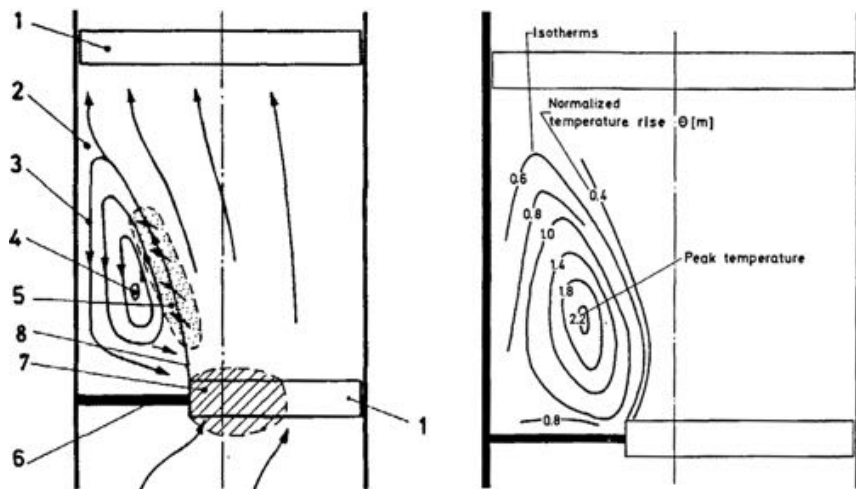


Figure 4.18: The qualitative temperature and flow profile inside an SFR subassembly with a 21% corner blockage as predicted by a subassembly code [7]. Left: Flow field.

Right: Temperature field. 1 - The spacer grid. 2 - Upper stagnation point. 3 - Reverse flow. 4 - Center of the vortex. 5 - Mixing zone. 6 - Planar corner blockage. 7 - Flow contraction. 8 - Pressure Recovery.

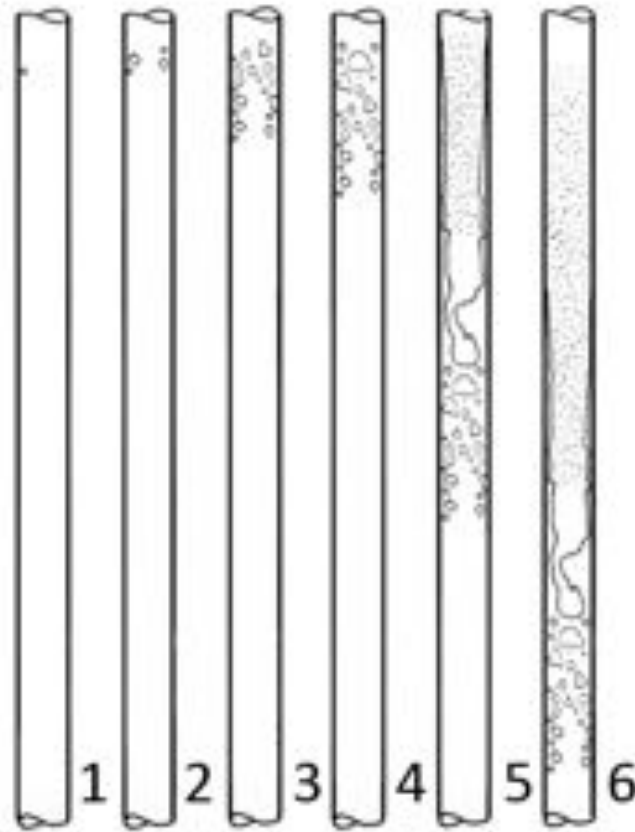


Figure 4.19: The typical convective water boiling pattern inside a uniformly heated tube, with a decreasing mass flow rate from left to right. The following heat transfer phenomena occur at the outlet: 1 - Subcooled nucleate boiling without net vapor generation. 2 - Subcooled nucleate boiling with net vapor generation. 3 - 4 - Saturated nucleate boiling. 5 - Liquid film boiling. 6 - Vapor cooling.

4.3.4 Boiling Regimes

Because the boiling regimes in water are quite well known and understood, we will start with a small discussion of these regimes and a comparison will be made in regards to sodium.

4.3.4.1 Water boiling regimes

The convective water boiling regimes are schematically given in figure 4.19. Due to the fact that the tube is assumed to be uniformly heated in the figure, first boiling phenomena occur at the outlet.

At the onset of boiling a hissing sound can be heard, while practically no bubbles can be visually observed. This is the start of subcooled nucleate boiling: Very small, practically invisible, bubbles are formed in the narrow superheated layer (see figure 4.16). But after the bubble has grown and the bubble tip encounters the subcooled liquid phase, condensation sets in and the bubble collapses violently [25]. As the temperature of the bulk liquid increases, vapor bubbles can detach from the wall and condense a distance from their original nucleation site. This is still subcooled nucleate boiling, but past the net vapor generation point [61]. Past this point, a noticeable void fraction can be observed. As the bulk liquid continues to heat up, the saturated nucleate boiling regime is reached when the bulk temperature attains the saturation temperature.

4.3.4.2 Sodium boiling regimes

For sodium, the near-wall temperature profile is far less steep (see figure 4.16). Hence bubbles will become much larger before they encounter subcooled liquid and a noticeable void fraction can exist after the onset of nucleate boiling, hence the point of net vapor generation does not exist. Furthermore, the bulk temperature is close to saturation and the regime of subcooled nucleate boiling will be practically inexistent and, in most cases, saturated nucleate boiling will be observed directly at the onset of boiling. This however does not mean that subcooled boiling is inexistent at the level of a subchannel or at the level of the fuel assembly [62] (see figure 4.20, deduced from quasi-steady state boiling conditions).

Hot Spot Boiling This is a form of subcooled boiling that has only been reported for fuel assemblies with wire spacers. The wire spacer (or other local flow obstructions) creates, at reduced flow rates, a local stagnant zone of sodium between the wire spacer and the fuel pin [64]. The stagnant zone can be identified in the flow field simulations of Hamman and Berry [55] (figure 4.21). For high heat fluxes, boiling conditions can be present in the small stagnant volume and a vapor bubble can be created. This vapor bubble can only grow until it encounters the subcooled core of the subchannel flow. In this case, the wire spacer geometry creates the conditions that can lead to a relatively steep temperature profile (that typically exists at the wall in a water flow) and the associated subcooling. Some hypotheses exist for the hot spot boiling phenomenon: e.g. a small bubble is formed that grows and becomes stable, creating local dry-out on a small cladding area. Another hypothesis is that the bubble collapses when it encounters the subcooled liquid. However, none of these hypotheses have been directly verified in the past and at present it was impossible to do so.

Local Boiling It is a known fact of the current SFR fuel assembly design that a significant mass flow passes through the corner and edge subchannels, which can

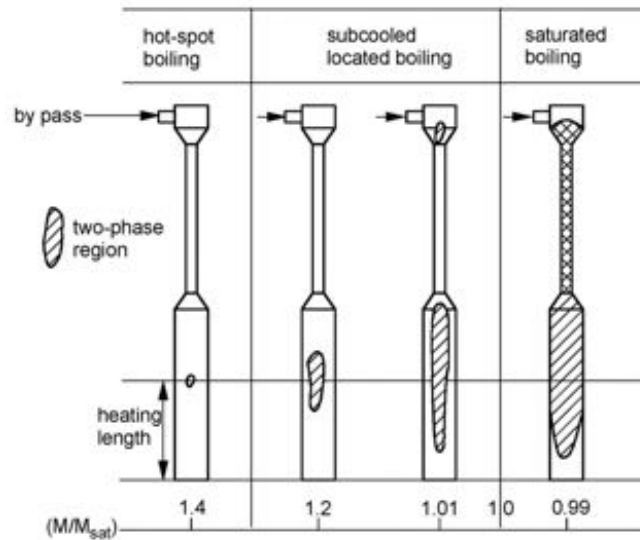


Figure 4.20: The typical boiling zones in a 19-pin bundle with wire spacer after Menant [63] as a function of the mass flow rate (M) relative to the mass flow rate to reach the the saturation temperature (M_{sat}). These observations were done under quasi-steady state conditions.

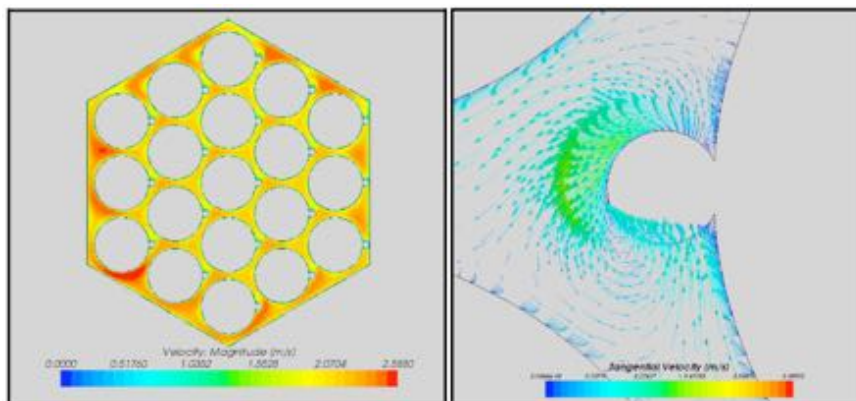


Figure 4.21: The velocity profile calculated by Hamman and Berry [55] in a 19-pin SFR fuel assembly with a wire spacer. Notice the reduced flow velocity between the wire and the fuel cladding. Also note the relatively higher velocities in the edge subchannels.

also be seen in the simulations of Hamman and Berry [55] (figure 4.21) or Rolfo and Péniguel [56]. Hence the exterior subchannels are overcooled, leading to a relatively important radial temperature profile. Therefore, saturated boiling can take place in the interior subchannels while the assembly mean enthalpy is still lower than the saturated enthalpy. The vapor created in the interior subchannels will therefore recondensate before the exit of the fuel assembly. In this case there is never any steep temperature gradient present inside of the subchannels and sub-cooling is only created because of the flow redistribution of the current SFR fuel assembly design.

Downstream of the fuel pins the coolant is mixed and the enthalpy can approach the saturation enthalpy corresponding to the pressure inside the convergent. Due to the pressure losses in the section and at the outlet, the liquid can be superheated in comparison to the local pressure and flashing can occur.

Saturated Boiling When the liquid reaches the saturation enthalpy over an entire cross-section of the heated length, saturated boiling is attained.

4.3.5 Two-Phase Flow Patterns

Although the boiling regimes discussed in the previous section already give an insight in the boiling behavior of sodium, they only refer to the extent two-phase zone, the saturation zone and the subcooling zones. They, however, do not provide any in-depth knowledge of the microscopic structure of the two-phase boiling flow as given for water in figure 4.19. But before we start the discussion on this subject, we introduce the typical two-phase flow patterns as presented by Taitel and Dukler [65].

4.3.5.1 Flow Pattern Classification in a Vertical Tube

In a flow with two phases with quite different properties, especially very different densities, the two phases can be distributed along the flow channel in a variety of ways. Although this exact microscopic distribution is quite chaotic and stochastic, there are certain tendencies or spatial similarities that allow us to classify their general distribution. And although the definition and description of such patterns is subjective in nature, literature mentions generally the bubbly flow, slug flow, churn flow and annular flow in a vertical tube. These are schematically given in figure 4.22. It must nonetheless be stated that these flow patterns are defined for non-reactive flows, i.e. without chemical reactions or phase changes.

Bubbly Flow In a bubbly flow, the gas phase is distributed more or less uniformly in the form of discrete “bubbles” in a continuous liquid.

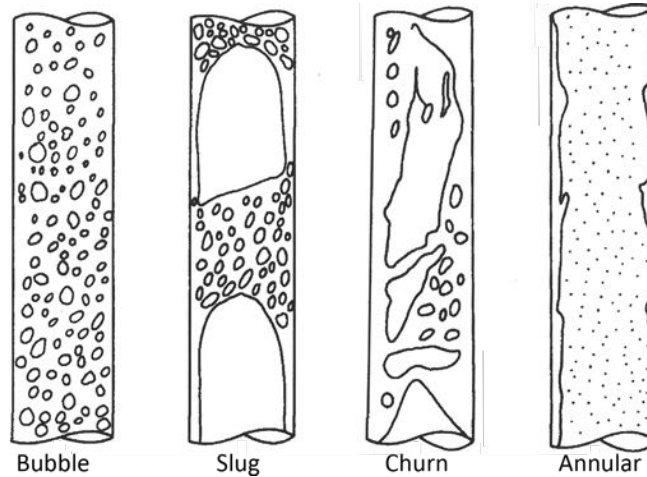


Figure 4.22: Typical liquid/gas two-phase flow patterns in a vertical tube from Taitel and Dukler [65].

Slug Flow For a slug flow, the gas flows largely in a so-called large, bullet-shaped, Taylor bubble that occupies most of the pipe's cross-sectional area with only a liquid film remaining. The Taylor bubbles are separated axially by liquid slugs.

Churn Flow Churn flow is somewhat similar to slug flow. However, the Taylor bubbles are deformed.

Annular Flow Annular flow is characterized by an axial continuity of both phases. The gas phase is located in the core of the flow, whereas the liquid is only present as a liquid film.

Flow Maps It is possible to model the transitions between each flow regime, which leads to flow maps as given in figure 4.23 as has been proposed by Mishima and Ishii [66]. And although these flow maps have been constructed for a non-reactive flow, we can deduce (qualitatively) the flow pattern information during boiling. If we assume a constant mass flow rate at the inlet of the tube of figure 4.19:

- For subcooled nucleate boiling the mass fraction of vapor is low. Hence we can assume, even with the low value of the vapor density, that the vapor velocity will be low too. On top of that, the liquid velocity will be unchanged. The two-phase flow regime will thus certainly be bubble, as it has been shown in figure 4.19 for situations 1-3.

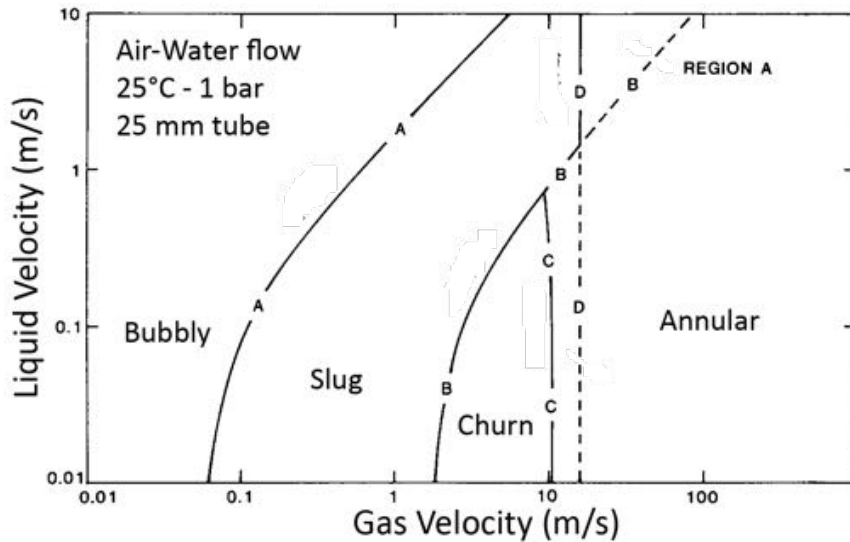


Figure 4.23: Typical liquid/gas two-phase flow map for a vertical 25 mm tube under atmospheric conditions and at room temperature. From Mishima and Ishii [66].

- For an increasing vapor mass fraction, e.g. for saturated nucleate boiling, the liquid velocity decreases slightly whilst the gaseous velocity becomes more and more important. The two-phase flow regime changes however to slug flow as can be seen in figure 4.19 for situation 4.
- For higher vapor mass fractions, the vapor velocity becomes so high that the flow regime changes to annular flow. As such, a liquid film remains on the heated wall and the heat transfer mechanism is liquid film boiling, as shown for situation 5-6 in figure 4.19.

4.3.5.2 Flow Pattern Classification in a Pin Bundle

The flow patterns in a reactor system occur in a pin bundle. The geometry from this pin bundle is very different from the geometry in a tube, which influences the two phase flow. Dukler and Taitel [65] mention however that in general the same flow patterns as for round tubes are observed. But there is one important exception for the slug flow regime. Independent slugs can also occur inside the subchannels of the bundle. However, a slug can also occur in the form of a large bubble that encapsulates many rods. Both configurations are given in figure 4.24. It appears that the large bubble slug flow regime occurs only when there is a sudden rapid increase in the gas flow rate.

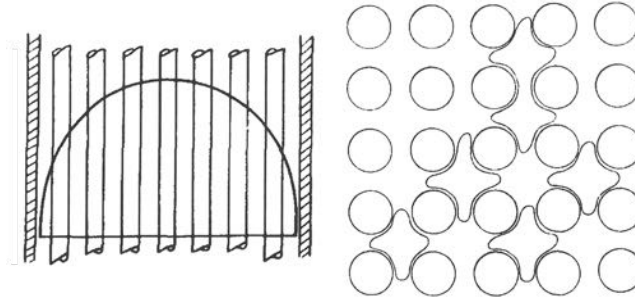


Figure 4.24: Slug flow patterns in a vertical pin bundle. Left: the large bubble slug that occurs with a sudden increase in the gas flow rate. Right: Individual slugs inside the subchannels of the pin bundle. From Dukler and Taitel [65].

4.3.5.3 Flow Patterns in a Small Vertical Tube

The studies referenced in the document of Dukler and Taitel [65] or the study by Mishima and Ishii [66] discuss the flow pattern in relatively large channels. Even the study for the pin-bundle of figure 4.24 were conducted for a rectangular 24 pin-bundle with a subchannel hydraulic diameter of about 14 mm with a pin diameter of about 13 mm, whereas the geometry of interest in our study have a much smaller hydraulic diameter with a triangular lattice and a wire spacer. No specific flow maps exist for the specific geometry under consideration here¹¹.

To have an idea about the flow patterns that may occur in the specific geometry under consideration, reference is made to the study of Mishima and Hibiki [67]. In their study they identified certain flow regimes that are particular for capillary tubes as they used tubes with a diameter of 1-4 mm. These peculiar flow regimes are given in figure 4.25. The most radical changes are for the bubble, slug and churn flow pattern:

Bubbly Flow The bubbles in a minichannel tend to accumulate along the tube's axis¹². Smaller bubbles form a spiral train, whereas the larger bubbles tend to align next to each other to form intermittent bubble trains.

Slug Flow The slugs in a minichannel tend to be very long, with bridges of thin liquid in the long slugs.

¹¹Or better, during the three year study no specific flow maps have been found for the specific geometry under consideration.

¹²This is for a non-heated flow.

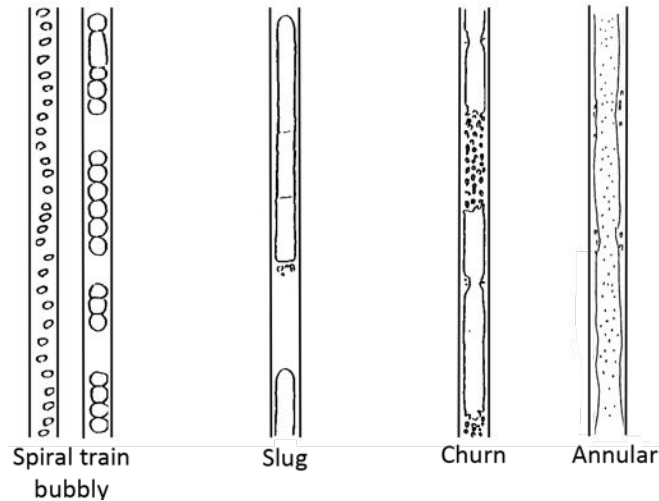


Figure 4.25: Typical liquid/gas two-phase flow patterns in a small vertical tube from Mishima and Hibiki [67].

Churn Flow For a churn flow inside a minichannel, the resemblance to the slug flow pattern is maintained. The only distortion that occurs is the deformation of the bullet-formed nose of the slug. Behind the slug, a finely dispersed bubbly flow is observed.

Flow Maps For the flow transitions in a minichannel, Mishima and Hibiki [67] concluded that the model of Mishima and Ishii [66] could be used to reproduce them well.

4.3.5.4 Identified Flow Patterns for Sodium Boiling

For the more common fluids, the flow pattern can be observed visually, by optical probes, by conductivity probes or by wire mesh sensors. For liquid sodium, only a few of these can be used as the conductive or opaque properties of sodium don't always allow any meaningful measurement. Furthermore, not all of these devices can be used under the high temperature conditions inside the mini-channels of a subassembly. Hence only nuclear measurements, e.g. X-ray imaging or neutron radiography, can reveal the information of the flow pattern during boiling. This type of measurement techniques doesn't seem to have been applied to a sodium boiling loop. The only available elements are, according to Seiler [16], temperature, pressure, axial void fraction and mass flow rate. With these elements, most sources mention a slug flow pattern (more a multi-slug pattern) or an annular flow pattern [57]. But before going into the details of such a boiling flow pattern, a

closer look is taken to the earliest arguments that led to this conclusion.

Historical Context Historically, the slug flow pattern is related to the hypothesis of a high boiling inception superheat and the typical vapor ejection phenomena that follow: Following boiling inception long slugs would grow that fill up the entire subchannel area (see figure 4.5): A slug would form during forced convection that results in local cooling and a pressure rise from the slug expulsion. This inhibited the formation of further vapor, until the original slug became stable and local superheat was re-established. As such a new slug could form, resulting in a multi-slug pattern.

We have already discussed in detail the absence of any superheat in a typical reactor system, thus this argumentation for the (multi-) slug flow pattern is invalid.

“Recent” Observations In 1987 Yamaguchi studied the flow patterns of boiling sodium at decay power levels [68]. For this experimental study the flow regime identification was based upon the pressure and temperature signals:

- *Bubbly Flow*
Bubble flow was identified by the appearance of irregular fluctuations in the measured pressure signal, whilst the saturation temperature was observed for at least one thermocouple.
- *Slug Flow*
The transition from bubble to slug flow was observed by the onset of oscillatory boiling, whilst a temperature decrease occurred in the non-boiling region due to an expected enhanced heat transfer.
- *Annular Flow*
A decay in the oscillatory boiling was interpreted as a sign of the transition to annular flow.

This type of pressure-measurement flow regime identification method isn't mentioned in the review article of Taitel and Dukler [65]. But because Yamaguchi identified bubbly flow during sodium boiling [68], we take our refuge to a theoretical view on the problem to obtain some more clarity.

Theoretical View Sheriff writes in a chapter for the Liquid Metals Thermalhydraulics handbook [7] that boiling is initiated in the regime of slug or churn flow due to the high expansion factor for evaporation under reactor conditions. In fact, the expansion factor of sodium under reactor conditions is in the order of magnitude of 1000. However, the expansion factor for water at low pressure has the same order of magnitude. It is the second remark of Sheriff that reveals most of

the information: the temperature difference between the wall and the fluid (i.e. the flow average temperature). The latter, as demonstrated already, is in the order of magnitude of 10 K. But yet again, this can also be the case for water at low heat fluxes (see figure 4.17). The subtlety is in the temperature profile: the temperature drop between the wall and the center of the channel is very gradual for sodium, whereas the temperature drop is more important at the wall for water. And it is just this gradual temperature drop that will make the vapor stable for a large fraction of the flow channel, certainly if we're discussing the mini-channels of a subassembly.

The only thing that remains is to establish that this large vapor fraction inside the subchannel will result in a slug flow. For that we can rely on the paper of Taitel and Dukler [65] that mentions that this happens at a void fraction of 0.25-0.3. Although nowhere mentioned explicitly (also not in the work of Mishima and Ishii [66]), the procedures used to relate this value to a certain area averaged gas-velocity, implies that this is the area averaged void fraction. From the profile in figure 4.16 and figure 4.17, we can deduce that such a value is most likely easily reached.

Final Remarks The gradual and small temperature drop between the wall and the center of the flow, combined with the high expansion factor during evaporation, yields directly a high void fraction. Due to this high void fraction, sodium boiling initiates with a slug flow regime. The latter has however never been directly observed!

It is clear that the wire-spacer in the wire-wrapped subassembly design will influence the flow pattern. However, no specific details have been found on the latter subject.

4.3.6 Boiling Zone

The previous analysis doesn't give any information on the stability of the generated vapor slug in the slug flow, i.e. the reactive part of the flow. The stability of the generated vapor, independent of the flow pattern, is important to delimit the two-phase zone. The presence of vapor in a subassembly is limited by:

- The contact of vaporous sodium with a structure that is not at the sodium saturation temperature. This contact leads to a very large heat loss from the vapor due to condensation (see figure 4.10 that indicates values of 0.1 MW/m^2 for the heat transfer coefficient.). The sodium vapor will thus quickly condensate.
- The high thermal diffusivity of liquid sodium that leads to a rapid condensation of a sodium vapor "bubble" contacted with subcooled liquid. A

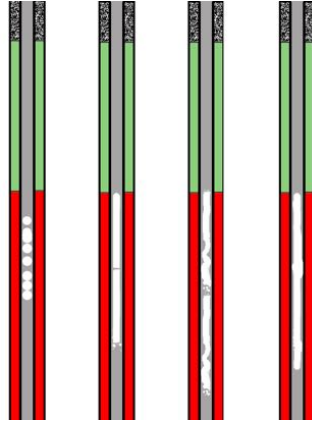


Figure 4.26: A graphical representation of the flow patterns in a typical boiling SFR subchannel: “spiral train” bubbly flow, slug flow, churn flow and annular flow. The lower part represents the heated length whereas the upper parts represent the fertile part and the upper gas plenum. The penetration of the vapor inside the non-heated parts is governed by the structural heat-up.

sodium vapor bubble that enters a subcooled liquid zone will thus quickly implode [69].

The consequences of this behavior is summarized by an important remark given by Seiler [16]: “The penetration of vapor in subcooled regions means condensation. Boiling-zone propagation is governed by structure heating-up”. This is especially important for the gas plena and fertile blankets of a fuel assembly (see figure 4.26 that gives the typical boiling flow patterns in a small-diameter channel.) and due to the non-uniform cooling of the sub-assembly.

4.4 Boiling Crisis

With the knowledge of the temperature profile and typical flow pattern during sodium boiling, it is also possible to give an idea of the limiting boiling heat transfer mechanism in SFRs (see figure 4.12). It has thus to be determined whether the dryout crisis or the DNB crisis is most important. And although a quantitative argumentation is possible (see for example the review article on sodium boiling [9] or Ishii and Fauskes consideration [42]), a more qualitative approach is taken here.

To distinguish clearly between the physics of both limiting mechanisms, their behavior in the case of more common liquids is given in figure 4.27. And although Shah [70] mentions the importance of the DNB mechanism, figure 4.27 already indicates that for the typical sodium boiling behavior the DNB mechanism is un-

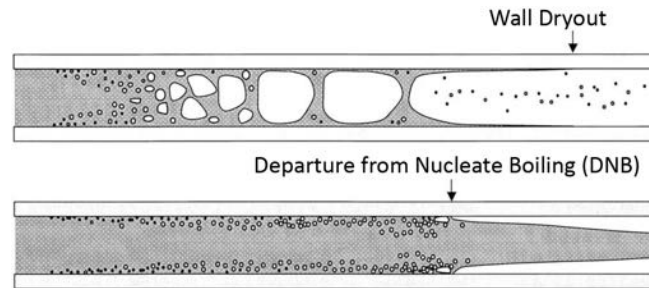


Figure 4.27: A graphical representation of the phenomena that occur during dryout and Departure from Nucleate Boiling.

likely as the slug flow regime prevails at the onset of boiling in a reactor system. Hence a slug is formed and the evaporation of the remaining liquid film will be determinate as a limiting heat transfer mechanism.

4.5 Conclusion

Sodium as a perfectly wetting fluid with a high saturation temperature has the tendency to initiate boiling with a high superheat. However, the superheat in actual convective boiling loops and reactor systems is limited as long as it can be shown that argon bubbles are present. The typical gradual temperature profile combined with the high expansion factor during evaporation leads to a high void fraction and most likely to a typical slug flow pattern for minichannels. This two-phase region inside the subassembly is however limited by condensation heat transfer to the structure or subcooled liquid, maintained by the non-uniform cooling of the subassembly.

It is undeniable that a lot of knowledge has been built on the topic of sodium boiling in the past, with only a small fraction discussed in this chapter. The total liquid metal boiling knowledge is sufficient for the safety analysis of SFRs. However, it is also clear from the discussion in this chapter that still some microscopic information is missing.

References

- [1] D. Mills. *Advances in solar thermal electricity technology*. Solar Energy, 76:19–31, 2004.

-
- [2] D.L. Katz, R.R. Miller, C.B. Jackson, R.M. Adams, E.C. Miller, H.F. Poppendiek, T. Trocki, I.R. Kramer, and R.N. Lyon. *Liquid-Metal Handbook*. Office of Naval Research, Department of the Navy, 2nd edition, January 1954.
- [3] V.I. Subbotin, D.N. Sorokin, D.M. Ovechkin, and A.P. Kudryavtsev. *Heat Transfer In Boiling Metals By Natural Convection*. Academy of Sciences of the USSR. Scientific Council for High Temperature-Physics, 1969.
- [4] C.C. Addison. *The Chemistry of the Liquid Alkali Metals*. John Wiley & Sons, Inc, 1984.
- [5] R.T. Lahey and F.J. Moody. *The Thermal-Hydraulics of A Boiling Water Reactor*. American Nuclear Society, 2nd edition, 1993.
- [6] Hens Zeger. *Concepts in Physical Chemistry*. University of Ghent - Academia Press, 2005.
- [7] H.M. Kottowski-Dümenil, editor. *Liquid Metal Thermal-Hydraulics*. INFORUM Verlag, 1994.
- [8] H. Kottowski and G. Grass. *Influence on superheating by suppression of nucleation cavities and effect of surface microstructure on nucleation sites*. In John C. Chen and A. A. Bishop, editors, *Liquid-Metal Heat Transfer and Fluid Dynamics*, pages 108–115, 1970.
- [9] Matthias Vanderhaegen and Alix Le Belguet. *A Review on Sodium Boiling Phenomena in Reactor Systems*. Nuclear Science and Engineering, 2013.
- [10] J. M. Delhaye, M. Giot, and M.L. Riethmuller. *Thermohydraulics of Two-Phase Systems for Industrial Design and Nuclear Engineering*. Hemisphere Publishing, 1981.
- [11] Magnus Holmgren, *Matlab X Steam, Thermodynamic properties of water and steam, 2007*.
- [12] O.E. Dwyer. *Boiling Liquid-Metal Heat Transfer*. American Nuclear Society, 1975.
- [13] M. Bader and C.A. Busse. *Wetting By Sodium at High Temperatures in Pure Vapour Atmospheres*. *Journal of Nuclear Materials*, 67:295–300, 1977.
- [14] H.K. Fauske. *Nucleation of Liquid Sodium in Fast Reactors*. *Reactor Technology*, 15(4):278–302, Winter 1972-1973.
- [15] K.T. Claxton. *The Influence of Radiation on the Inception of Boiling in Liquid Sodium*. In *Proceedings of the International Conference on the safety of Fast Reactors*, Aix-en-Provence, France, September 19-22 1967.

- [16] J.M. Seiler. *Studies on Sodium-Boiling Phenomena in Out-of-Pile Rod Bundles For Various accidental situation in LMFBR: Experiments and Interpretations*. Nuclear Engineering and Design, 82:227–239, 1984.
- [17] Suizheng QIU, Minoru TAKAHASHI, Dounan JIA, and Guanghui SU. *Density Wave instability of sodium boiling Two-phase flow in a vertical annulus at low Pressure*. Journal of Nuclear Science and Technology, 40(7):439–500, July 2003 2003.
- [18] A. Chenu, K. Mikityuk, and R. Chawla. *TRACE simulation of sodium boiling in pin bundle experiments under loss-of-flow conditions*. Nuclear Engineering and Design, (2417-2429), 2009.
- [19] Ze-Jun Xiao, Gui-Uin Zhang, Jian-Qiang Shan, Xue-Song Bai, and Dou-Nan Jia. *Experimental research on heat transfer to liquid sodium and its incipient boiling wall superheat in an annulus*. Nuclear Science and Techniques, 17(3):177–184, 2006.
- [20] Zicheng Qiu, Suizheng Qiu, Yingwei Wu, Wenxi Tian, and Guanghui Su. *Experimental Study on Boiling Wall Superheat of Sodium Flowing in Annulus*. In The 15th International Tropical Meeting on Nuclear Reactor Thermal-Hydraulics (NURETH), Pisa, Italy, May 12-17 2013.
- [21] J.B. Van Erp, D.R. MacFarlane, and H.K Fauske. *Protection against local core accidents in liquid metal fast breeder reactors*. Nuclear Engineering and Design, 15:441–457, 1971.
- [22] K. Thormeier. *Solubility of the Noble Gases in Liquid Sodium*. Nuclear Engineering and Design, 14:69–82, 1970.
- [23] E. Veleckis, S.K. Dhar, F.A.Cafasso, and H.M. Feder. *Solubility of Helium and Argon in Liquid Sodium*. Journal of Physical Chemistry, 75(18):2832–2838, 1971.
- [24] J.R. Welty, C.E. Wicks, R.E. Wilson, and G. Rorrer. *Fundamentals of Momentum, Heat and Mass Transfer*. John Wiley & Sons, Inc, 2001.
- [25] John Lienhard. *A Heat Transfer Textbook*. Phlogiston Press, 2006.
- [26] A. Yamaguchi and A. Hashimoto. *A Computational Model for Dissolved Gas and Bubble Behavior In The Primary Coolant System of Sodium-Cooled Fast Reactor*. In 11th International Topical Meeting on Nuclear Reactor Thermal-Hydraulics, Avignon, France, October 2005.
- [27] J.B. Moreno, C.E. Andraka, and T.A. Moss. *Boiling Behavior of Sodium-Potassium Alloy in A Bench-Scale Solar-Receiver*. In Proceedings of the 27th Intersociety Energy Conversion Conference, 1992.

- [28] A.B. Reynolds and G. Berthoud. *Analysis of EXCOBULLE Two-Phase expansion test*. Nuclear Engineering and Design, 67:83–100, 1981.
- [29] T. Theofanous, L. Biasi, H.S. Isbin, and H. Fauske. *A Theoretical study on bubble growth in constant and time-dependent pressure fields*. Chemical Engineering Science, 24:885–897, 1969.
- [30] T. Ytrehus. *Molecular-Flow effects in Evaporation and Condensation at Interfaces*. Multiphase Science and Technology, 9:205–327, 1997.
- [31] J.W. Rose. *Condensation Heat Transfer*. Heat and Mass Transfer, 35:479–485, 1999.
- [32] Van P. Carey. *Liquid-Vapor Phase-Change Phenomena: An Introduction to the Thermophysics of Vaporization and Condensation Processes in Heat Transfer Equipment*. Number ISBN 0-89116-836-2. Hemisphere Publishing, 1992.
- [33] S.P. Sukhatme and W.M. Rohsenow. *Heat Transfer During Film Condensation Of A Liquid Metal Vapor*. Technical Report 9167-27, Department of Mechanical Engineering, MIT, April 1964.
- [34] E.M. Sparrow and J.L. Gregg. *A boundary layer treatment of laminar film condensation*. Transactions of the ASME: Journal of Heat Transfer, 81(1):13–18, February 1959.
- [35] B. Misra and C. Bonilla. *Heat Transfer in the Condensation of Metal Vapors: Mercury and Sodium up to Atmospheric Pressure*. In F.J. Van Antwerpen, editor, Chemical Engineering Progress Symposium Series, volume 52, pages 7–21, January 1956.
- [36] Jhan Jhu Shu. *Similarity Solutions for laminar filmwise condensation on a vertical, non-isothermal, semi-infinite plate*. Computational Heat and Mass Transfer, 1:271–278, 2001.
- [37] S.J. Wilcox and W.M. Rohsenow. *Film Condensation of Liquid Metals - Precision of Measurement*. Technical Report DSR 71475-62, Department of Mechanical Engineering, MIT, April 1969.
- [38] E.D. Fedorovich and W.M. Rohsenow. *The Effect of Vapor Subcooling on Film Condensation of Metals*. Technical Report DSR 70586-53, Department of Mechanical Engineering, Engineering Projects Laboratory, MIT, May 1968.
- [39] W.M. Rohsenow. *Film Condensation of Liquid Metals*. In Progress of Heat and Mass Transfer, volume 7, page 469, 1973.

- [40] N.N. Kochurova. *Effects of Surface Properties of the condensate on the condensation coefficients of alkali metals*. Journal of Engineering Physics, 21(5):876–880, 1971.
- [41] H. Ninokata. *Analysis of Low-heat-flux sodium boiling test in a 37-pin bundle by the two-fluid model computer code SABENA*. Nuclear Engineering and Design, 97:233–246, 1986.
- [42] M. Ishii and H. Fauske. *Boiling and Dryout Behavior in a Liquid-Metal Fast Breeder Reactor Subassembly Bundle Under Low Heat Flux and Low Flow Conditions*. Nuclear Science and Engineering, 84:131–146, 1983.
- [43] M.M.K. Farahat, D.T. Eggen, and D.R. Armstrong. *Pool Boiling in Subcooled Sodium at Atmospheric Pressure*. Nuclear Science and Engineering, 53:240–253, 1974.
- [44] H.-J. Zimmer, W. Pepler, and H. Jacobs. *Thermal Fragmentation of Molten Alumina in Sodium*. In U. Mueller, editor, 4th International Topical Meeting on Nuclear Reactor Thermal Hydraulics (NURETH), 1989.
- [45] P.J. Berenson. *Film Boiling Heat Transfer from a Horizontal Surface*. Transactions of the ASME: Journal of Heat Transfer, 83:351–358, August 1961.
- [46] R.E. Henry. *A Correlation for the minimum film boiling temperature*. Heat Transfer - Research and Design, AIChE Symposium Series, 70(138):81–90, 1974.
- [47] Satish G. Kandlikar. *Fundamental issues related to flow boiling in minichannels and microchannels*. Experimental Thermal and Fluid Science, 26:389–407, 2002.
- [48] John R. Tome. *Boiling in microchannels: a review of experiment and theory*. International Journal of Heat and Fluid Flow, 25:128–139, 2004.
- [49] Novak Zuber. *Hydrodynamic Aspects of Boiling Heat Transfer*. PhD thesis, University of California, Los Angeles, 1959.
- [50] J.C. Chen. *Incipient Boiling Superheat in Liquid Metals*. Journal of Heat Transfer, 90(3):303–312, 1968.
- [51] S.G. Bankoff and H.K. Fauske. *Inert Gas Effects in the incipient Boiling Of Alkali Liquid Metals*. International Journal of Heat and Mass Transfer, 17:461–462, 1974.
- [52] C.E. Brennen. *Cavitation and Bubble Dynamics*. Number ISBN 0-19-509409-3. Oxford University Press, 1995.

- [53] T.G. Leighton. *The Acoustic Bubble*. Number ISBN-0-12-441920-8. Academic Press, 1997.
- [54] G. Le Guillou, B. Berger, and M. Brunet. *Boiling Detection in Fast Reactors By Noise Analysis*. Progress in Nuclear Energy, 1:409–426, 1977.
- [55] Kurt D. Hamman and Ray A. Berry. *A CFD simulation process for fast reactor fuel assemblies*. Nuclear Engineering and Design, 240:2304–2312, 2010.
- [56] Stefano Rolfo, Christophe Péniguel, Matthieu Guillaud, and Dominique Laurence. *Thermal-Hydraulic study of a wire spacer fuel assembly*. Nuclear Engineering and Design, 243:251–262, 2012.
- [57] Alan Edward Waltar and Albert Barnett Reynolds. *Fast Breeder Reactors*. Pergamon Press, 1981.
- [58] N.E. Todreas and M.S. Kazimi. *Nuclear Systems I*. Taylor & Francis, 1990.
- [59] *Handbook on Lead-bismuth Eutectic Alloy and Lead Properties, Materials Compatibility, Thermal-hydraulics and Technologies*. Number ISBN 978-92-64-99002-9. Nuclear Energy Agency, 2007.
- [60] R.C. Martinelli. *Heat Transfer to Molten Metals*. Transactions of the ASME, 69:947–959, 1947.
- [61] William C. Press, Saul A. Teukolsky, William T. Vetterling, and Brian P. Flannery. *Numerical Recipes in C: The Art of Scientific Computing*. Number ISBN 0-521-43108-5. Cambridge University Press, 1992.
- [62] B. Menant. *Preliminary Results of Sodium Boiling Through a 19 Heating Rod Bundle*. In 6th Liquid Metal Boiling Working Group Meeting, Risley, UK, October 1-3 1975.
- [63] B. Menant. *Quelques particularités des écoulements de sodium bouillant dans les grappes d'aiguilles chauffantes*. PhD thesis, Institut Polytechnique de Grenoble, 1976.
- [64] *Liquid Metal Coolants for Fast Reactors Cooled by Sodium, Lead and Lead-Bismuth Eutectic*. Number NP-T-1.6. IAEA, 2012.
- [65] A.E. Dukler and Y. Taitel. *Flow Pattern Transitions in Gas-Liquid Systems: Measurement and Modeling*. Multiphase Science and Technology, 2(1):1–94, 1986.

-
- [66] K. Mishima and M. Ishii. *Flow Regime Transition Criteria For Upward Two-Phase Flow In Vertical Tubes*. International Journal of Heat and Mass Transfer, 27(5):723–737, 1984.
- [67] K. Mishima and T. Hibiki. *Some Characteristics of Air-Water Two-Phase Flow in Small Diameter Vertical Tubes*. International Journal of Multiphase Flow, 22(4):703–712, 1996.
- [68] K. Yamaguchi. *Flow Pattern and Dryout Under Sodium Boiling Conditions at Decay Power Levels*. Nuclear Engineering and Design, 99:247–263, 1987.
- [69] T.G. Theofanous, Luigi Biasi, H.S. Isbin, and H.K. Fauske. *Nonequilibrium bubble collapse: a theoretical study*. Chemical Engineering Progress Symposium Series, 66(102), 1969.
- [70] M. Mohammed Shah. *Survey of Critical Heat Flux Data for Pool Boiling of Liquid Metals and New Correlations*. Heat Transfer Engineering, 17(2):54–66, 1996.

5

Acoustic Boiling Noise Analysis

“A hypothetical theory is necessary, as a preliminary step, to reduce the expression of the phenomena to simplicity and order before it is possible to make any progress in framing an abstractive theory” ***The Edinburgh New Philosophical Journal***

William J.M. Rankine
1855

5.1 Introduction

The aim of this study is to model the acoustic boiling noise during a subassembly blockage, i.e. the noise related to the hydrodynamics of boiling. Fitzpatrick and Strasberg describe in their paper the origin of many hydrodynamic sound sources [1], where especially the strong coupling between hydrodynamics and acoustics is mentioned. It is thus not surprising that in this chapter both acoustic and hydrodynamic phenomena will be discussed

Fitzpatrick and Strasberg define underwater sounds (or basically sound traveling and being observed in a liquid medium) as fluctuating pressures associated with the flow. The hydrodynamic noise is thus a second order effect that has little effect on the more obvious characteristics [1]. The original definition of Fitzpatrick and Strasberg stated that such second order effects wouldn't have any influence at all.

The experiments of Chekanov, as described by Nesis, show however that the boiling inception in one liquid volume can trigger boiling in a saturated non-boiling volume by an acoustic connection [2]. Hence it can't be stated that the noise has no influence at all.

However, with the previous definition of the origin of the sound in the liquid in mind, it is already clear that the proposed model of the boiling noise is practically impossible. There is simply too much sodium boiling microscopic data missing (see chapter 5). It is thus the aim to give a hypothetical theoretical model based on the available thermodynamic knowledge, and as such to compare to processed experimental data that is found in literature to deduce some tendencies or to confirm some hypotheses.

5.2 Hydrodynamic Noise

5.2.1 Introduction

Fitzpatrick and Strasberg classified the hydrodynamic noise according to the macroscopic flow phenomena. In general, it can be written that the noise is related to unsteady flow phenomena (i.e. turbulence) and the unsteady motion of a two-phase interface (i.e. entrained gaseous bubbles, free surface disturbances, boiling, cavitation, . . .). To characterize the boiling noise, we thus have to look to the two-phase flow equations.

5.2.2 Two-Phase flow equations

As we have to look to the microscopic unsteady flow phenomena, we have to write down the local instantaneous differential equations for each phase and the interface. These equations can for example be found in the work of Delhaye [3], Van Carey [4] or in the article of Hsieh [5]. The article of Hsieh takes into account most, if not all, phenomena that can occur and as such we'll base our discussion on his publication.

5.2.2.1 Vapor phase equation

Inside the vapor/gaseous phase both vapor (subscript v) and incondensable gasses (subscript g) are present, and as such the conservation equation for each constituent should be written down:

$$\frac{\partial \rho_v}{\partial t} + \nabla \cdot (\rho_v \vec{v}_v) = 0 \quad (5.1a)$$

$$\frac{\partial \rho_g}{\partial t} + \nabla \cdot (\rho_g \vec{v}_g) = 0 \quad (5.1b)$$

The latter equations can be summed and as such we obtain the conservation equation of the gas-vapor mixture (subscript m):

$$\frac{\partial \rho_m}{\partial t} + \nabla \cdot (\rho_m \vec{v}_m) = 0 \quad (5.1c)$$

$$\rho_m = \rho_v + \rho_g \quad \rho_m \vec{v}_m = \rho_g \vec{v}_g + \rho_v \vec{v}_v \quad (5.1d)$$

with this mixture equation the momentum equation can be written:

$$\rho_m \left(\frac{\partial \vec{v}_m}{\partial t} + \vec{v}_m \cdot \nabla \vec{v}_m \right) = \nabla \cdot \bar{\bar{\tau}}_m + \rho_m \vec{g} \quad (5.1e)$$

where \vec{g} is the gravity (body) force and $\bar{\bar{\tau}}_m$ is the stress tensor that can normally be written as a function the pressure p and the velocity gradient (for simplicity written without any subscript):

$$\bar{\bar{\tau}}_{i,j} = -p\delta_{i,j} + \mu \left[\left(\frac{\partial \vec{v}_i}{\partial \vec{r}_j} + \frac{\partial \vec{v}_j}{\partial \vec{r}_i} \right) \right] + \delta_{i,j} \left(\mu_{bulk} - \frac{2}{3}\mu \right) (\nabla \cdot \vec{v})$$

In this equation the normal dynamic viscosity is given by μ , while μ_{bulk} is the bulk viscosity. This bulk viscosity is normally negligible, but it is notably important for acoustic and shock-wave effects. $\delta_{i,j}$ is the classical Kronecker delta.

The internal energy conservation (u) in the vapor phase (without internal heat generation) is given by:

$$\rho_m \left[\frac{\partial u_m}{\partial t} + \vec{v}_m \cdot \nabla u_m \right] = -\nabla \cdot \vec{q}'_m + Tr(\nabla v_m \cdot \bar{\bar{\tau}}_m) \quad (5.1f)$$

The first term in the right hand side gives the heating (or cooling) by the heat flux vector. This heat flux vector can be related to the temperature difference by Fourier's law:

$$\vec{q}' = -k\nabla T$$

The second term in the right hand side, i.e. the trace of the matrix product, gives the viscous heating and pressure-work. For simplicity these equations have been written in their most compact form.

5.2.2.2 Liquid phase equation

Similar equations for the liquid phase can be formulated. As for the vapor phase, we also have to take into account that there is some dissolved gas fraction in the

liquid (subscript s). This then leads to the mass conservation equations:

$$\frac{\partial \rho_l}{\partial t} + \nabla \cdot (\rho_l \vec{v}_l) = 0 \quad (5.2a)$$

$$\frac{\partial \rho_s}{\partial t} + \nabla \cdot (\rho_s \vec{v}_l) = -\nabla \cdot \vec{j}_s \quad (5.2b)$$

$$(5.2c)$$

The latter equation is the convective mass transfer equation in which the diffusional mass flux can be given by Fick's law [6]:

$$\vec{j}_s = -\rho D \nabla \left(\frac{\rho_s}{\rho} \right)$$

In the latter equation ρ is the mixture density. The density of the dissolved fraction is however sufficiently low that the mixture and liquid density can be taken equal. The momentum equation for the mixture (without subscripts) becomes:

$$\rho_l \left(\frac{\partial \vec{v}}{\partial t} + \vec{v} \cdot \nabla v \right) = \nabla \cdot \bar{\bar{\tau}} + \rho \vec{g} \quad (5.2d)$$

and similar to the the vapor phase, a conservation equation can be formulated for the energy of the mixture:

$$\rho \left[\frac{\partial u}{\partial t} + \vec{v} \cdot \nabla u \right] = -\nabla \cdot \vec{q}'' + Tr(\nabla v \cdot \bar{\bar{\tau}}) \quad (5.2e)$$

Again, these equations have been written in their most compact form.

5.2.2.3 Liquid-Vapor interface

The set of equations given in the previous paragraphs are valid only in the liquid or the vapor domain. On the mathematical/thermophysical (see figure 4.2) representation of the liquid-vapor interface, $S(r, t) = 0$, conservation laws also apply. ~~It are~~ these interface equations ~~that~~ couple the set of equations for the gas phase with the set of equations for the liquid phase.

The condensation/evaporation mass transfer at the boundary must respect the mass conservation. Hence any vapor or liquid actually "passing" the interface, i.e. having a normal component with the interface, and thus contributing to condensation/evaporation is subjected to conservation laws. However, the interface isn't necessarily stationary. The conservation law should thus take into account all these phenomena, which are schematically given in figure 5.1. This leads, after applying the mass conservation integral to the system in figure 5.1, to the differential equation for the liquid/vapor:

$$\rho_l \left(\vec{v}_l \cdot \nabla S + \frac{\partial S}{\partial t} \right) = \rho_v \left(\vec{v}_v \cdot \nabla S + \frac{\partial S}{\partial t} \right) \quad (5.3a)$$

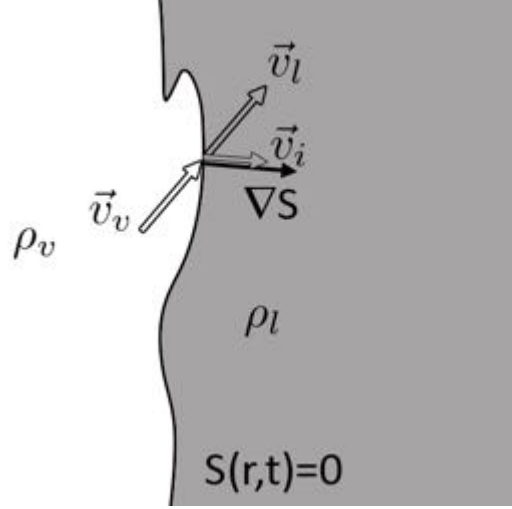


Figure 5.1: Graphical representation of the flow properties at a liquid (subscript l)/vapor (subscript v) interface (subscript i).

For the dissolved gas in the liquid and the gas in the vapor/gas-mixture, the interface conservation equation reads:

$$\rho_g \left(\vec{v}_g \cdot \nabla S + \frac{\partial S}{\partial t} \right) = \rho_s \left(\vec{v}_l \cdot \nabla S + \frac{\partial S}{\partial t} \right) + \vec{j}_s \cdot \nabla S \quad (5.3b)$$

Similarly, an interface equation exists for the mixture conservation:

$$\rho \left(\vec{v} \cdot \nabla S + \frac{\partial S}{\partial t} \right) = \rho_m \left(\vec{v}_m \cdot \nabla S + \frac{\partial S}{\partial t} \right) \quad (5.3c)$$

Similar conservation equations can be written for the momentum and for the energy respectively:

$$\begin{aligned} \rho \vec{v} \left(\vec{v} \cdot \nabla S + \frac{\partial S}{\partial t} \right) - \bar{\tau} \cdot \nabla S = \rho_m \vec{v}_m \left(\vec{v}_m \cdot \nabla S + \frac{\partial S}{\partial t} \right) \\ - \bar{\tau}_m \cdot \nabla S - \sigma \nabla S \left(\nabla \cdot \frac{\nabla S}{|\nabla S|} \right) - \nabla_{S=0} \sigma \end{aligned} \quad (5.3d)$$

The last two terms in the momentum balance include the normal capillary forces and the tangential (by use of the surface gradient $\nabla_{S=0}$) Marangoni forces. The

energy conservation equation reads:

$$\begin{aligned} \rho \left(u + \frac{v^2}{2} \right) \left(\vec{v} \cdot \nabla S + \frac{\partial S}{\partial t} \right) - \bar{\tau} \cdot \vec{v} \cdot \nabla S + \vec{q}'' \cdot \nabla S = \\ \rho_m \left(u_m + \frac{v_m^2}{2} \right) \left(\vec{v}_m \cdot \nabla S + \frac{\partial S}{\partial t} \right) - \bar{\tau}_m \cdot \vec{v}_m \cdot \nabla S \\ + \vec{q}_m'' \cdot \nabla S + \sigma \frac{\partial S}{\partial t} \left(\frac{\nabla S}{|\nabla S|} \right) \end{aligned} \quad (5.3e)$$

Hsieh assumed local thermodynamic equilibrium at the boundary. This leads to a temperature equilibrium between the vapor phase and the liquid:

$$T_m = T$$

However, a temperature drop or a heat transfer resistance should be taken into account at the liquid/vapor interface. This is especially true for liquid sodium, where this temperature drop can be more important than the temperature drop inside the liquid or the vapor. The temperature drop and mass flux across the interface are for example given by equation 4.12:

$$\dot{G} = \frac{\beta}{\sqrt{2\pi\mathcal{R}}} \left[\frac{p_{sat}}{\sqrt{\rho}} - \frac{p_v}{\sqrt{T_v}} \right] \quad (4.12)$$

where the interface is assumed **not** to have any curvature. Also assuming that there is no interface resistance or curvature effect for Henry's law, the non-condensable fraction at the liquid side and vapor side of the interface can be related:

$$\rho_s = k_h p_g \quad (5.4)$$

5.2.2.4 Solution

The latter equations have to be applied inside the complex geometry of a sub-assembly, with the respective no-slip boundary condition at the wall. The flow properties inside the subassembly should then be propagated towards the acoustic sensor location. Additionally, an initial condition should be given. This initial condition is the small 100 μm incondensable bubble from which nucleation initiates. This nucleation process is a hypothesis that has been formulated in the previous chapter and the actual nucleation process is an important lack of knowledge that already hinders a reliable prediction. Nonetheless, starting from the initial bubble, the growth of the vapor volume and possible condensation can be tracked and propagated. Whilst the solution of the full set of previous equations for this problem is already a challenge, we haven't mentioned the fact that turbulence modeling can't be used. Or in other words, a full two-phase flow direct numerical simulation (DNS) should be done.

And although that this two-phase DNS study was initially an objective, this type of DNS is far beyond the reach of the present-day simulation capabilities. A more simple, hypothetical theory should thus be deduced.

5.2.3 Simplified form

5.3 Bubble Dynamics

5.3.1 Analytical Development

5.3.1.1 Bubble Growth

5.3.1.2 Bubble Oscillation

5.3.1.3 Bubble Condensation

5.3.2 Condensation Dynamics

5.3.3 Condensation Models

5.4 Acoustic Development

5.5 Theory vs. Documented Experimental Data

5.6 Conclusion

References

- [1] H.M. Fitzpatrick and M. Strasberg. *Hydrodynamic sources of sound*. In First Symposium on Naval Hydrodynamics, pages 241–283. National Academy of Sciences, September 1959.
- [2] E.I. Nesis. *Boiling of Liquids*. Soviet Physics USPEKHI, 8(6):883–907, 1966.
- [3] J.M. Delhaye. *Thermohydraulique des réacteurs*. EDP Sciences – INSTN - Génie Atomique, 2008.
- [4] Van P. Carey. *Liquid-Vapor Phase-Change Phenomena: An Introduction to the Thermophysics of Vaporization and Condensation Processes in Heat Transfer Equipment*. Number ISBN 0-89116-836-2. Hemisphere Publishing, 1992.
- [5] Din-Yu Hsieh. *Some Analytical Aspects of Bubble Dynamics*. Journal of Basic Engineering, pages 991–1005, December 1965.
- [6] John Lienhard. *A Heat Transfer Textbook*. Phlogiston Press, 2006.

6

Acoustic Boiling Noise Experiments

*“The intensity of the boiling songs has been variously described by investigators as singing, howling, high frequency screams, a wailing banshee, or ultrasonic generator-type noise”, **Boiling Songs and Associated Mechanical Vibrations***

*H. Firstenberg, Nuclear Development Corporation of America,
1960*

6.1 Introduction

insert text here...

7

Acoustic Boiling Noise Detection

7.1 Introduction

insert text here...

8

Conclusion



Conversion and Breeding: from fertile to fissile isotopes

A.1 Introduction

Start text here...

B

Sodium Properties

B.1 Introduction

In this section, all the sodium properties in relation to sodium boiling are given. To interpret these properties, they are presented in relation to similar properties for water as has been done in a recent publication in the ANS journal of Nuclear Science and Engineering . The water properties are deduced from the Matlab steam tables, given by the XSteam module [2]. The sodium properties come from the reference work of Fink and Leibowitz [3, 4], other properties not mentioned by the latter document were taken from another reference work by Ohse [5]. Furthermore, we limit ourself to the discussion of properties at saturation. This is one the one hand because sodium can be considered to be fairly incompressible, but on the other hand also because simple compressible data of sodium are rare or there calculation requires a more complicated implementation as been discussed by Morita et al. for the SIMMER approximation of sodium properties [6, 7].

It is also important to mention that sodium, even reactor grade, does never exist in its pure form. It always contains some impurities. And even if the sodium would not contain any impurities, its vapor must be considered as a mixture of electrons, sodium ions Na^+ , monomer Na , dimer Na_2 and even tetramer Na_4 sodium-molecules [5, 8]. The contribution of the ions is practically negligible as can be easily calculated with the data of Vargaftik and Voljak [5] for the ionization reaction. A similar remark can be made for the tetramer content. To calculate

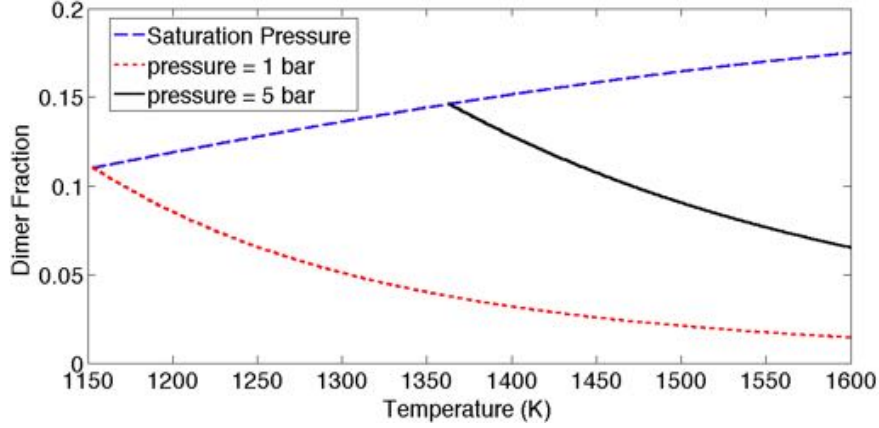


Figure B.1: The relative molar dimer Na_2 content in sodium vapor as a function of pressure and temperature.

the relative concentration of the dimer, which is non negligible, the equilibrium constants of Ewing et al [8] can be used for the association reaction (with the temperature T given in Kelvin):

$$2 Na \rightleftharpoons Na_2 \quad \log(k_2) = -4.3249 + \frac{4002.3}{T}$$

Figure B.1 shows the dimer fraction as a function of temperature and pressure. Taking into account the previous graph, we repeat the conclusion of Ewing: the dimer content is shown to increase with increasing pressure, while superheating the vapor tends to decrease the dimer fraction. These tendencies are important for the vapor properties of sodium.

B.2 Thermodynamic Properties

B.2.1 Vapor Pressure

The vapor pressure (in units of MPa as a function of the temperature T in Kelvin) given by:

$$p_l = \exp\left(11.9463 - \frac{12633.73}{T} - 0.4672 \log(T)\right) \quad (B.1)$$

is shown in figure B.2, showing the different scale in temperature for sodium and water at atmospheric conditions. Not only does it explain the interest to use liquid sodium in a reactor system (high temperatures can be obtained without excessive pressures), but it also makes the presentation of properties more difficult. To obtain

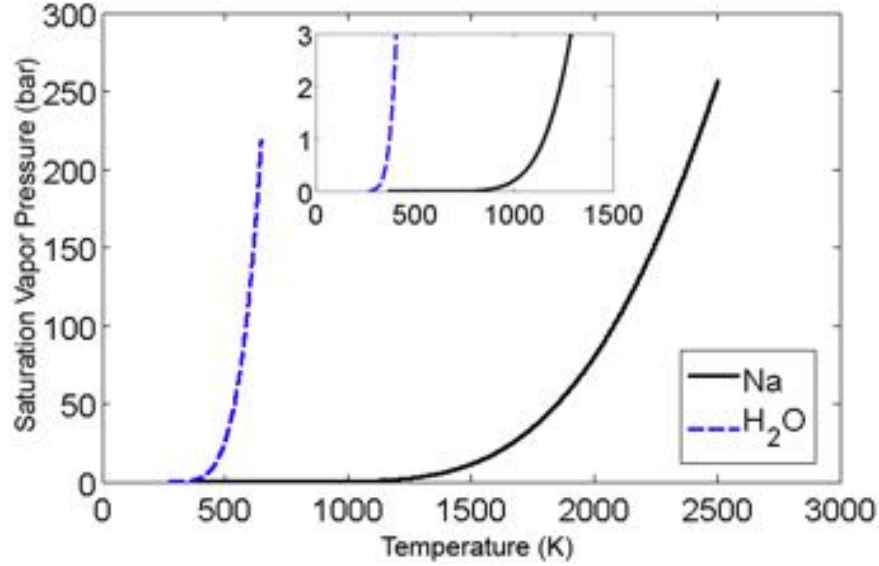


Figure B.2: The vapor pressure at saturation for sodium and water, as a function of the absolute temperature.

comprehensible graphs of the properties of interest, the temperature needs to be non-dimensionalised. Although the temperature is often non-dimensionalised by the critical temperature, we propose the following non-dimensional temperature:

$$(T - T_{melt}) / (T_{sat}^{1\text{ bar}} - T_{melt}) \quad (\text{B.2})$$

with T_{melt} the reference melting temperature of 371K defined in the work of Fink and Leibowitz [3]. $T_{sat}^{1\text{ bar}}$ is the saturation temperature at 1 bar (1154.7K). The advantage of this formulation stems from the fact that the range of interest is close to 1. We can thus elegantly come to conclusions between water and sodium properties.

B.2.2 Heat Of Vaporization

The heat of vaporization given (in units of kJ/kg) by:

$$h_{lv} = 393.37 \left(1 - \frac{T}{2503.7}\right) + 4398.6 \left(1 - \frac{T}{2503.7}\right)^{0.29302} \quad (\text{B.3})$$

with T given in Kelvin and given in figure B.3, shows a high value about twice that of water.

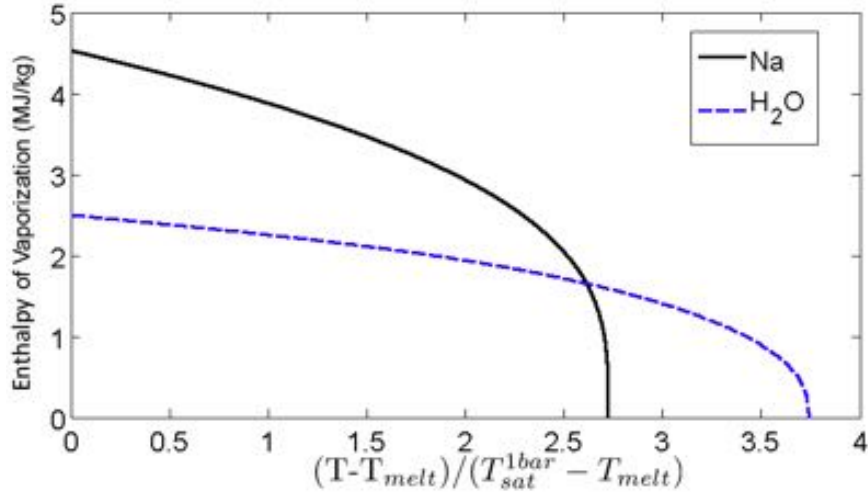


Figure B.3: The heat of vaporization of sodium and water, as a function of a dimensionless temperature: $(T - T_{melt}) / (T_{sat}^{1bar} - T_{melt})$, with T_{melt} the reference melting temperature.

B.2.3 Density

Figure B.4 shows the liquid density correlation (in units of kg/m^3):

$$\rho_l = 219 + 275.32 \left(1 - \frac{T}{2503.7}\right) + 511.58 \left(1 - \frac{T}{2503.7}\right)^{0.5} \quad (B.4)$$

with T given in Kelvin. The relatively complex correlation for the vapour density is shown in figure B.5, but for the exact calculation reference is made to the work of Fink and Leibowitz [3].

B.2.4 Heat Capacity

The heat capacity behavior for the sodium vapor and liquid are given in figure B.6, showing the peculiar behavior of the sodium vapor heat capacity caused by the dimerization at higher temperatures. This behavior can not be given by a simple correlation and reference is made to the work of Fink and Leibowitz. However, remark that the values for sodium vapor and steam are very similar. And although the heat capacity of liquid sodium and water are of the same order of magnitude, there is a factor four difference between them.

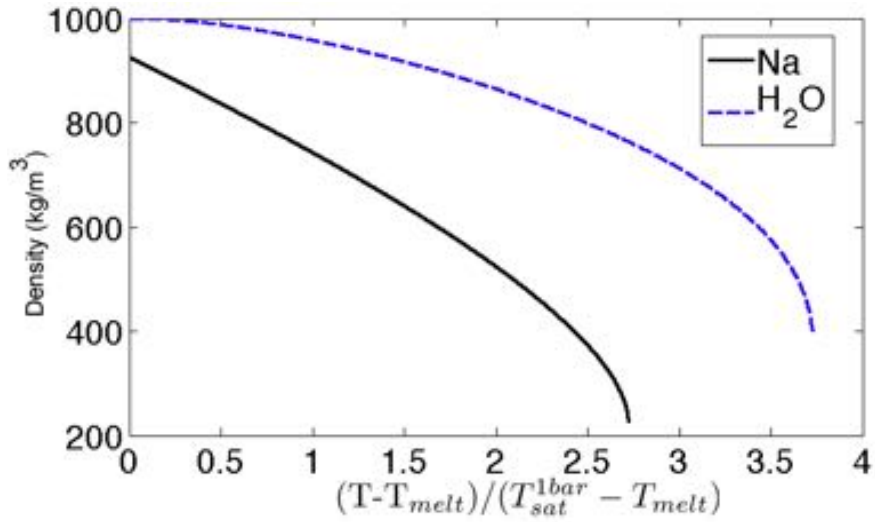


Figure B.4: The density of saturated liquid sodium and water, as a function of a dimensionless temperature: $(T - T_{melt}) / (T_{sat}^{1bar} - T_{melt})$, with T_{melt} the reference melting temperature.

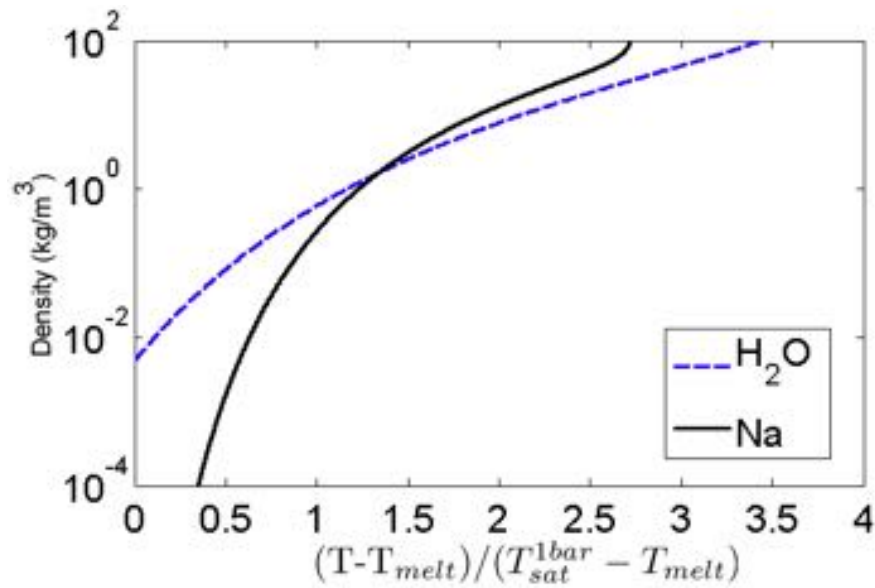


Figure B.5: The density of saturated sodium vapor and steam, as a function of a dimensionless temperature: $(T - T_{melt}) / (T_{sat}^{1bar} - T_{melt})$, with T_{melt} the reference melting temperature.

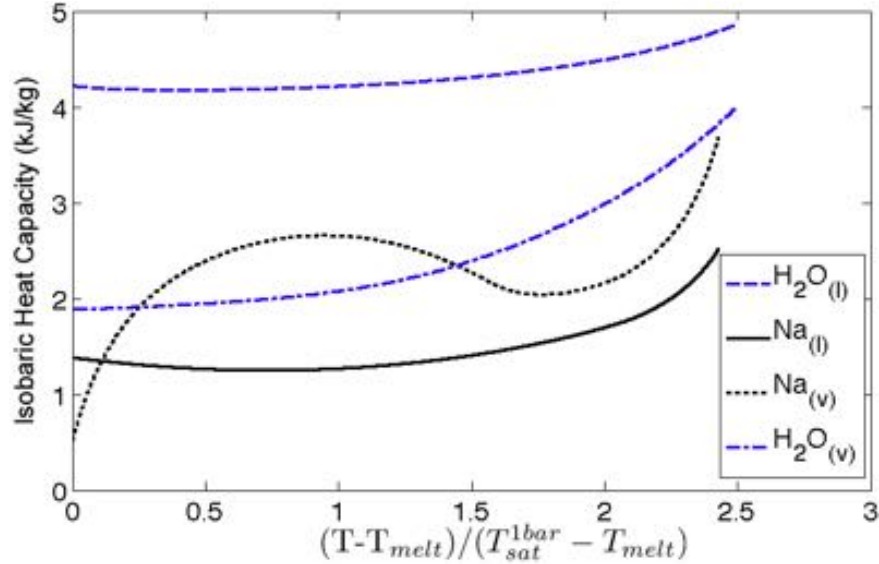


Figure B.6: The saturated heat capacity at constant pressure of water, liquid sodium and their vapor as a function of a dimensionless temperature: $(T - T_{melt}) / (T_{sat}^{1bar} - T_{melt})$, with T_{melt} the reference melting temperature.

B.2.5 Surface Tension

The surface tension between the liquid and the vapor (in units of mN/m):

$$\sigma = 240.5 \left(1 - \frac{T}{2503.7} \right)^{1.126} \quad (\text{B.5})$$

with T given in Kelvin and given in figure B.7 shows a relatively high value for the sodium surface tension, in comparison with water, at typical SFR operating and boiling conditions.

B.2.6 Sensitivity

Most of those properties do not change by a small impurity content. However, the surface tension for water is known to be particularly sensitive to impurities such as surface active substances. There exist two different positions on this subject:

- Allen mentions that oxide impurities act like surface active agents [5]. According to the data available to Allen, oxide impurities can form an insoluble sodium-oxide layer that significantly reduces the surface tension at high oxide content.

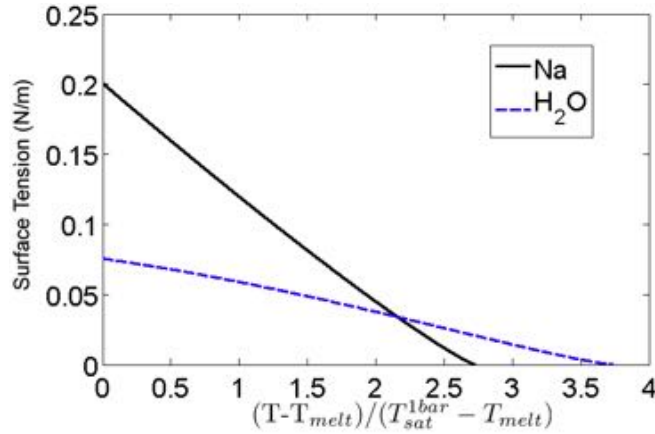


Figure B.7: The surface tension between the saturated liquid and the saturated vapor of sodium and water, as a function of a dimensionless temperature: $(T - T_{melt}) / (T_{sat}^{1bar} - T_{melt})$, with T_{melt} the reference melting temperature.

- Addison argues that surface-active substances do not exist for liquid metals, at least not in the usual sense as, for instance, for water [9]. Whilst he noticed a slight influence on the oxide level, it was not being perceived as notable as a typical surface active agent in water.

The aforementioned authors agree however that there is a change in surface tension due to metallic impurities:

- Allen mentions that a concentration of 0.025 at% Ca can change the surface tension by $0.01 \cdot 10^{-3} N/m$
- Addison states that the surface tension of Na-Cs alloy becomes practically equal to the Cs surface tension for a concentration below 60 at% of Na. This effect can be seen in figure B.8. The transition, between $\sigma_{Cs} < \sigma_{Na}$, is linear between 60 and 100 at% of sodium. Assuming that the effect of K (also an alkali metal with $\sigma_K < \sigma_{Na}$) in liquid sodium is similar to that of Cs, we can conclude that the amount of K-impurities in liquid sodium that is in the order of 1000 ppm gram will only change the surface tension value marginally.

B.3 Transport Properties

B.3.1 Viscosity

The kinematic viscosity of the liquid and vaporous state are given in figure B.9 and B.10 respectively. The kinematic viscosity deduced from the dynamic viscosity (η)

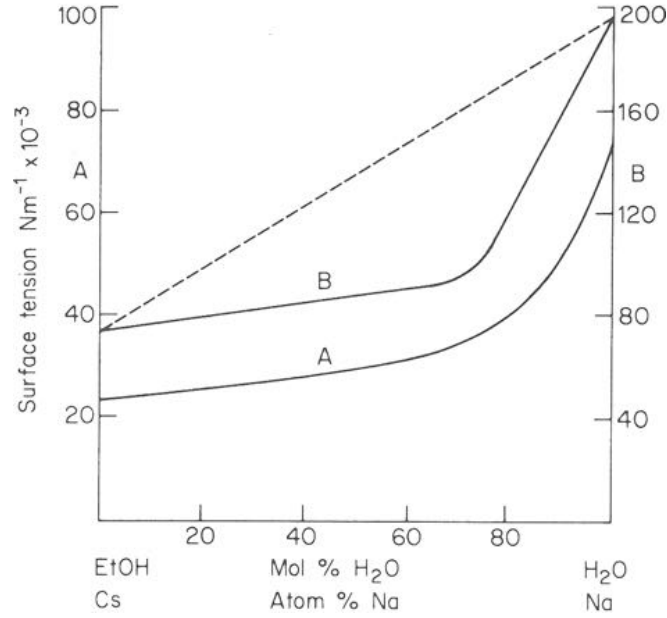


Figure B.8: The surface tension variation for an alcohol-water system (A) at 20°C and a cesium-sodium system (B) at 120°C. From Addison [9].

in units of $Pa.s$):

$$\eta = \exp\left(-6.4406 - 0.3958 \log(T) + \frac{556.835}{T}\right) \quad (B.6)$$

with T the temperature in Kelvin, is quite similar for water and liquid sodium. The viscosity of the vapor, given in the work of Ohse, depends on the dimer fraction and a simple representation is impossible.

B.3.2 Thermal Conductivity

The liquid thermal conductivity (in units of W/Km) is given by:

$$k = 124.67 - 0.11381 T + 5.5226 \cdot 10^{-5} T^2 - 1.1842 \cdot 10^{-8} T^3 \quad (B.7)$$

with T given in units of Kelvin and represented in figure B.11. For the sodium vapor thermal conductivity, as for the vapor's viscosity, the dimer fraction intervenes and a simple representation is impossible. Reference is thus made to the work of Ohse.

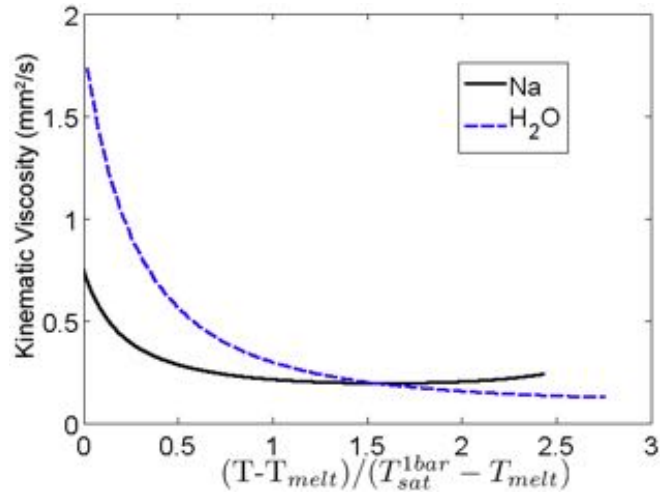


Figure B.9: The kinematic viscosity of saturated water and liquid sodium as a function of a dimensionless temperature: $(T - T_{melt}) / (T_{sat}^{1bar} - T_{melt})$, with T_{melt} the reference melting temperature.

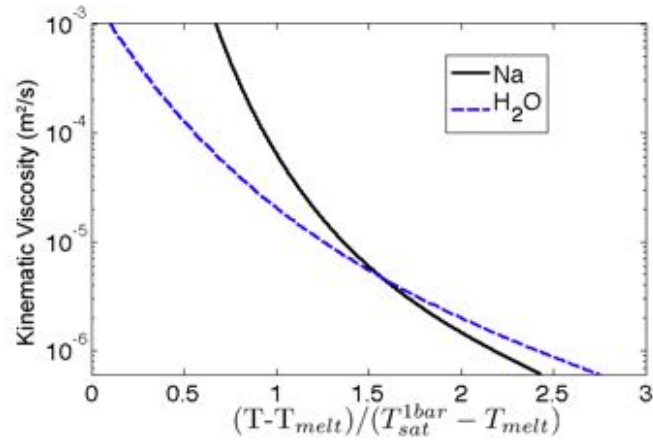


Figure B.10: The kinematic viscosity of saturated steam and sodium vapor as a function of a dimensionless temperature: $(T - T_{melt}) / (T_{sat}^{1bar} - T_{melt})$, with T_{melt} the reference melting temperature.

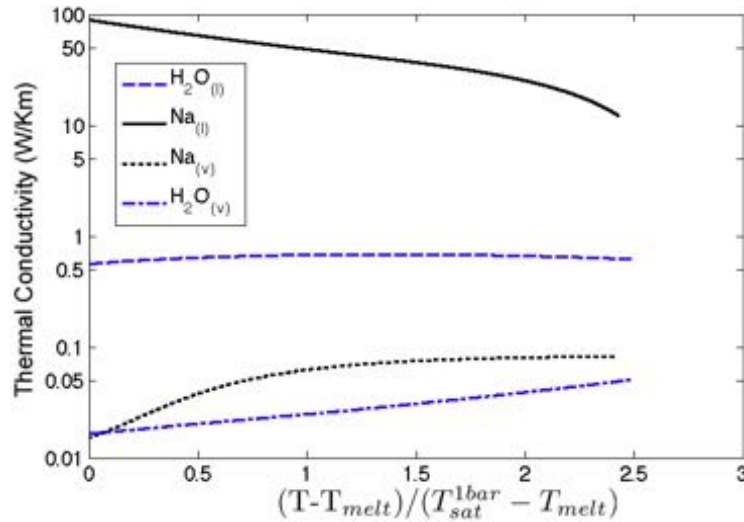


Figure B.11: The saturated thermal conductivity of water, liquid sodium and their vapors as a function of a dimensionless temperature: $(T - T_{melt}) / (T_{sat}^{1bar} - T_{melt})$, with T_{melt} the reference melting temperature.

B.3.3 Prandtl number

The thermal diffusivity, given by the ratio of the thermal conductivity k and the volumetric heat capacity ρc_p , is given in figure B.12. In this figure it can be seen that liquid sodium has a very high thermal diffusivity.

The ratio of the momentum diffusivity and the thermal diffusivity result in a dimensionless parameter that is called the Prandtl number that intervenes in the heat transport equation. Due to the high thermal diffusivity of liquid metals, this dimensionless parameter is very small. Due to this, the study of heat transfer in liquid metals is also often referred to as the analysis of low-Prandtl number flows. The Prandtl-number for liquid sodium and water is given in figure B.13, confirming its low value in comparison with more common fluids such as water.

B.4 Non-Condensables

It is important to notice that the solubility of the noble gases, argon and helium, is a few orders of magnitude lower in sodium than in water as can be seen in table B.1. But there is an important difference between the typical non-condensable behavior in sodium compared with the non-condensable behavior in water as demonstrated

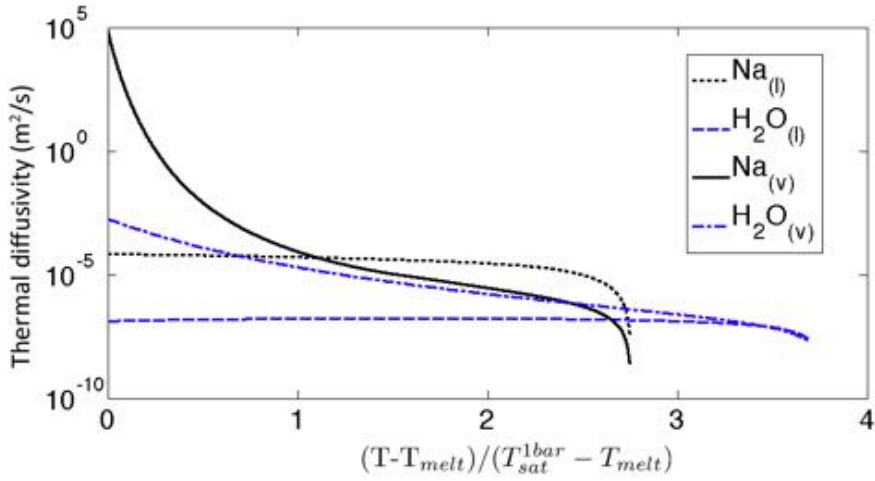


Figure B.12: The saturated thermal diffusivity of water, liquid sodium and their vapors as a function of a dimensionless temperature: $(T - T_{melt}) / (T_{sat}^{1bar} - T_{melt})$, with T_{melt} the reference melting temperature.

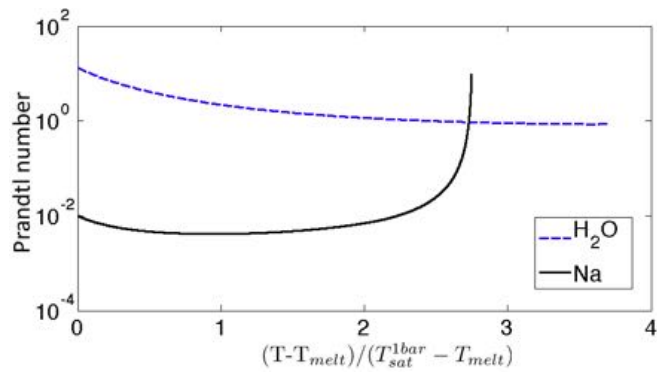


Figure B.13: The Prandtl number at saturation conditions for liquid sodium and water as a function of a dimensionless temperature: $(T - T_{melt}) / (T_{sat}^{1bar} - T_{melt})$, with T_{melt} the reference melting temperature.

Noble gas	Helium	Argon
Sodium [600°C]	$3.49 \cdot 10^{-7}$	$5.47 \cdot 10^{-8}$
Water [30°C]	$6.96 \cdot 10^{-6}$	$2.3 \cdot 10^{-5}$

Table B.1: Solubility of typical non-condensables, expressed as mole fractions, in sodium [10] compared to their solubility in water [12] for 1 atmosphere of partial gas pressure.

with Thormeier's correlation for the most important cover gas argon [10]:

$$x_g = p_g \cdot 5.49 \cdot 10^{-3} \exp(-10055 K/T) \quad (\text{B.8})$$

where the proportionality constant between the solubility (x_g) and the partial gas pressure (p_g) has units of mole fraction per unit of kilogram-force per square meter (practically equal to 1 atmosphere). While the solubility of non-condensables in water generally decreases with an increased solvent temperature, the solubility in liquid sodium increases with an increasing solvent temperature according to equation B.8. For completeness, we add that Veleckis made similar observations [11].

References

- [1] Matthias Vanderhaegen and Alix Le Belguet. *A Review on Sodium Boiling Phenomena in Reactor Systems*. Nuclear Science and Engineering, 2013.
- [2] Magnus Holmgren, *Matlab X Steam, Thermodynamic properties of water and steam, 2007*.
- [3] J.K. Fink and L. Leibowitz. *Thermodynamic and Transport Properties of Sodium Liquid and Vapor*. Technical Report ANL/RE-95/2, Argonne National Laboratory, Reactor Engineering Division, January 1995.
- [4] J.K. Fink and L. Leibowitz. *A Consistent Assessment of the Thermophysical Properties of Sodium*. High Temperature and Material Science, 35:65–103, 1996.
- [5] Roland W. Ohse, editor. *Handbook of Thermodynamic and Transport Properties of Alkali Metals*. Blackwell Scientific Publishing, 1985.
- [6] K. Morita and E.A. Fischer. *Thermodynamic properties and equations of state for fast reactor safety analysis. Part I: Analytic equation-of-state model*. Nuclear Engineering and Design, 183:177–191, 1998.

-
- [7] K. Morita, E.A. Fischer, and K. Thurnay. *Thermodynamic properties and equations of state for fast reactor safety analysis. Part II: Properties of fast reactor materials*. Nuclear Engineering and Design, 183:193–211, 1998.
- [8] C.T. Ewing, J.P. Stone, J.R. Spann, and R.R. Miller. *Molecular Association in Sodium, Potassium and Cesium Vapors at High Temperatures*. The Journal of Physical Chemistry, 71(3):473–477, 1967.
- [9] C.C. Addison. *The Chemistry of the Liquid Alkali Metals*. John Wiley & Sons, Inc, 1984.
- [10] K. Thormeier. *Solubility of the Noble Gases in Liquid Sodium*. Nuclear Engineering and Design, 14:69–82, 1970.
- [11] E. Veleckis, S.K. Dhar, F.A. Cafasso, and H.M. Feder. *Solubility of Helium and Argon in Liquid Sodium*. Journal of Physical Chemistry, 75(18):2832–2838, 1971.
- [12] Emmerich Wilhelm, Rubin Battino, and Robert J. Wilcock. *Low Pressure Solubility of Gases in Liquid Water*. Chemical Reviews, 77(2):219–262, 1977.

